The Role of Glucocorticoid Signaling in Adult Muscle Stem Cell and Myogenic Differentiation

by

Rashida Rajgara

Thesis submitted to the University of Ottawa
in partial Fulfillment of the requirements for the degree of
Doctor of Philosophy

Cellular and Molecular Medicine
Faculty of Medicine

University of Ottawa

ABSTRACT

Glucocorticoids are the most widely prescribed medications due primarily to their anti-inflammatory and immunosuppressive actions, however, their use is not without side effects. Among these, glucocorticoids cause profound muscle atrophy, yet paradoxically are used as the first line of treatment for muscle wasting disorders such as Duchenne Muscular Dystrophy (DMD) and inflammatory myopathies. In DMD patients, glucocorticoid treatment can improve muscle strength during the first 6 months of treatment and can delay loss of muscle function by up to three years. While recent advancements have been made to understand the effect of glucocorticoids (GCs) on the myofiber, the impact of GCs on skeletal muscle stem cells (MuSCs), the adult stem cells responsible for muscle regeneration, and their role in myogenic differentiation, are relatively unknown. To study the role of glucocorticoid signalling during muscle repair, I developed a conditional null mouse ($GR^{MuSC-/-}$) model in which glucocorticoid receptor (GR) expression is knocked out specifically in MuSCs ($GR^{MuSC-/-}$). One-week following acute muscle injury, WT and $GR^{MuSC-/-}$ mice both underwent robust repair assessed by myofiber cross-sectional area (CSA) analysis. However, the $GR^{-/-}$ MuSCs failed to return to quiescence following repair resulting in a significant increase in average myofiber CSA at 28- and 42- days post-injury, as compared to controls. Loss of the GR led to a significant increase in the percentage of PAX7+Ki67+ cycling cells in $GR^{MuSC-/-}$ mice (as compared to controls) at 42 days post injury. In the uninjured contralateral limb, I observed significantly fewer MuSCs in $GR^{MuSC-/-}$ mice with a concomitant increase in fibers with centrally located nuclei, indicating that these PAX7+ MuSCs progressed to differentiation in the absence of direct injury. In an uninjured model, two weeks following loss of GR expression there was an increase in the percentage of BrdU+ and Ki67+ cycling cells in resting $GR^{MuSC-/-}$ tibialis anterior muscles as compared to WT, suggesting that the GR acts to maintain MuSC quiescence. Consistent with this, immunostaining of single EDL myofiber fibers at T2h post-dissociation revealed that loss of GR in MuSCs lead to precocious activation and subsequent proliferation of MuSCs as compared to controls. Bulk RNA-sequencing from *in situ* fixed MuSCs in resting muscle revealed that the gene signature of $GR^{-/-}$ MuSCs was consistent with cells that have exited from the quiescent state and are activated for differentiation. Despite precocious activation, $GR^{-/-}$ myoblasts differentiate and fuse normally, however the myotubes produced had abnormal morphology and aberrant myonuclear placement in regenerated muscle fibers *in vivo*.

Conversely, dexamethasone (DEX) treatment increased myoblast fusion but resulted in the formation of stellate-shaped myotubes in culture. In myofibers, DEX treatment enhanced parallel microtubule bundling. Taken together my results demonstrate that the glucocorticoid receptor is critical to maintain MuSC quiescence and to regulate cell morphology upon differentiation; at least in part, by microtubule bundling.

TABLE OF CONTENTS

LIST OF FIGURES

LIST OF TABLES

LIST OF ABBREVIATIONS

ABD1	Actin-binding amino-terminal domain
AMPK	AMP-activated protein kinase
ANG1	Angiopoietin 1
ASCs	Activated MuSC
ASO	Antisense oligonucleotides
BPVC	Bupivacaine hydrochloride
BrdU	Bromodeoxyuridine
CDK	Cyclin-dependent kinases
CNM	Central Nuclear Myopathies
CRH	Corticotropin-releasing hormone
CSA	Cross-sectional area
CSC	Contralateral satellite cells
CTX	Cardiotoxin
DBD	DNA binding domain
DEGs	Differentially Expressed Genes
DEX	Dexamethasone
DGC	Dystrophin-glycoprotein complex
DLL4	Delta-like canonical Notch ligand 4
DMD	Duchenne Muscular Dystrophy
DMEM	Dulbecco's modified Eagle's medium
DSHB	Developmental Studies Hybridoma Bank

EB1	End-binding protein 1
ECM	Extracellular matrix
EDL	Extensor Digitorum Longus
EDTA	Ethylenediaminetetraacetic acid
ETC	Electron transport chain
FACS	Fluorescence Activated cell Sorting
FAP	Fibroadipogenic precursors
FBD	Flexor digitorum brevis
FFPE	Formalin-fixed parafilm embedded
FGF	Fibroblast growth factor
FIJI	Fiji Is Just ImageJ
GCs	Glucocorticoids
GSEA	Gene Set Enrichment Analysis
GOBP	Gene Ontology for Biological Processes
GR	Glucocorticoid Receptor
GREs	Glucocorticoid response elements
HGF	Hepatocyte growth factor
IGF-I	Insulin-like growth factor 1
JNK	c-Jun N-terminal kinase
LINC	Linker of Nucleoskeleton and Cytoskeleton
MAP1b	Microtubule-binding proteins
MAPK	Mitogen-activated protein kinase
MAPs	Microtubule-associated proteins

MHC	Major histocompatibility complex
MPCs	Myogenic precursor cells
MR	Mineralocorticoid receptor
MRF	Myogenic Regulatory Factor
mRNA-seq	messenger RNA sequencing
MT	Microtubule
MTJ	Myotendinous junction
MTOC	Microtubule Organizing Centres
mTOR	Mechanistic target of rapamycin
MuSCs	Muscle Stem Cells
MyHC	Myosin heavy chain
MYOD	Myogenic Differentiation
MYOG	Myogenin
NE	Nuclear envelope
NES	Normalized enrichment score
NMJ	Neuromuscular junctions
NTD	N-terminal transactivation domain
OCT	Optimal Cutting Temperature
OXPHOS	Oxidative phosphorylation
PAX	Paired Box
PCM	Pericentriolar matrix
PCNT	Pericentrin
PCP	Planar cell polarity

PDGF-BB	Platelet-derived growth factor-BB
PFA	Paraformaldehyde
PTM	Post-translational modification
QSCs	Quiescent satellite/stem cells
*RB*1	Retinoblastoma 1
*RB*L1	Retinoblastoma-like 1
RNA	Ribonucleic Acid
ROS	Reactive oxygen species
RT-qPCR	Real-time quantitative polymerase chain reaction
TCA	Citric Acid Cycle
TEM	Transmission electron microscopy
TLR	Toll-like receptors
UMI	Unique molecular identifiers
VEGF	Vascular Endothelial Growth Factor
WT	Wild Type

ACKNOWLEDGEMENTS

Firstly, I would like to express my heartfelt thanks to my mentor and research supervisor Dr. Nadine Wiper-Bergeron, whose guidance and support has been invaluable throughout the past 6 years and beyond. Her expertise, encouragement, and insights have greatly contributed to the success of my professional research career and personal growth.

I would also like to extend my appreciation to my thesis advisory committee members; Dr. Alexandre Blais, Dr. Rashmi Kothary and Dr. David Lohnes, whose critical feedback, encouragement, and suggestions helped me shape my research ideas and develop the necessary skills to become a resilient researcher with the highest integrity.

I am immensely grateful to the diligent staff of the animal care and veterinary services, autoclaving, technical support, procurement and logistics, graduate office, and the CMM/NSC secretaries. Your unwavering dedication and assistance have been invaluable in enabling me to carry out my work. I cannot thank you enough for all that you do.

I am grateful to my past lab members, specifically Dr. Hamood Alsudais, Dr. Neena Lala-Tabbert, Dr. Emilie Sarazin and Kira Slivitzky for helping me navigate the early challenges of graduate school and showing me the ropes. To the current NWB lab team: Aisha Saleh, Leanne Dawe, Alex Brown, Natasha Strong, Jocelyn Nguyen and Konstantin Alexeev, whose camaraderie, support, and friendship helped me to stay motivated and inspired throughout the ups and downs of this journey. One of the mentionable downs being the Covid-19 pandemic, which did negatively impact the planet, people, and plans; but has also reminded us of the importance of resilience, flexibility, and compassion.

I would like to thank my parents Firoz and Rehana, whose unwavering support, encouragement, prayers, and sacrifices have been instrumental in my success. Their love,

guidance, and wisdom have been the foundation upon which I have built my academic and personal achievements. You are the back-up that never fails. Special mention to my in-laws Farida and Imran for always being avid listeners and my biggest supporters.

To all my loved ones, including family, relatives, and friends, who are too numerous to list individually but too important to overlook, I thank you for the love and laughs that transpired. The strong bond I share with my sisters Fatema and Umme proved to be a vital source of support and encouragement, enabling me to successfully complete my PhD.

I am deeply grateful to my best friend and husband Akil, who has been my rock, my confidante, and my cheerleader. His love, support, and deep understanding has sustained me through the long hours of research and writing. Thank you for your constant presence.

I would like to thank our cat Purrcy, who wasn't the most motivating writing companion, but his physical presence, purrs, and playfulness reminded me to take breaks, relax, and enjoy the simple pleasures of life. To all of you, I express my deepest gratitude and appreciation. Thank you for being part of my journey, and for helping me to reach this milestone.

I also want to acknowledge the invaluable contribution of the mice that were used in this study. Their sacrifice and contribution to science cannot be overstated, and I am deeply grateful for their role in advancing our understanding in this field.

Finally, I would like to end with a land acknowledgement for Ottawa. I acknowledge that the land on which this research was conducted is the traditional and unceded territory of the Algonquin Anishinaabe Nation. I recognize and respect the enduring presence, resilience, and knowledge of the Indigenous peoples who have lived on this land for thousands of years, and I commit to engaging with them in a spirit of reconciliation, respect, and collaboration.

CONTRIBUTION OF COLLABORATORS

This work was supported by a grant from the Canadian Institutes of Health Research (CIHR) to Dr. Nadine Wiper-Bergeron (NWB). Rashida Rajgara (RR) is supported by the Ontario Graduate Scholarship (OGS) from the University of Ottawa, ON. The B10 Scotty Snell WT (C57BL/10ScSnJ, The Jackson laboratory, stock #000476) and *mdx* (C57BL/10ScSn-Dmd*mdx*/J, The Jackson laboratory, stock #001801) mice were generously gifted by Dr. Rudnicki and Dr. Korneluk's laboratory. Studies on microtubule dynamics and cytoskeletal staining were performed with the assistance of Dr. John Copland. Previous and present lab members (particularly Dr. Hamood Alsudais, Aisha Saleh, Leanne Dawe, Alex Brown, Jocelyn Nguyen, Laura Mardiros and Amina Mohammed) for their help with sample collection, processing, and data quantification. The Cell Biology and Image Acquisition Core (RRID: SCR_021845) and the staff members (Dr. Chloë Van Oostende-Triplet and Skye Green) funded by the University of Ottawa, Ottawa, Natural Sciences and engineering Research Council of Canada, and the Canada Foundation for Innovation for help with image acquisition, processing, and quantification. The Louise Pelletier Histology Core (RRID: SCR_021737) and staff for performing H&E staining on TA muscles used in this study. I acknowledge the use of instruments (SH800 cell sorter) and expertise (Dr. Vera Tang) from the uOttawa Flow Cytometry Core Facility, which is funded by the University of Ottawa, Natural Sciences and Engineering Research Council of Canada, and the Canadian Foundation for Innovation. I would also like to thank the Donnelly Sequencing Center (University of Toronto, ON) and Genome Quebec (Montréal, QC) staff for library preparation and bulk RNA sequencing. Special mention to Ines Barrakad and Dabo Yang from Dr. Alexandre Blais (AB) lab for assistance with *in-situ* fixed cell isolation, optimization, and sorting. To Philippos Mourikis (Institut Mondor, Paris) for advice on RNA-extraction from *in situ*-fixed samples. I personally thank Dr. Alexandre

Blais for performing quality check and processing of raw data files to generate differentially expressed gene lists from bulk RNA-sequencing experiments performed in this study. CIHR grant (PJT 183839) to AB. MDA Idea grant #874651 to AB and NWB.

INTRODUCTION

i. Skeletal muscle and the satellite cell niche

Skeletal muscle is one of the most dynamic tissues in the human body that forms approximately 40% of total body weight and contains up to 50–75% of all body proteins. The contractile component of skeletal muscle is composed of multinucleated muscle cells called myofibers (M. Buckingham, 2001). During development, myofibers are formed by the fusion of mesodermal progenitors that express the Paired Box (PAX) transcription factors PAX3 and PAX7. The PAX3+/7+ population present in the central dermomyotome also gives rise to adult muscle stem cells, which have an important role in maintaining skeletal muscle throughout the life of an organism (Margaret Buckingham & Relaix, 2007). At approximately E16, which marks the end of fetal myogenic development, PAX3+/7+ progenitor cells begin to accumulate under the basal lamina that forms around muscle fibers and enter quiescence (Frédéric Relaix et al., 2005). These cells, called muscle satellite/stem cells (MuSCs) were hypothesized to be the stem cell responsible for adult vertebrate muscle regeneration (Mauro, A. 1961), and the conditional depletion of these Pax7-expressing cells (MuSCs) from mice using diphtheria toxin expression driven by the Pax7 promoter caused a complete loss of muscle regeneration and was associated with increased fibrosis and fatty tissue in injured muscle (Lepper et al., 2011; Mccarthy et al., 2011; Murphy et al., 2011a; Sambasivan et al., 2011). Transplantation of donor MuSCs rescued the defective regeneration in these mice, indicating the indispensability of MuSCs in muscle regeneration (Sambasivan et al., 2011). These findings suggest that other resident muscle cell populations, referred to as non-MuSCs, are incapable of fully regenerating damaged muscle. As such *Pax7*-expressing satellite cells are indispensable for post-natal skeletal muscle regeneration (Sambasivan et al., 2011). MuSCs are characterized by their unique anatomical position, which is located between the basal

lamina and the sarcolemma of individual muscle fibers, and their expression of Pax7 (Cornelison & Wold, 1997; Gnocchi et al., 2009; Kuang et al., 2007; P. Seale, L. A. Sabourin, A. Girgis-Gabardo, A. Mansouri, P. Gruss, 2000; So-ichiro Fukada, Akiyoshi Uezumi, Madoka Ikemoto, Satoru Masuda, Masashi Segawa, Naoki Tanimura, Hiroshi Yamamoto, Yuko Miyagoe-Suzuki, 2007) (Fig. a).

Skeletal muscle regeneration is a highly orchestrated process involving the activation of various cellular and molecular responses and any defect seen in even one of these processes leads to impaired regeneration. Upon injury, caused by exercise or myotrauma, MuSCs re-enter the cell cycle (Zammit et al., 2004). Proliferating muscle stem cells are commonly referred to as myogenic precursor cells (MPCs), or myoblasts, and are characterized by the expression of the myogenic regulatory factors (MRFs), MYOD and MYF5 (Cooper et al., 1999; Cornelison & Wold, 1997; Grounds et al., 1992). Subsequently, myoblasts downregulate PAX7, withdraw from the cell cycle irreversibly, upregulate the expression of the MRFs myogenin and MRF4, and commit to terminal differentiation to become myocytes (J. C. J. Chen & Goldhamer, 1999; Hasty et al., 1993; Tedesco et al., 2010; Zammit et al., 2004). Myocytes then fuse to form a multinucleated syncytium that becomes the myofiber (known as myotube in culture). In addition to undergoing differentiation and fusion, some myogenic precursor cells can escape differentiation, downregulate MYOD expression and self-renew, re-entering quiescence to maintain the MuSC population (Collins et al., 2005; Zammit et al., 2004, 2006). This ability to self-renew allows the muscle to sustain multiple rounds of injury during the adult lifespan.

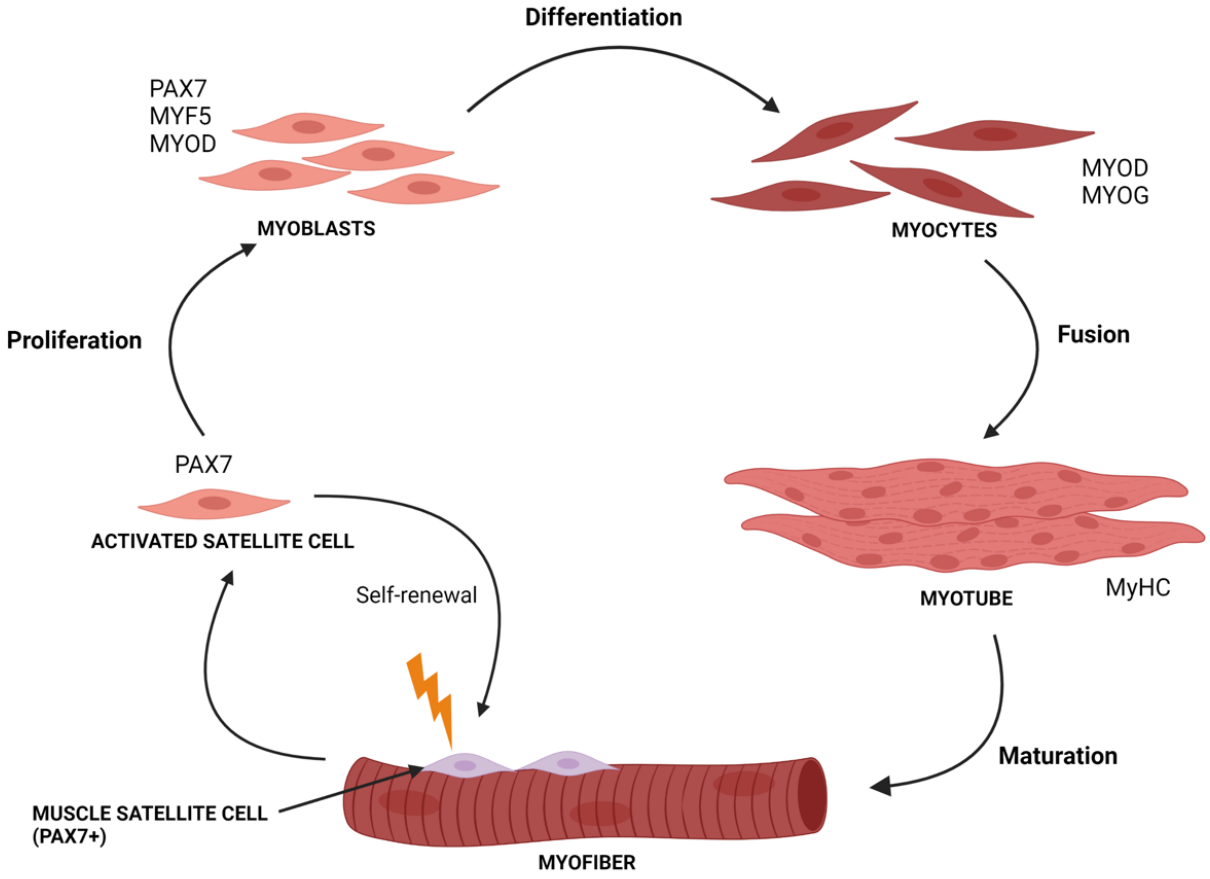

Figure a: Transcriptional regulation of adult skeletal myogenesis.
A schematic representation of the series of molecular and cellular events involved in adult muscle stem cell activation and differentiation into skeletal muscle. When muscle fibers are damaged due to injury, exercise, or a diseased state, PAX7+ muscle stem/satellite cells (MuSCs) exit quiescence to proliferate to increase the muscle progenitor cell pool (myoblasts; PAX7+/MYOD+). After expansion, myoblasts differentiate and express myogenin (MYOG) then fuse to form new fibers or fuse with existing muscle fibers to repair damaged tissue and restore muscle function. A proportion of MuSCs do not differentiate but rather undergo self-renewal to repopulate the MuSC niche. The pivotal transcription factors and structural genes involved in skeletal muscle formation are illustrated. Created with BioRender.com

ii. Muscle stem cell quiescence

In tissues with low turnover such as skeletal muscle, adult stem cells remain quiescent (in the G0 state of the cell cycle) for extended periods of time until activated for regeneration and repair (Arai et al., 2004; Cotsarelis et al., 1990; N. Li & Clevers, 2010; Study et al., 1978). Cellular

quiescence refers to a state of reversible cell cycle arrest in which cells are in the resting phase of the cell cycle (G_0) but can re-enter mitosis in response to various internal and external cues. Even though quiescent MuSCs show similarities to other non-dividing cell types such as terminally differentiated cells that are also in G_0, they are not irreversibly arrested. Quiescent MuSCs (qMuSCs) are characterized by decreased cell size and reduced histone methylation, RNA content, protein synthesis and metabolism (Llorens-Bobadilla et al., 2015; Passegué et al., 2005; Shin et al., 2015; Signer et al., 2014; Simsek et al., 2010). Whether a cell enters G_0 or continues through the cell cycle is determined by several key factors, including cyclins, cyclin-dependent kinases (CDKs) and the CDK inhibitors. CDK inhibitors, including p21 (CDKN1A), p27 (CDKN1B), and p57 (CDKN1C) promote cell cycle exit, and quiescent cells typically display high levels of these proteins (Aktas et al., 1997; Arora et al., 2017; Barr et al., 2017; Fujimaki et al., 2019; B. Li et al., 2019; L. Wang et al., 2020). The dynamic interactions between MuSCs and their niche also regulate satellite cell function including the maintenance of quiescence and self-renewal. MuSCs are found in a highly specified niche, which consists of the adjacent myofiber, surrounding cells (fibro/adipogenic precursors, FAPs; immune cells), blood vessels and the extracellular matrix (ECM), all of which interact with quiescent cells using indirect (soluble factors) or direct (cell-cell; cell-matrix) contact (Fiore et al., 2018) (Fig. b). Furthermore, MuSCs, as one of the niche components themselves, also influence each other by means of cell-cell interactions and autocrine/paracrine signaling (Yin et al., 2013).

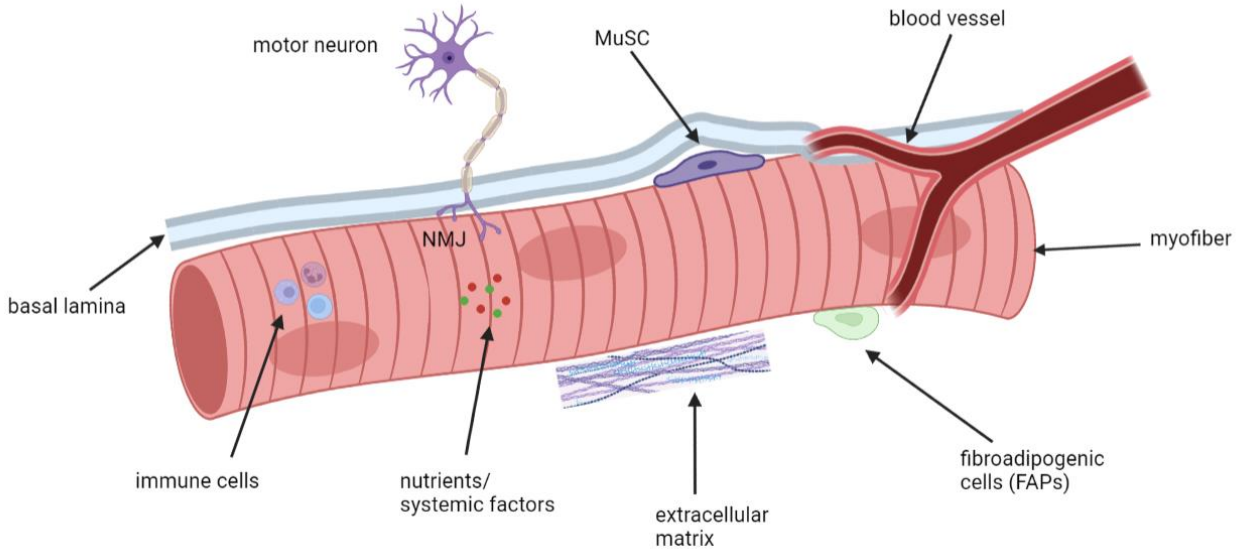

Figure b: The muscle stem cell niche.
The muscle stem cell niche is the microenvironment surrounding satellite cells (MuSCs) between the basal lamina and the myofiber sarcolemma. The niche consists of the extracellular matrix (ECM), vascular (blood vessels) and neural (motor neuron) networks, fibroadipogenic cells (FAPs) and immune cells among others and diffusible molecules (nutrients, growth factors). Adapted from: The emerging biology of muscle stem cells: implications for cell-based therapies by Bentzinger, C. F., Wang, Y. X., von Maltzahn, J., & Rudnicki, M. A. (2013). Bioessays. 35(3):231-41. Doi: 10.1002/bies.201200063. Created with BioRender.com

Wnt ligands function to promote satellite cell proliferation during muscle regeneration, whereas Wnt antagonists inhibit proliferation by sequestering β-catenin to the cell membrane in quiescent satellite cells (Otto et al., 2008). Notch signaling is also involved in the maintenance of cell quiescence in healthy muscle. Genetic removal of *Rbpj*, the main effector for canonical Notch signaling in MuSCs, results in the loss of their quiescent state and spontaneous differentiation to form myofibers, with concomitant depletion of the stem cell pool (Philippos et al., 2012). Delta-like canonical Notch ligand 4 (DLL4) is another example of niche factors that regulate MuSC function. Eliazer *et al.*, demonstrated that DLL4 expression is unequally distributed along the muscle fiber and MuSCs located in low DLL4 regions are primed for activation at the onset of

injury (Eliazer et al., 2020). Therefore, the deletion of *Dll4* in myofibers depletes the MuSC pool, confirming the requirement of the niche DLL4 for MuSC self-renewal (Eliazer et al., 2020).

Indeed, the myofiber plays an important role in maintaining MuSC function. This finding was revealed through selective necrosis of myofibers with bupivacaine hydrochloride (BPVC) which leaves the basal lamina intact. BPVC treatment resulted in greater numbers of proliferating satellite cells compared to viable myofibers (Richard Bischoff, 1975), suggesting that the myofiber provides a quiescence-inducing signal either by its physical proximity or by releasing secreted factors (R. Bischoff, 1990; Richard Bischoff, 1986). Interstitial cells (such as fibroblasts, FAPs, adipocytes, telocytes), motor neurons and the vasculature (blood vessels) also tightly regulate MuSC function. Fibro/adipogenic progenitors (FAPs) are a population of progenitor cells that express PDGFRα and have the capacity to differentiate into both fibroblasts and adipocytes, as reported by Uezumi *et al* (Uezumi et al., 2010). Following injury, FAPs are activated and undergo expansion. Although FAPs do not contribute to myofiber formation, they support the expansion and differentiation of muscle stem cells through the secretion of factors that regulate the extracellular matrix (ECM) (Uezumi et al., 2010; Wosczyna et al., 2019). The establishment of a suitable niche for MuSC expansion and myofiber formation is a critical function of FAPs. Studies by the Rando group have demonstrated that depletion of FAPs from skeletal muscle not only impairs muscle regeneration, but also reduces MuSC numbers and muscle size, as described by Wosczyna *et al.* (Wosczyna et al., 2019). The depletion of FAPs from skeletal muscle tissue leads to a significant reduction in MuSC numbers in uninjured muscle, suggesting that FAPs play a crucial role in maintaining the MuSC pool. Furthermore, skeletal muscle atrophy and reduced function were observed after FAP depletion, highlighting the importance of FAPs in skeletal muscle homeostasis and function, as reported by (Wosczyna et al., 2019).

Literature has further emphasized the supportive role of non-muscle stem cells in muscle regeneration. Specifically, studies have shown that fibroblasts play a critical role in regulating the extracellular matrix and myogenic differentiation during muscle regeneration. In murine models, the ablation of fibroblasts via Tcf4 promoter-driven diphtheria toxin resulted in decreased MuSC proliferation, premature differentiation, smaller regenerating fibers, and a depletion of the MuSC pool (Murphy et al., 2011b). *In vitro* co-culture experiments have indicated that the fibroblast-derived secretome suppresses myogenic differentiation (Rao et al., 2013). Additionally, fibroblasts are major regulators of the skeletal muscle ECM, which undergoes extensive remodeling during muscle regeneration (Thomas et al., 2015; Urciuolo et al., 2013; Zou et al., 2008). Fibroblasts secrete several collagens, including collagen VI, which has been shown to play a critical role in both muscle regeneration and MuSC self-renewal in mice lacking collagen VI (Urciuolo et al., 2013). Furthermore, fibroblasts secrete factors such as angiopoietin 1 (ANG1), which promote MuSC quiescence and stimulate Pax7 expression (Abou-Khalil et al., 2009).

Chiristov *et al* showed that in co-culture, endothelial cells promote myoblast proliferation by secreting growth factors, such as insulin-like growth factor 1 (IGF-I), hepatocyte growth factor (HGF), fibroblast growth factor (FGF), platelet-derived growth factor-BB (PDGF-BB), and VEGF (Chiristov et al., 2007). MuSCs are functionally and molecularly heterogeneous (Chakkalakal et al., 2012; Kuang et al., 2007; Rocheteau et al., 2012; Sacco et al., 2008). They also found that periendothelial cells (smooth muscle cells and endomysial fibroblasts) promote reserve stem cells, stem cells that escape differentiation, to return to the quiescent state (Chiristov et al., 2007). MuSCs are in close proximity to endothelial cells and exhibit a dynamic interplay with them, as demonstrated *in vivo* (Verma et al., 2018). Verma *et al.* revealed that MuSCs secrete Vascular Endothelial Growth Factor (VEGF), a potent pro-angiogenic factor, which plays a crucial role in

the recruitment of endothelial cells in the vicinity of MuSCs (Verma et al., 2018). This recruitment of endothelial cells in the vicinity of MuSCs is necessary for the maintenance of the quiescent state of MuSCs through the interaction between endothelial-derived DLL4 and the NOTCH receptor on MuSCs (Verma et al., 2018).

The diverse constituents of the MuSC (muscle stem cell) niche underscore the intricate interplay of niche factors essential for the preservation and specification of MuSC destiny. Such findings promote the concept of manipulating MuSC niche regulation as a potential therapeutic strategy for managing muscular disorders.

iii. Nuclear positioning and microtubule dynamics

During myogenic differentiation, the maturation of the myofiber produced through the fusion of precursor cells, involves the movement of nuclei to the periphery of myofiber. The process of nuclear migration involves five separate events: centration, alignment, spreading, peripheral movement and anchoring (Cadot et al., 2015) (Fig. c). As these multinucleated myofibers form from the fusion of mononucleated myoblasts, the myonuclei first arrange themselves in the center (centration) of the cytoplasm parallel with the long axis of the cell (Cadot et al., 2012). Once centered, these nuclei align (alignment) on a central axis (Espigat-Georger et al., 2016) and space themselves out along the length of the cell as it elongates into a fiber (spreading) (Metzger et al., 2012; Wilson & Holzbaur, 2015). As the fibers mature post-fusion, the myonuclei then migrate towards the plasma membrane (peripheral migration), where they assume their final position. Peripheral migration is also characterized by the development of a dense myofibril network throughout the cell. Roman *et al.*, showed that myofibril crosslinking and contraction actively move nuclei toward the periphery of the skeletal muscle fibers (Roman et al., 2017). They also reported that nuclear movement is coordinated with the development of a dense

myofibril network, which provides the necessary force to propel nuclei to the periphery (Roman et al., 2017). Roman *et al.*, suggest that the coupling between myofibril contraction and nuclear movement is essential for maintaining the structural integrity of the muscle fiber (Roman et al., 2017). Following peripheral migration, nuclei become anchored (anchoring) beneath the plasma membrane (Roman & Gomes, 2018). The positioning of nuclei at the periphery of the myofiber is believed to be important as it allows for more efficient distribution of nuclei along the length of the myofiber, which is important for proper muscle function and governance (myonuclear domain) and more efficient communication between the nucleus and the rest of the cell (Cadot et al., 2015). Interestingly, while nuclei are for the most part evenly spaced along a myofiber, clusters of nuclei are present at neuromuscular (NMJ) or myotendinous (MTJ) junctions. Mispositioned nuclei were first observed in a shared group of laminopathies called Central Nuclear Myopathies (CNM).

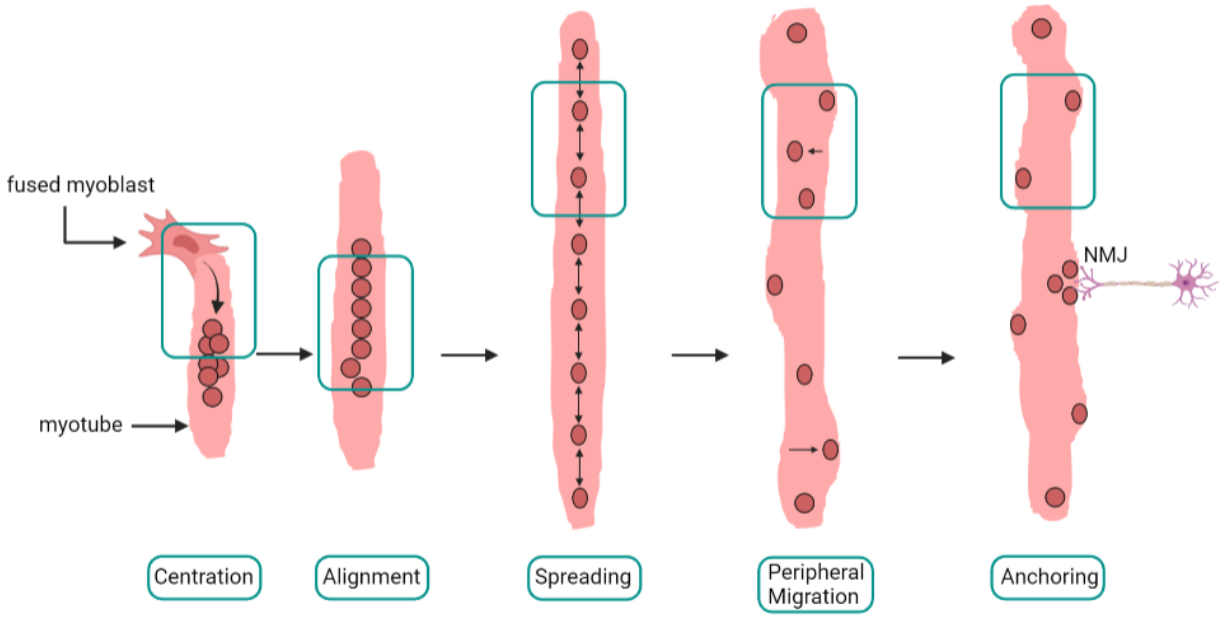

Figure c: Nuclear movements during myoblast fusion.
A diagrammatic representation of myoblast fusion. A process that occurs during muscle development and repair, where individual myoblasts merge to form multinucleated myotubes. The five steps involved during

nuclear movements include: 1. Centration: migration of myonuclei from fused myoblasts to the center of the newly formed cell. 2. Alignment: the arrangement of these nuclei along the central longitudinal axis. 3. Spreading: the longitudinal movement of these cells as the myotube elongates into a fiber. 4. Peripheral migration: migration of these nuclei from a central position to the cell periphery right below the plasma membrane. And finally in the 5th and last movement termed Anchoring, in which these nuclei become secured under the plasma membrane. Adapted from: Nuclear positioning in skeletal muscle by Roman W., Gomes E (2018). Semin Cell Dev Biol. 82:51-56. doi: 10.1016/j.semcdb.2017.11.005. Created with BioRender.com

Nuclear mispositioning results in hindered muscle contraction and is a characteristic of many muscle disorders (e.g., CNM, DMD among others). In muscular dystrophy, the nucleus can become mispositioned due to defects in the connections between the cytoskeleton and the nucleus, leading to muscle weakness and wasting.

Most of the nuclear movements during skeletal myogenesis are microtubule (MT) dependent. Microtubules (MTs) are highly dynamic polymeric cytoskeletal filaments that are required for diverse cellular processes, such as cell division, motility, and determination of cell shape. The α- and β-tubulin dimers form both stable and dynamic networks originating primarily from two major Microtubule Organizing Centres (MTOCs), the centrosome and the Golgi complex; although the Akhmanova & Steinmetz group also found these tubulin dimers on the spindle pole, cell nucleus and cell cortex (Akhmanova & Steinmetz, 2019). New MTs are nucleated at MTOCs by ɤ-tubulin and the ɤ-tubulin ring complex (ɤ-TuRC), which caps the MT (-) end by binding to the exposed β -tubulin subunits that are only exposed at distal MT (-) ends (Kollman et al., 2011). The ɤ-TuRC serves as a template for MT assembly and tethers and protects the vulnerable (-) end of the MT at the MTOC, which if exposed would undergo rapid depolymerization. Pericentrin (PCNT), is an integral component of the pericentriolar matrix (PCM), a centrosome scaffold that interacts with MT nucleation component ɤ-tubulin and anchors the ɤ-TuRC complex to the centrosome (M. Chen et al., 1996) (Fig. d).

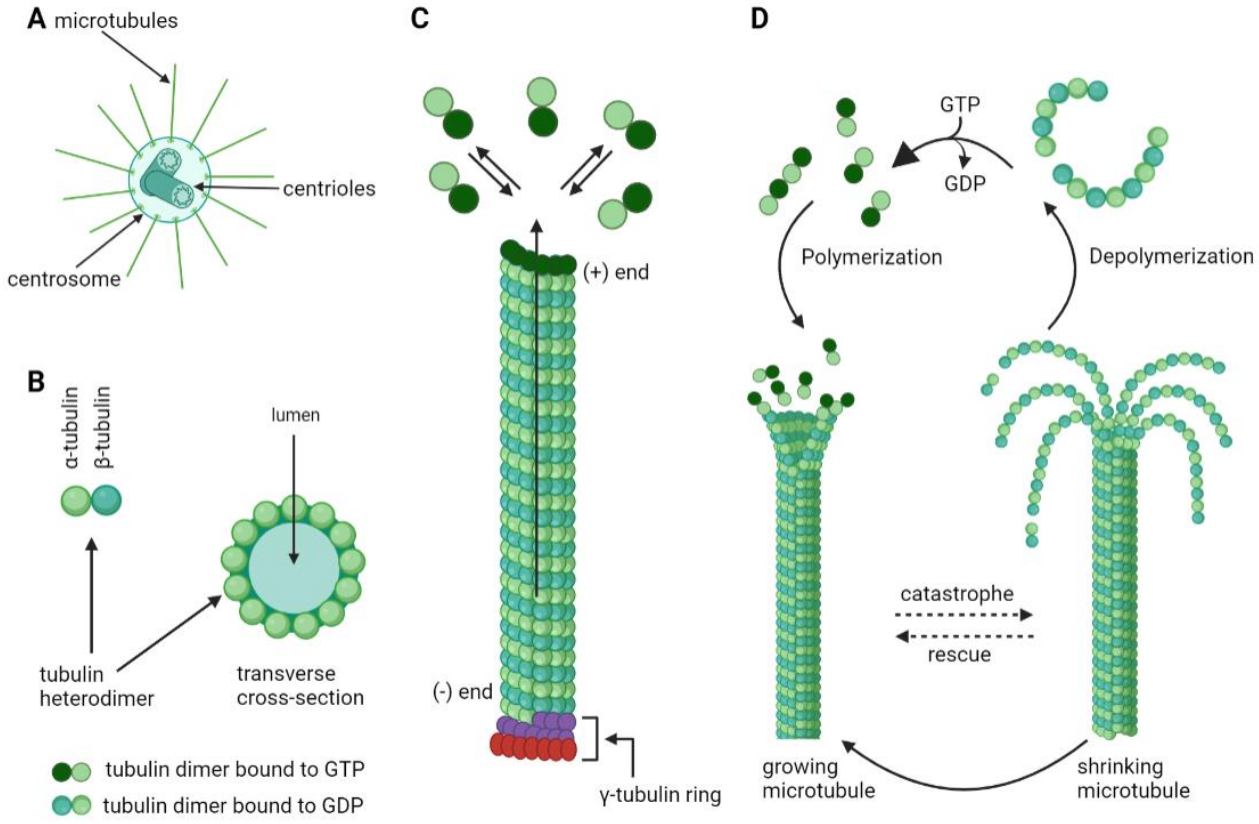

Figure d: Microtubule formation, structure, and dynamics.
(A) Centrosomes are one of the main microtubule-organizing centers (MTOCs) in eukaryotic cells along with Golgi elements. Each centrosome consists of a pair of centrioles surrounded by a matrix of proteins. MTOCs are involved in the organization of microtubules. **(B)** Microtubules (MTs) are highly dynamic polymers formed of α and β tubulin heterodimer subunits assembled into linear protofilaments. A single microtubule contains ~13 protofilaments that loop together to form a 24 nm wide hollow cylinder consisting of an inner space (lumen). **(C)** The αβ-heterodimers are added to the exposed MT (+) end, in a manner dependent on the concentration of tubulin subunits. The ϒ-tubulin ring complex (ϒ-TuRC) functions as a structural framework (tether) for microtubule assembly, while simultaneously anchoring the unstable (-) end of the MT at the MTOC which undergoes rapid depolymerization upon exposure. **(D)** Microtubule dynamics refers to the constant turnover of microtubules within the cell. This process involves the addition of new tubulin dimers to the plus (+) end of the microtubule (polymerization), and the removal of dimers from the minus (-) end (depolymerization). This combination of growth, shrinkage, and rapid transitions between the two is known as dynamic instability. A cap of GTP–tubulin at the plus (+) end of GDP–tubulin-containing microtubules is thought to stabilize the growth phase. The rate of turnover is regulated by several proteins, including microtubule-associated proteins (MAPs) and motor proteins. Adapted from: Growth, fluctuation and switching at microtubule plus ends by Howard, J., Hyman, A (2009). Nat Rev Mol Cell Biol 10, 569–574. doi.org/10.1038/nrm2713. Created with BioRender.com

MTs are firm structures that form by the dimerization of α- and β-tubulin that align in an apical-basal manner to form protofilaments, which associate with each other to form a hollow tube (Nicholas Dias, Yung Peng, 2017). These polarized tubes have a fast growing plus (+) end; where α-tubulin is exposed and is responsible for dynamic interactions, and a slow growing (-) end; where β-tubulin is present and are more stably anchored to its original nucleated sites (Desai & Mitchison, 1997; Nogales & Wang, 2006). The αβ-heterodimers are thus added to the exposed MT (+) end, in a manner dependent on the concentration of tubulin subunits and regulated by the (+) tip binding proteins such as end-binding protein 1 (EB1) and XMAP215 (Akhmanova & Steinmetz, 2019; Brouhard & Rice, 2018). In a population of microtubules, at any given point in time, some microtubules are rapidly growing while others are quickly shrinking (although sometimes microtubules also sit still in a 'paused' state). This combination of growth, shrinkage, and rapid transitions between the two is known as dynamic instability. When MTs shrink rapidly, the event is known as a "catastrophe" and occasionally, a rapidly shrinking MT is "rescued", switching from shrinkage back to growth. Catastrophe is promoted by the interaction with destabilizing proteins such as katanin (Goodson & Jonasson, 2018). MT stability, on the other hand, is associated with post-translational modifications of tubulin subunits and is promoted by microtubule-binding proteins (MAP1b, tau) (Wloga et al., 2017). MTs serve as scaffolds for organelle and other intracellular vesicle transport, along with the help of microtubule-associated proteins (MAPs), by exerting a pull and push force on these structures.

iv. Microtubule networks during muscle development

During early differentiation of myoblasts, the radial MT array found in proliferating undifferentiated cells is replaced by MTs parallel to the long axis of the cell, which contribute to the elongated cell shape (Zaal et al., 2011). The Golgi apparatus can interact with microtubules via

various microtubule-binding proteins, such as CLASP and AKAP450 (P. M. Miller et al., 2009). During myoblast fusion and fiber maturation, the Golgi complex is re-distributed both to the nuclear envelope (NE) and into small Golgi elements that localize below the plasma membrane, clustered at neuromuscular junctions, where they recruit myonuclei (Oddoux et al., 2013b). Pericentriolar proteins (such as Pericentrin and Cep135) are recruited to the NE by Nesprin1α, a LINC (Linker of Nucleoskeleton and Cytoskeleton) complex component (Espigat-Georger et al., 2016). The LINC complex is used as an anchor to complete the transport of these centrosomal proteins from the centrosome to the NE. The static, peripherally-located plasma membrane Golgi element MTOCs nucleate a regularly spaced MT network under the sarcolemma that is made up of single and bundled MTs (which are both stable and dynamic) and interact with dystrophin at the membrane and connect to the contractile proteins in the core of the fiber to form a unique orthogonal grid in myofibers during maturation (Oddoux et al., 2013a, 2019).

During myoblast fusion, the myoblast nucleus migrates to the center of the newly formed cell, where it aggregates with the already centered myonuclei (Cadot et al., 2015). These already centrated nuclei pull the MTs of the incoming myoblast towards the center of the myotube. The myoblast nucleus in turn may also pull on MTs from previously centered nuclei to reach the center of the cell. This mechanism of clustering of nuclei at the center of the cell is MT and dynein (MT-dependent motor protein) dependent. In mammals, centration is regulated by Cdc42 and the PAR polarity complex proteins PAR6 and PAR3. PAR6 and PAR3 form a complex that recruits the dynein/dynactin complex to the NE in muscle cells. Knockdown studies in myotubes have shown that Nesprin1α and Pericentriolar Material 1 (PCM-1) are important in the alignment of nuclei, the step following centration. Nesprin1α and PCM-1 are required for the recruitment of centrosomal

and microtubule motor proteins (such as dynein and kinesin, another MT-dependent motor protein) required for centration.

Peripheral migration of myonuclei is intermediate filament (desmin/actin) dependent (Cadot et al., 2015), and desmins have been implicated in nuclear anchoring (Capetanaki et al., 1997). Since myotubes *in vitro* never fully mature to the extent of nuclear anchoring, studies of this step are limited. Further, in mice after regeneration, the process of nuclear anchoring is extremely slow and is rarely observed in mouse models used to study degeneration.

Anchored myonuclei can be segregated into two groups: those that aggregate at myotendinous junctions (MTJs) and neuromuscular junctions (NMJs) (Carlsson et al., 1999; Razafsky & Hodzic, 2015) and these junctions are evenly distributed along the length of the myofiber (Falcone et al., 2014; Razafsky & Hodzic, 2015). Clustering of nuclei at both junctions have their own anchoring mechanisms and appear to have different functions as evidenced by unique gene expression profiles (Rossi et al., 2000). The NMJ and MTJ nuclei have been implicated in the monitoring of muscle excitation and stretching respectively, whereas the equally distributed nuclei may maintain the myonuclear domain in myofibers. Myonuclear domain theory postulates that each nucleus oversees the regulation of a certain volume of myofiber cytoplasm (Bothe & Baylies, 2016; Gundersen & Bruusgaard, 2008).

v. Duchenne Muscular Dystrophy

Muscular dystrophies (MD) are genetic disorders that cause progressive degeneration of the skeletal muscle (Emery, 2002). Most common are the dystrophinopathies, which as the name suggests, are caused by mutations in the gene for dystrophin (*Dmd*) (Emery, 2002) of which Duchenne Muscular Dystrophy (DMD) is the most common, affecting approximately 1 in 3500 male births (Hoffman et al., 1987). Characterized by progressive skeletal muscle wasting, loss of

ambulation and scoliosis, the average life expectancy of a DMD patient is 26 years; however, with excellent care, some individuals live into their third or fourth decade of life. Most patients, however, are wheelchair-bound by adolescence. Respiratory failure, resulting from the weakening of the diaphragm muscle, reduces lifespan unless mechanical support is introduced. In DMD and other forms of muscular dystrophy, the heart muscles are also affected resulting in cardiac complications such as heart failure and irregular cardiac rhythm.

In DMD, muscle function is directly correlated with the extent of muscle pathology. DMD fetal muscle shows very little evidence of disease pathology, despite the loss of dystrophin at the myofiber plasma membrane (Nevo et al., 1999). However, soon after birth and before the onset of clinical symptoms, multiple components of the innate immune system get activated, including altered signaling via Toll-like receptors (TLR4, TLR7), nuclear factor κB (NF-κB) activation, and expression of major histocompatibility complex (MHC) class I molecules on muscle cells. A second pathological process, which is superimposed on the chronic inflammatory state includes successive cycles of degeneration and regeneration of myofibers leading to the depletion of the myogenic progenitor cell pool (Lu et al., 2014). Moreover, because dystrophin is also expressed in satellite cells, its loss results in altered polarity of the satellite cells and decreased asymmetric divisions (Dumont et al., 2015; Y. X. Wang et al., 2019). As a result of this, the DMD muscle becomes progressively unable to repair damaged muscle fibers, further contributing to wasting. Ultimately, with age, the interplay between chronic activation of the innate immunity and the cycles of degeneration followed by regeneration combine to produce a poorly orchestrated repair response that promotes disease progression (Rosenberg et al., 2015). As repair struggles to keep up with myofiber damage, DMD myofibers are gradually replaced by fat and fibrotic tissue, which

reduces the mechanical and physiological activity of skeletal muscle (Alvarez et al., 2002; Rahimov & Kunkel, 2013; Serrano & Muñoz-Cánoves, 2010).

The *mdx* mouse is a genetic model of Duchenne's Muscular Dystrophy, in which a single point mutation in the dystrophin gene produces a premature stop codon resulting in the production of a truncated, non-functional protein (Ryder-Cook et al., 1988; Sicinski et al., 1989). In *mdx* mice, extensive muscle damage and regeneration of the hindlimb muscles begins shortly after mice are weaned (3– 4 week of age) and by 8 weeks of age more than 50% of fibers have undergone a damage induced regeneration as quantified by the presence of centrally located nuclei (Ryder-Cook et al., 1988). However, unlike human patients, *mdx* mice recover from the wasting crisis, suggesting that the phenotype is milder in this model. Numerous other models have been developed to recapitulate the human disease trajectory with the goal of understanding the pathogenesis and developing new therapeutic avenues.

vi. Dystrophin and the Dystrophin-Glycoprotein Complex

The dystrophin gene is the largest known human gene, containing 79 exons and spanning > 2,200 kb, which is roughly 0.1% of the whole genome (Koenig et al., 1987). Dystrophin is expressed primarily in skeletal and cardiac muscles though small amounts of dystrophin are present in brain neurons, where its function is unclear (Gao & McNally, 2015). The dystrophin protein is comprised of four main functional domains: an actin-binding amino-terminal domain (ABD1), a central rod domain, a cysteine-rich domain, and a carboxyl-terminus. The rod domain consists of a unique collection of spectrin-like repeats which mediates the interaction with microtubules and spectrin repeats 20-23 are required for the organization of microtubule networks responsible for intracellular transport in skeletal muscle cells (Belanto et al., 2014; Prins et al., 2009). The altered microtubule network in *mdx* mouse skeletal muscle cells has been linked to

increased reactive oxygen species (ROS) signaling and increased flux of intracellular calcium, contributing to the pathophysiological phenotype observed in the *mdx* mice (Khairallah et al., 2012).

Dystrophin is an essential component of the dystrophin-glycoprotein complex (DGC) that spans the sarcolemma and serves as a framework to connect the cytoskeleton to the extracellular matrix. In healthy muscle fibers, dystrophin acts as an actin-binding protein that links the cytoskeleton via the α/β-dystroglycan complex to the extracellular matrix (ECM) protein laminin through the outer cell membrane (Holland et al., 2013). This transmembrane complex stabilizes the muscle membrane thereby preventing membrane rupture during continuous contraction-relaxation cycles, and supports muscle fiber integrity by reducing muscle stiffness, increasing sarcolemmal deformability, and helping to prevent muscle fiber injury (Holland et al., 2013; Matsumura et al., 1993). In dystrophinopathies, the mechanical stress of contraction can lead to muscle fiber degeneration and leakage, leading to a rise in intracellular Ca^{2+} levels (Kunkel et al., 1985; Moser, 1984). In DMD, the dystrophin deficiency causes a drastic reduction in dystrophin-associated glycoproteins, which renders muscle fibers more susceptible to injury and necrosis (Holland et al., 2013). Although injury can be repaired in wild-type muscle, muscle regeneration in DMD muscle produces regenerated fibers also lacking dystrophin that are destined to degeneration. Therefore, dystrophin plays a pivotal role in maintaining muscle cell structure and integrity of muscle fibers (Matsumura et al., 1993).

Dystrophin is an MT guide, and modifications of the MT network have been observed in the myofibers of the *mdx* mouse model (Oddoux et al., 2019). When compared to wild-type (WT) mice, *mdx* MTs are more disordered and denser, and these observations are corelated to the dystrophic pathology (Oddoux et al., 2019). Further, the Golgi elements are mispositioned and

increased in number and size. MTs in *mdx* fibers also grow more rapidly and in shorter bursts during the recovery period after being treated with Nocodazole (a MT depolymerizing agent) as compared to WT cells, with an overall denser and more disorganized network. These results show that muscle fibers lacking dystrophin are more fragile in part because the sarcolemmal connection to an organized MT network is disrupted (Oddoux et al., 2019).

vii. Glucocorticoids, its receptor, and mechanism of action

Currently, there is no known cure for muscular dystrophy, although significant headway is being made with exon-skipping technologies (Aartsma-Rus et al., 2004; Aoki et al., 2010; Bremmer-Bout et al., 2004; Qi et al., 2005), gene-replacement therapies (Bowles et al., 2012; Harper et al., 2002; Sakamoto et al., 2002), and cell-based therapies such as myoblast transplantation (Huard et al., 1992; Mouly et al., 2005; Partridge et al., 1978; Skuk et al., 2007), direct engraftment of satellite/stem cells (Collins et al., 2005; Jankowski et al., 2002; Webster & Blau, 1990), and allogenic delivery of muscle stem cells (MuSC) (Gussoni et al., 1999; Mu et al., 2011; Torrente et al., 2007). Currently, glucocorticoid treatment is recommended as a standard of care for DMD patients, improving muscle strength and function in the short term (12 months), and survival up to 3 years (McDonald et al., 2018a).

Glucocorticoids (GCs) are naturally occurring steroid hormones produced and released by the adrenal cortex in response to biological cues and stress such as fasting, exercise and disease (W. L. Miller & Auchus, 2011) to regulate protein and glucose metabolism, development, immune function, skeletal growth, reproduction, cognition and cardiovascular function (Rhen & Cidlowski, 2005). Synthetic glucocorticoids (GCs) such as prednisone, are also commonly used therapeutically as powerful anti-inflammatory and immunosuppressive agents (Ramamoorthy & Cidlowski, 2016). In 2020, ~20 million total prescriptions for prednisone, one of many synthetic

glucocorticoids, were given to ~9 million patients in North America alone, out of which ~3 million patients are chronic users (https://clincalc.com/DrugStats/Drugs/Prednisone). Despite their therapeutic potential, chronic use of GCs also have serious side effects including muscle wasting, which affects up to 60% of patients (Surmachevska, N. & Tiwari, V).

GCs can stimulate dystrophin expression in normal human myoblasts (Sklar & Brown, 1991) and can induce the expression of utrophin in long-term GC-treated DMD myotubes (Pasquini et al., 1995). As long-term GC treatment results in side effects including obesity and osteoporosis, steroid dosing also plays an important role in GC action, with a single weekly dose of prednisone improving sarcolemmal repair via increased expression of annexin A1 and A6 with fewer side effects as compared to daily dosing (Quattrocelli et al., 2017a). Interestingly, sex-based differences in muscle response to GCs has been noted, such that distinct pathways are stimulated in male and female mice following GC treatment that results in improved force in both (Salamone et al., 2022). The exact mechanisms by which GCs cause short-term ergogenic effects and detrimental long-term effects as well as their target cells in muscle, are still unknown.

High circulating GCs result in a decrease in skeletal muscle protein anabolism and an increase in protein catabolism to generate elevated levels of free amino acids, which can serve as substrates for gluconeogenesis by the liver to help the body maintain blood glucose levels (glucose homeostasis) (Kuo et al., 2013). Therefore, sudden increases in glucocorticoids are beneficial in that they maintain circulating glucose levels to support vital brain function under stressful conditions. However, when circulating glucocorticoid levels are elevated for a prolonged duration due to a pathological condition (Cushing's syndrome, cancer cachexia or sepsis) or as a part of a medical treatment (drug given to treat inflammation) the effects on skeletal muscle are detrimental,

resulting in loss of mass and weakness (GC-induced muscle atrophy) as well as insulin resistance (Bodine & Furlow, 2015).

The physiological and pharmacological functions of glucocorticoids are carried out by the intracellular glucocorticoid receptor (GR, encoded by the *Nr3c1* gene), which is a member of the nuclear hormone receptor family of ligand-activated transcription factors. The GR is a modular protein comprising of three functional domains: an N-terminal transactivation domain (NTD) which is the least conserved and thus most variable domain, a central DNA binding domain (DBD) which is the most conserved domain among family members and binds target DNA sequences called glucocorticoid response elements (GREs), and lastly a C-terminal ligand-binding domain (LBD) (Kumar & Thompson, 2005). When GCs are not present, the GR is primarily located in the cytoplasm of nucleated cells as part of a larger multi-protein complex that includes chaperone proteins such as hsp90, hsp70, and p23 and immunophilins (FKBP51 and FKBP52) (Grad & Picard, 2007; Pratt & Toft, 1997). Upon ligand binding, the GR undergoes a conformational change (Moras & Gronemeyer, 1998), which results in the dissociation of the heat shock proteins, and reveals a nuclear localization signal, allowing for rapid translocation of the receptor into the nucleus (Giouchon-Mantel et al., 1992). Once inside the nucleus, GR binds directly to GREs and can act as an activator or repressor of transcription in a ligand dependent manner. While binding to specific response elements in the promoter and enhancer regions of many steroid responsive genes (dependent on direct DNA binding) has for a long time been considered as the major mode of GC action, an increasing number of alternative transcriptional control mechanisms have been identified. Indeed, while deletion of the GR leads to perinatal death (Cole et al., 1995), mice carrying a point mutation known to impair dimerization and DNA binding of the glucocorticoid receptor are viable, highlighting alternative mechanisms of action including crosstalk with other

transcription factors through protein-protein interactions (independent of direct DNA binding) (Reichardt & Schütz, 1998). For example, GR can inhibit the activity of AP-1 (Reichardt & Schütz, 1998) and NF-kB (Heck et al., 1997) and can enhance the action of CCAAT/Enhancer Binding Protein β (C/EBPβ) (Wiper-Bergeron et al., 2003, 2007).

viii. Glucocorticoid action in muscle

Duchenne Muscular Dystrophy is primarily treated with glucocorticoid therapy as the first-line of treatment. This treatment can lead to improved muscle strength for the first 6 months and delay the loss of muscle function for approximately 3 years (McDonald et al., 2018b). Longer GC treatment (more than 1 year) increases patient survival (McDonald et al., 2018b). The use of GCs as the primary treatment for DMD seems counterintuitive given that skeletal muscle wasting is a feature of both pharmacological GC treatment and conditions where endogenous cortisol levels are elevated (for example: Cushing's syndrome, sepsis, starvation, and cancer cachexia). Indeed, while GCs can promote proteolysis (breakdown), this appears to be largely reserved to the fasting state (Khairallah et al., 2012; Prins et al., 2009). In fed animals, only very high doses of GCs can promote muscle protein catabolism (Kerr et al., 2015). GCs have also been implicated in the expression of the atrogenes MuRF-1 and MAFbx/atrogin-1, although treatment of C57BL/6 mice for up to 2 weeks with the synthetic GC dexamethasone (DEX) failed to increase proteasome activity (Baehr et al., 2011), suggesting that the effects of glucocorticoids on muscle catabolism appear to be dependent on the nutritional status of the animal (Britto et al., 2014).

Developmentally, the role of the glucocorticoid receptor (GR) in muscle has been studied from embryonic to adult myogenesis. Whole-body GR-knockout (KO) mice die within hours of birth due to respiratory failure (Cole et al., 1995) and demonstrate underdeveloped lungs, reduced liver capacity (blood volume) and enlarged adrenal glands due to cortical hypertrophy (Cole et al.,

1995). A muscle fiber-specific conditional knockout of the glucocorticoid receptor has also been shown to protect mice from diabetes-induced muscle wasting (Hu et al., 2009) but not denervation-induced atrophy (Watson et al., 2012; Zhao et al., 2009). To identify genomic targets of glucocorticoids in C2C12 myotubes, Kuo *et al* performed ChIP-seq and microarray, identifying 173 direct target genes, of which 8 were known to be involved in the regulation of insulin signaling (Kuo et al., 2012). Myofiber-specific knockout of the GR revealed that GR and MYOD1 interact with the promoters of genes via the CpG-bound transcription factor *Nrf1* to activate gene expression of the skeletal muscle program (Rovito et al., 2021). Further, GR negatively controls the hypertrophy (muscle mass) and striated muscle contraction (muscle strength) in mice, by downregulating anabolic pathways (Rovito et al., 2021). Despite a role for GR in the myofiber, there has been no MuSC-specific knockout of the GR described.

ix. Rationale and Hypothesis

While glucocorticoid treatment has been shown to stimulate utrophin expression and promote membrane resealing in the context of DMD, the effect of GCs on the MuSC population has not been described. The objective of this project was to define the role of glucocorticoid signaling mediated by the glucocorticoid receptor in the MuSC population both in culture and *in vivo*. To this end, I developed a conditional genetic deletion (knockout) mouse in which GR is knocked out in MuSCs and investigated the phenotype of both uninjured and injured muscle in young and older mice as well as the in-culture differentiation of primary myoblasts derived from this model. I hypothesized that the glucocorticoid receptor is necessary for MuSC homeostasis and for myotube cytoskeletal organization.

The specific aims of this study were**:** (1) to assess the impact of the GR on muscle satellite cell function during repair and regeneration, (2) to identify GR gene targets that regulate quiescence in MuSCs, and (3) identify the gene targets that regulate microtubule assembly, dynamics, and organization in myotubes.

MATERIALS AND METHODS

i. Generation of GR conditional knockout mice and animal care

Nr3c1$^{fl/fl}$ floxed mice (Mittelstadt et al., 2012) (B6.Cg-*Nr3c1*$^{tm1.1Jda/J}$, The Jackson laboratory, stock # 021021) were crossed with *Pax7*^{CreER} mice (B6.Cg-*Pax7*$^{tm1(cre/ERT2)Gaka}$/J, The Jackson laboratory, stock #017763) (Murphy et al., 2011a) to produce *Nr3c1*$^{+/fl}$*Pax7*$^{creER/+}$ and *Nr3c1*$^{+/fl}$*Pax7*$^{+/+}$ progeny. The *Nr3c1*$^{+/fl}$*Pax7*$^{CreER/+}$ male studs were then crossed with *Nr3c1*$^{fl/fl}$*Pax7*$^{+/+}$ females to produce WT (*Nr3c1*$^{fl/fl}$*Pax7*$^{+/+}$) and GR$^{MuSC-/-}$ (*Nr3c1*$^{fl/fl}$*Pax7*$^{CreER/+}$) pups at Mendelian ratios. Temporal control of the GR knockout was achieved via treatment with tamoxifen (Sigma Aldrich, T5648) through five daily intraperitoneal (i.p.) injections of pups (1.5-2 mg/20 g body weight) at 4-6 weeks of age. All animals were maintained at 22°C with 30% relative humidity on a 12 hr light/dark cycle and provided food and water *ad libitum*. All animal experimentation was approved by the University of Ottawa Animal Care Committee and conducted in accordance with the guidelines set out by the Canadian Council on Animal Care.

ii. Isolation and culture of primary myoblasts

Primary myoblasts were isolated as described in (Megeney et al., 1996). Briefly, hindlimb muscles from adult (aged 6-8 weeks) WT and *Nr3c1*$^{MuSC-/-}$ conditional knockout (GR$^{MuSC-/-}$) mice were dissected and digested with collagenase type II (2 mg/mL in DMEM: Worthington Biochemical, LS004176). The muscle slurry was then filtered (70 μm cell strainer) to remove undigested connective tissue and the filtered solution was successively washed with MACS Buffer and the pellet was incubated with anti-PE magnetic beads conjugated to negative sort (CD45, CD31, CD11b, and Sca1^{-}) and positive sort (Integrin α7+) surface markers to sequentially isolate muscle stem cells by magnetic labeling (Pasut et al., 2012). Cell suspension was eluted using the magnetic separator. Cells were washed with serum-free media and enriched for myoblasts by

selective plating (to get rid of contaminating fibroblasts) for 30-45 min. Primary myoblasts were grown on matrigel-coated plates in growth media (GM; Dulbecco's modified Eagle's medium [DMEM] containing 20% fetal bovine serum [FBS], 10% horse serum [HS]) supplemented with basic fibroblast growth factor (10 ng/ml) (Peprotech, cat# 100-18B-50UG) and hepatocyte growth factor (2 ng/ml) (Peprotech, cat# 100-39-10UG). *In vitro* excision of *Nr3c1* exon 3 was achieved by treating primary myoblasts with 4-OH-tamoxifen (Sigma Aldrich, H7904). Dexamethasone (DEX) was used at concentrations of 10 nM, 100 nM, or 1 μM with DMSO (100%) as the vehicle control. For differentiation assays, primary myoblasts were induced to differentiate (DM; DMEM containing 2% FBS, 10% HS) in the presence or absence of DEX for 2 days.

iii. Cardiotoxin injury and analysis of muscle histology

Seven-week-old mice were anesthetized with isofluorane, and 30 μL of 10 μM CTX (Latoxan, France) in PBS was injected intramuscularly into the left Tibialis anterior (TA) muscle, the right TA was left uninjured. Mice were sacrificed by cervical dislocation, 7- 28- and 42-days post injury, and the dissected muscles were flash frozen using Optimal Cutting Temperature compound (OCT) dipped in isopentane cooled by liquid nitrogen. Eight μm-thick sections of TA muscle were fixed on charged slides using the HM525NX cryostat and stained with hematoxylin & eosin following fixation in 4% paraformaldehyde (PFA) for 15 min (Louise Pelletier Histology Core Facility, University of Ottawa). Images were acquired on the EVOS FLAuto2 (Cell Biology & Image Acquisition Core Facility, University of Ottawa). A minimum of 500 fibers were counted for analysis of the average fiber cross-sectional area and Feret diameter using FIJI (Fiji Is Just ImageJ) for quantification.

iv. Analysis of cell morphology and nuclear defects

The differentiation (% of nuclei in myosin heavy chain (MyHC) positive cells) and fusion indices (average number of nuclei per MyHC+ myotube) were calculated on WT and $GR^{MuSC-/-}$ myoblasts that were differentiated for two days under low serum conditions (DM) using the cell counter plug-in on FIJI. To quantify cell shape, I used the circularity index on FIJI to threshold and calculate the circularity of the myotubes. Myotube length was calculated as the average length of myotubes divided by the number of nuclei within the myotube. To measure myotube branching following treatment with DEX, the FIJI line tool was used to measure the angle of the branches (less than 180°C) from the myotubes radially. Alignment and spreading defects were quantified in FIJI by counting the nuclei that deviate from the central longitudinal axis of WT and $GR^{MuSC-/-}$ myotubes. Spreading defects were similarly calculated by quantifying the internuclear distance between myonuclei in myotubes to measure the distance (length) between the two nuclei (in microns).

v. Immunofluorescence

Single EDL myofibers were fixed in 4% paraformaldehyde (PFA) in PBS and 1% glycine. Fibers were blocked in PBS containing 0.2% Triton X-100, 2% BSA, 5% normal donkey serum (Cedarlane, 017-000-121), and 1% azide. The TA muscle sections (cryopreserved at -80°C) were first dehydrated at 65°C on a heating block and then fixed in 4% paraformaldehyde (PFA). Membrane permeabilization was carried out using 0.5% Triton X-100 in PBS and blocked using 0.1% TritonX-100 in PBS with 5% normal donkey serum (Cedarlane, 017-000-121). Specifically, for PAX7 staining, antigen retrieval was performed in a citrate buffered solution (pH 6.0) at 92°C for 30 min prior to permeabilization. Next, the sections were blocked for 30-1hr, following primary antibody incubation at 4°C overnight. Primary myoblasts were fixed using PFA and permeabilized

in PBS containing 0.3% Triton X-100 and 10% normal donkey serum (Cedarlane, 017-000-121). Detection was performed according to standard procedures using the following primary antibodies: PAX7-c (DSHB), Glucocorticoid receptor (Cell Signalling, D6H2L), MF-20 (DSHB), Dystrophin (Abcam, ab15277), Laminin (Abcam, ab11575), Ki67 (Abcam, ab15580), BrdU (Shp pAb to Biotin) (Abcam, ab2284) and α-tubulin (Sigma Aldrich, T5168). Detection of immunoconjugates was achieved using, (1) biotinylated secondaries such as donkey anti-mouse IGG (H+L) Fab fragments (Jackson ImmunoResearch Laboratories, 715-066-150) with Cy3-streptavidin (Jackson ImmunoResearch Laboratories, 016-160-084), or Alexa Flour 488-Streptavidin (Jackson ImmunoResearch Laboratories, S11223) for biotinylated BrdU and (2) non-biotinylated secondary antibodies such as Dylight 488 donkey anti-rabbit (Jackson ImmunoResearch Laboratories, 016-540-084) and Cy3 anti-mouse (Jackson ImmunoResearch Laboratories, 715-166-150). Nuclei were counterstained with DAPI and mounted in vectashield antifade mounting medium (Vectorlabs, H-1000). Images were taken on the Zeiss AxioImager.M2 Microscope (Cell Biology & Image Acquisition Core Facility).

vi. *In vivo* BrdU labeling

6-week-old mice were intraperitoneally injected for 5 consecutive days with tamoxifen to excise the GR. Two weeks following the last injection, *Nr3c1*$^{fl/fl}$*; Pax7*$^{+/CreER}$ (GR$^{MuSC-/-}$) and *Nr3c1*$^{fl/fl}$*; Pax7*$^{+/+}$ (WT) female mice were intraperitoneally injected once with 100 mg/kg of body weight of BrdU for 24 hours. TA muscles and hindlimbs were collected a day later.

vii. Single EDL myofiber isolation

Myofibers were isolated from the Extensor digitorum longus (EDL) muscle as described previously (Pasut et al., 2013). EDLs were removed from 8-week-old B10 Scotty Snell WT and *mdx* mice or WT (*Nr3c1*$^{fl/fl}$*; Pax7*$^{+/+}$) and GR$^{MuSC-/-}$ (*Nr3c1*$^{fl/fl}$*; Pax7*$^{+/CreER}$) mice two weeks

following the last intraperitoneal injection. Isolated myofibers were cultured for 3 days in suspension media before immunostaining for the myogenic cell populations. Briefly, after careful dissection from tendon-to-tendon the EDLs were digested with collagenase type I (2 mg/mL in DMEM; Sigma-Aldrich C0130) until fibers begin to separate. Muscles were then transferred under a dissecting microscope to horse-serum-coated plates and myofibers were separated by trituration using heat-polished glass Pasteur pipettes. Fibers were washed 2-3 times (placed in the incubator for 10 min in between washes) until hypercontracted fibers had been removed. Healthy fibers were then treated with nocodazole (a MT depolymerization agent, at 4 ug/ml for 4 hr) or vehicle (100% ethanol) and allowed to recover for 4 hrs before fixing and immunostaining the microtubule (MT) network. In a concurrent experiment to determine if glucocorticoids influence MT networks in fibers, EDLs were treated with vehicle (100% ethanol) or 100 nM DEX and for 48 hours in DMEM supplemented with 15% FBS and 2% chick embryo extract at 37°C, 5% CO2, before being fixed and immunostained. Separately, to determine the role of GR on the myogenic cell populations the same procedure as mentioned above was also performed on 8-week-old WT and $GR^{MuSC-/-}$ mice to isolate single myofibers. Briefly, these mice were treated with (1.5- 2 mg/20 g body weight) i.p. tamoxifen for 5 consecutive days to excise the receptor from $GR^{MuSC-/-}$ mice leaving normal glucocorticoid receptor expression in WT controls. Two weeks following the last injection, EDL myofibers were isolated from both genotypes and fixed for immunostaining ~2h post dissociation.

viii. Western analysis

Total protein was collected from WT and $GR^{MuSC-/-}$ whole cell extracts by homogenization in IPH lysis buffer (1 M Tris–HCl pH 7.5, 5 M NaCl, 500 mM EDTA, 010% NP-40) supplemented with 100 mM PMSF and 100 mM DTT (Dithiothreitol, Sigma Aldrich). Cells were resuspended in lysis buffer on ice for 30 min using a shaker and then centrifuged at maximum speed for 10 min

at 4°C. Supernatant was collected and protein concentration was quantified via Bradford assay and normalized prior to loading. Extracts were boiled on a heating block with 3X Laemmli loading buffer for 5 min at 95°C prior to loading on 4-15% Mini-PROTEAN TGX gels (Bio-Rad, 4561086) in SDS-PAGE running buffer (29 mM Tris, 144 mM glycine, 1% SDS) at 150 V for 1 hour. Protein samples were resolved on an 12% SDS-polyacrylamide gel electrophoresis and after transfer to polyvinylidene fluoride membrane (Bio-Rad), probed with specific antibodies: anti-Glucocorticoid Receptor D6H2L (1:1000 dilution, Cell Signaling, New England BioLabs #12041), anti- PAX7c (1:500 dilution, Developmental Studies Hybridoma Bank, DSHB), anti-MyoD5.8A (1:200 dilution, SantaCruz, sc-32758) and anti- Cyclophilin B (1:1000 dilution, Abcam, ab16045) antibodies. Antibodies were diluted in 1X milk-PBS-T overnight at 4°C on a shaker. Following incubation, the membrane was washed 3 times for 5 minutes in 1X PBS-T buffer. Glucocorticoid receptor (GR), PAX7, MYOD and Cyclophilin B were visualized using horseradish peroxide (HRP)-conjugated anti- rabbit (for GR and Cyclophilin B) and anti- mouse (for PAX7 and MYOD) at a 1:5000 dilution, GE Healthcare, Little Chalfont, U.K., respectively. This was followed by a chemiluminescence reaction using Pierce ECL substrate and luminal solution (Fisher Scientific, Nepean, ON, Canada) and visualized with the ChemiDoc MP Imaging System and the Image Lab Software (Bio-Rad). Proteins were compared to the Precision Plus Standard protein ladder (Bio-Rad) for molecular weight.

ix. Fluorescence Activated cell Sorting (FACS)

To isolate muscle stem cells from fixed tissues the procedure developed by Machado *et al.* was used (Machado et al., 2017). Briefly, the hind limb muscles of WT ($Nr3c1^{fl/fl}$; $Pax7^{+/+}$) and $GR^{MuSC-/-}$ ($Nr3c1^{fl/fl}$; $Pax7^{+/CreER}$) were dissected from tendon-to-tendon, further chopped, and exposed immediately to ice-cold 0.5% paraformaldehyde (PFA). Additional mincing using

scissors for 10 min in 0.5% w/v PFA was performed and muscle tissue was fixed for 45 mins by gentle rotation at 4°C. After the residual PFA was removed with repeated PBS washes, the cell pellet was digested in a Ham's F-10 digestion solution with 2% w/v of collagenase B (Roche, cat#11088831001) and 0.8% w/v Dispase II (Roche, cat#4942078001) enzymes at 37°C with agitation for 1.5 hour using the gentleMACS™ Octo Dissociator with Heaters (Miltenyi Biotec GmbH, Germany, catalogue# 130-096-427). 0.2% w/v of Bovine serum albumin (BSA) was also added to the cocktail. Post-digestion the cell pellet was washed and filtered with FACS buffer containing 3 mM Ethylenediaminetetraacetic acid (EDTA) and 1X PBS, sequentially through a 100 um, 70 um and 40 um cell strainer. Fixed MuSCs from WT and $GR^{MuSC-/-}$ mice were purified by FACS via gating for Streptavidin BV421-positive muscle stem cells conjugated to the positive marker, (VCAM- α mCD106 receptor) present on these cells, using a 4-laser Sony SH-800 cell sorter.

Antibody Panel:

Table 1. Antibody panel used for cell sorting.

Selection	Antibody	Antibody conjugate	Catalogue number	Concentration
Negative	CD31	PE-Cy7	561410 (BD Biosciences)	0.2 mg/mL
	CD45	PE-Cy7	552848 (BD Bioscience)	0.2 mg/mL
	Sca1	PE	553108 (BD Bioscience)	0.2 mg/mL
Positive	VCAM (a-Mcd106)		31-0057-05 (AbLab)	1.0 mg/mL
		Streptavidin BV421	563259 (BD Bioscience)	0.1 mg/mL

x. RNA-seq analysis

The RNA from sorted cells was isolated using the RecoverAll™ Total Nucleic Acid Isolation Kit for formalin-fixed parafilm embedded (FFPE) samples (Invitrogen, cat#AM1975). The RNA isolated from samples was sent to Donnelly Sequencing Center at the University of Toronto for library preparation and consecutive PCR amplification and sequencing. Briefly, total RNA was quantified using Qubit RNA HS (cat # Q32855, Thermo Fisher Scientific Inc., Waltham, USA) fluorescent chemistry and 1 ng was used to obtain the DV200 metric (percentage of RNA fragments > 200 nucleotides) using the Bioanalyzer RNA 6000 Pico kit (cat # 5067-1513, Agilent Technologies Inc., Santa Clara, USA). Lowest DV200 score was 28.6; median DV200 was 42.2. At the Donnelly Sequencing Center, 10 ng per sample of RNA was processed using the SMARTer Stranded Total RNA-Seq® v3 - Pico Input Mammalian Stranded Kit (cat # 634485; Takara Holdings Inc., Kyoto, Japan). This process leaves the library fragments originating from non-rRNA molecules untouched, with priming sites available on both 5' and 3' ends for further PCR amplification which was set to 14 cycles. 1 uL top stock of each purified final library was run on an Agilent Bioanalyzer dsDNA High Sensitivity chip (cat # 5067-4626, Agilent Technologies Inc., Santa Clara, USA). The libraries were quantified using the Qubit dsDNA HS (cat # Q32854, Thermo Fisher Scientific Inc., Waltham, USA) and were pooled at equimolar ratios after size-adjustment. The final pool was run on an Agilent Bioanalyzer dsDNA High Sensitivity chip and quantified using NEB Next Library Quant Kit for Illumina (cat # E7630L, New England Biolabs, Ipswich, USA). The quantified pool was hybridized at a final concentration of 460 pM and sequenced paired end on the Illumina NovaSeq 6000 platform using a S1 flow cell at 150 bp read lengths.

FASTQ files from RNA-seq were processed using a standard pipeline. Briefly, reads were processed first with UMI-tools (v. 1.1.2) (Smith et al., 2017), to extract unique molecular

identifiers (UMIs). Then fastp (v. 0.20.1) (S. Chen et al., 2018) was used to trim adapters and low-quality sections. Reads were aligned to the mouse genome (mm10 assembly) using STAR (v. 2.7.8a) (Dobin et al., 2013) and an index was created using a gene model GTF file (Mus_musculus.GRCm38.102.gtf, from ENSEMBL). UMI information was used to remove reads marked as duplicates. Reads overlapping exons were counted using Subread featureCounts (v. 2.0.1) (Liao et al., 2014) and counts were summarized over genes. Read counts were analyzed in R/Bioconductor using edgeR (Robinson et al., 2010), employing the TMM method to adjust library sizes. Genes with transcript shorter than 300 nucleotides or with expression less than three-fold from the median in at least 2 samples were removed from the analysis. Unwanted variation from the count table was removed using RUVseq (Risso et al., 2014): empirical tests using the RUVr, RUVs and RUVg algorithms and different values of k showed good performance with all methods; RUVs with k=2 was chosen. Contrasts tested the difference between genotype in one sex, or the difference between sexes in one genotype. Gene annotation term over-representation (GO) analyses and gene set enrichment (GSEA) analyses were performed in R/Bioconductor using the clusterProfiler (Wu et al., 2021) package. Volcano plots were generated using EnhancedVolcano (Blighe K, Rana S, 2022) and heatmaps using ComplexHeatmaps (Gu et al., 2016).

xi. Analysis and Statistics

All analysis was performed using a blinded design. Statistical differences between two means were calculated using the two-tailed paired Student's t-test for a minimum of three biological repeats. For multiple means, one-way or two-way ANOVA was conducted. If significant differences were identified, multiple comparison analysis was performed using a Tukey's post hoc test. P-values of less than 0.05 were considered significant, *$p<0.05$, **$p<0.01$, ***$p<0.001$. GraphPad Prism 9.4.1 was used for statistical analysis and graphical representation.

xii. Figure preparation

Photomicrographs from the results section were processed using FIJI (FIJI Is Just ImageJ) and the figures were assembled in Adobe Illustrator CS5.1™. Figures from the introduction were created using Biorender (BioRender.com).

RESULTS

Chapter 1: GR is required for efficient skeletal muscle regeneration.

To study GR action during myogenesis, I generated a temporally controlled conditional knockout of the GR in MuSCs ($GR^{MuSC-/-}$). The floxed *Nr3c1* mouse ($GR^{fl/fl}$) (Jackson Labs, B6. Cg-*Nr3c1*$^{tm1.1}$Jda/J) has loxP sites that flank exon 3 of the nuclear receptor subfamily 3, group C, member 1 (*Nr3c1*) gene (Mittelstadt et al., 2012). Deletion of exon 3 by Cre recombinase abolishes GR protein expression (Mittelstadt et al., 2012). To generate a *Nr3c1* knockout in MuSCs, the $GR^{fl/fl}$ mouse was crossed with the *Pax7*^{CreER} mouse (Murphy et al., 2011a), resulting in *Nr3c1*$^{fl/fl}$; *Pax7*$^{+/CreER}$ ($GR^{MuSC-/-}$, homozygous for the *Nr3c1* floxed allele) and *Nr3c1*$^{fl/fl}$; *Pax7*$^{+/+}$ ($GR^{fl/fl}$, or "WT" controls, homozygous for the *Nr3c1* wild-type allele) offspring. The *Pax7*^{CreER} allele expresses a tamoxifen inducible Cre recombinase under the control of the *Pax7* promoter and does not affect *Pax7* expression (Murphy et al., 2011a). This mouse model allows the study of adult skeletal myogenesis and the function of MuSCs in the absence of the GR, by loss of function analysis.

To evaluate GR expression during muscle injury and differentiation, I used the Single-Cell Muscle Project (scMuscle) transcriptomic database which aims to collect, analyze, and provide skeletal muscle transcriptomic data (McKellar et al., 2021) to measure *Nr3c1 (GR)* RNA expression up to 21 days following acute muscle injury and in quiescent muscle stem cells. In MuSCs, GR expression increased at 0.5 h post injury but was rapidly and drastically downregulated by day 1 until day 3 post-injury (Fig. 1 A). GR expression gradually increased from day 3 until the end of 3 weeks, culminating in a 1.5-fold increase at day 21, suggesting that at this time point, the MuSC population has not returned to the baseline GR mRNA expression found in uninjured muscle MuSCs (Fig. 1 A). In muscle progenitor cells (myoblasts), *Nr3c1 (GR)*

expression gradually increased from day 3 to its highest expression at day 10, with low or no expression throughout the rest of the time-course (Fig. 1 B). In myonuclei, *Nr3c1 (GR)* expression was only observed at day 10 and 21 post-injury for type IIb fibers (Fig. 1 C) and on day 21 in the type IIx myonuclei (Fig. 1 D). To explore GR protein expression during myogenic differentiation, I performed a differentiation assay on primary myoblasts isolated from WT mice. Following culture expansion for 48 hours in growth media (GM), primary myoblasts were induced to differentiate (differentiation media, DM) for another 48 hours. Cells were collected, and GR protein expression was assessed via western blot at 24- and 48- hours in GM and after 6, 12, 24 and 48 hours in DM (Fig. 1 E). Membranes were probed for GR, myosin heavy chain (MyHC) and cyclophilin B (CYPB, loading control). The protein expression of GR significantly decreased at 6 hours in DM and remained low until 24 hours of differentiation (Fig. 1 E, F). MyHC expression was observed at 48 hours into differentiation (Fig. 1 E, G). The changes in GR protein expression observed in primary myoblast cultures (Fig. 1 E, F) correlate with our observations in MuSCs and myoblasts/progenitors populations from the scMuscle database (Fig. 1 A, B). These data taken together suggest that differentiating myoblasts have reduced glucocorticoid sensitivity during early differentiation.

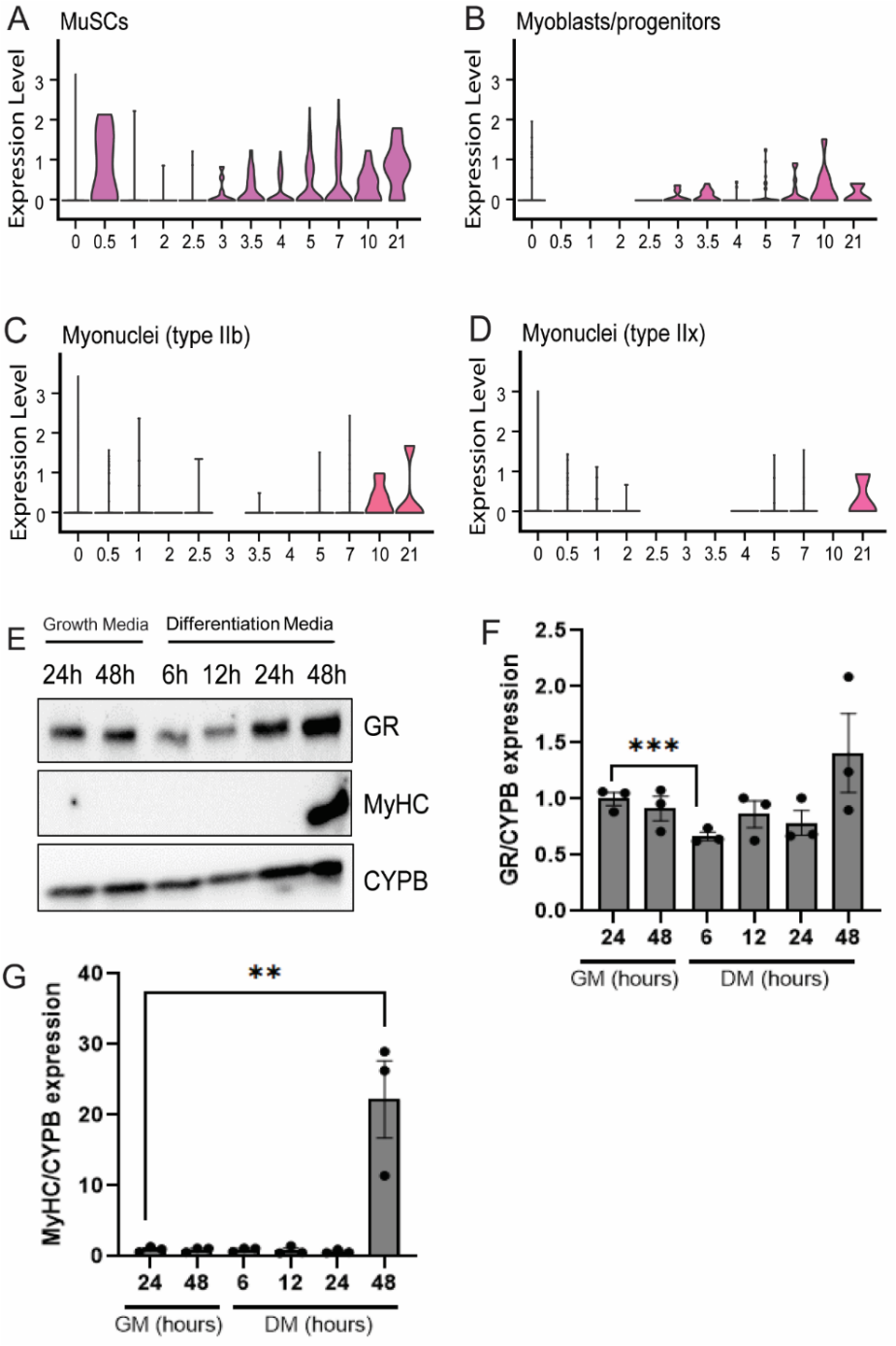

Figure 1: Differentiating myoblasts have reduced glucocorticoid sensitivity during early differentiation.

(A) scMuscle database (McKellar et al., 2021) was used to track expression level of *Nr3c1* transcripts in MuSCs, myoblasts/progenitors **(B)**, type IIb myonuclei **(C),** and type IIx myonuclei **(D)** for 21 days post injury. **(E)** Representative western blot of isolated satellite cells from *Nr3c1*$^{fl/fl}$; *Pax7*$^{+/+}$ (wild-type, WT) mice proliferated for 24 or 48 hours in growth media (GM) and then differentiated for another 48 hours in

differentiation medium (DM). Cyclophilin B (CyPB) is a loading control. **(F)** GR protein expression from (E) normalized to CYPB expression quantified, n=3. **(G)** Quantification of MyHC normalized (to CYPB) expression quantified from (E), n=3 pairs. *p<0.05, **p<0.01, ***p<0.001 by two-tailed paired Student t-test. Data is mean ± SD, using GraphPad Prism 9.4.1 for statistical analysis and graphical representation.

Since *in vitro* differentiation assays suggest a role for GR during early differentiation, I assessed muscle regeneration *in vivo* in six-week-old $GR^{MuSC-/-}$ (*Nr3c1*$^{fl/fl}$; *Pax7*$^{+/CreER}$) and WT control (*Nr3c1*$^{fl/fl}$; *Pax7*$^{+/+}$) mice. Mice in both groups were treated with 5 daily i.p. tamoxifen injections at 1.5-2.0 mg/20 g body weight beginning at 6 weeks of age to induce GR excision in PAX7+ muscle stem cells. Excision was verified upon necropsy following isolation of MuSCs in non-Tibialis anterior (TA) hindlimb muscle and western blot (Fig. 2 A). One-week following the last tamoxifen treatment, the left tibialis anterior (TA) muscle was injured with cardiotoxin (CTX), and the right (contralateral) TA remained uninjured. Both genotypes elicited a strong regenerative response to injury as evidenced by the presence of centrally located nuclei seen in the H&E staining performed at 7 days post-injury (Fig. 2 B). There were no observed differences in the average myofiber cross-sectional area (CSA) or the distribution of cross-sectional areas between contralateral (uninjured) TA muscles from WT and $GR^{MuSC-/-}$ mice (Fig. 2 B, C). Both WT and $GR^{MuSC-/-}$ mice displayed two distinctive fiber cross-sectional area peaks in uninjured muscles at ~1000 μm^2 and ~2250 μm^2 (Fig. 2 C). Following injury, the WT and $GR^{MuSC-/-}$ muscles both regenerated to ~55% of their uninjured cross-sectional area levels (Fig. 2 C, D), however the distribution of fiber CSA revealed only one peak of fibers at ~850 μm^2 present in both genotypes, representing a loss of larger fibers (Fig. 2 D), consistent with incomplete repair. Further, no significant differences were observed in fiber number between WT and $GR^{MuSC-/-}$ mice in uninjured or injured muscle (Fig. 2 E, F). Despite equivalent regenerative responses, the PAX7+ cell numbers were significantly lower in both injured and uninjured $GR^{MuSC-/-}$ muscle, though

MuSC numbers did expand in the $GR^{MuSC-/-}$ mouse (~88% increase) after injury like controls (~90% increase) (Fig. 2 G, H). Since reduced PAX7+ cell numbers can be due to many potential cell fates, I first assessed whether loss of GR results in precocious differentiation of MuSCs in the uninjured TA muscle. I quantified the number of fibers with centrally located nuclei in the TA muscle contralateral to the injury, a hallmark of muscle regeneration and found that while there was a trend towards increased number of fibers with centrally located nuclei in $GR^{MuSC-/-}$ mice as compared to littermate controls, it failed to reach statistical significance ($p=0.0647$, Fig. 2 I).

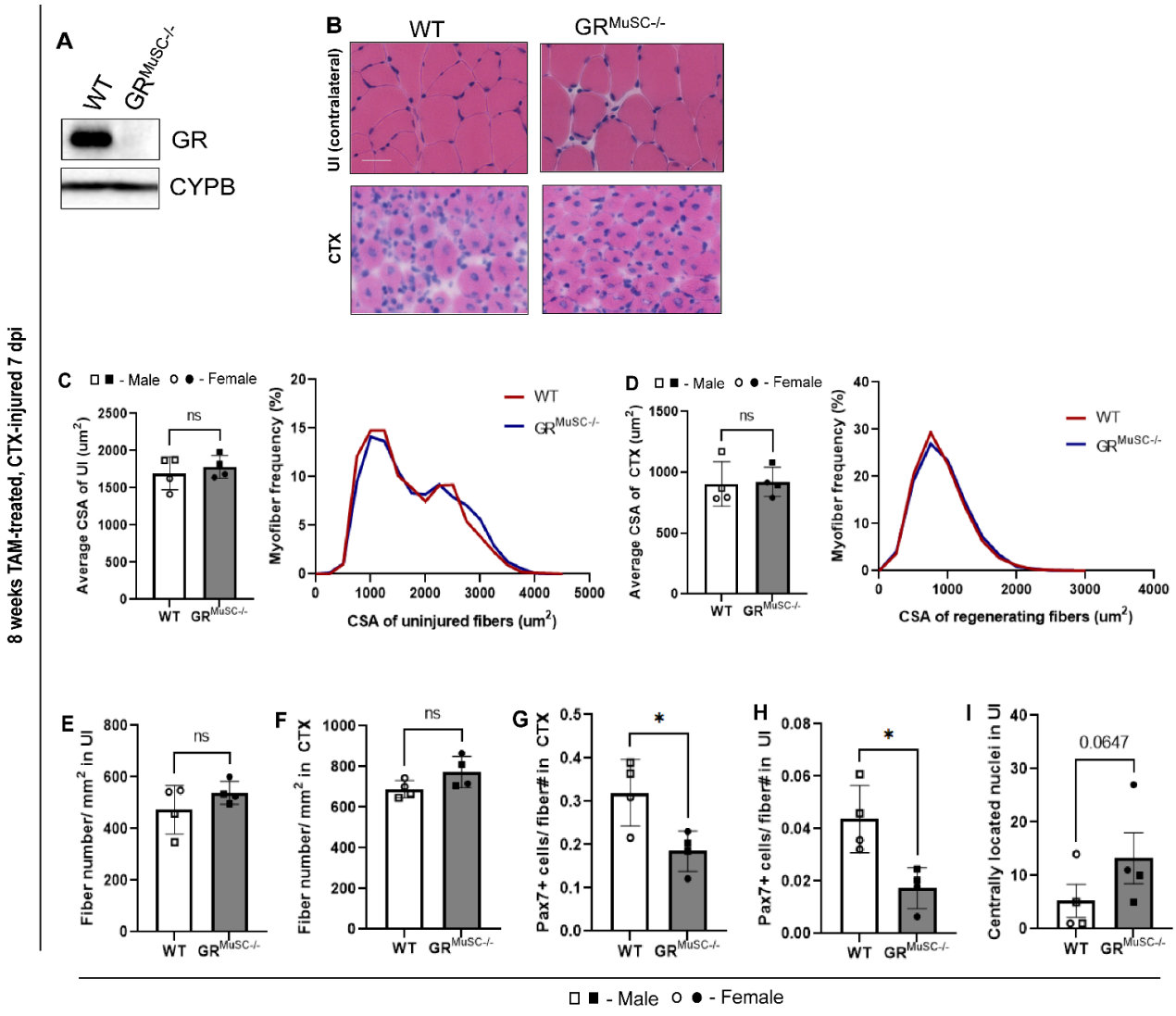

Figure 2: Loss of Glucocorticoid receptor expression leads to a reduction in the PAX7+ MuSC population 7 days post cardiotoxin injury.

(A) Western blot to confirm knockdown of the GR expression in primary myoblasts isolated from the *Nr3c1*$^{fl/fl}$; *Pax7*$^{+/CreER}$ (GR$^{MuSC-/-}$) and *Nr3c1*$^{fl/fl}$; *Pax7*$^{+/+}$ (WT) mice 2 weeks after intraperitoneal (i.p.) tamoxifen administration. Cyclophilin B (CyPB) is a loading control. **(B)** H&E-stained TA muscle sections from WT and GR$^{MuSC-/-}$ mice 7 days post injury (7 d.p.i) with cardiotoxin compared to uninjured muscle. Scale bar = 50 µm**. (C)** Mean fiber cross-sectional area (CSA) and distribution of cross-sectional areas of uninjured fibers from the right (contralateral) TA muscle of mice treated as in (A). **(D)** Average CSA and distribution of regenerating (CTX) fiber CSA from the injured left TA muscle of mice treated as in (A). **(E)** Average number of fibers per mm^2 in uninjured TA muscles from (A). **(F)** Average number of fibers per mm^2 in CTX-injured TA muscles from (A). **(G)** Average number of PAX7+ MuSCs per fiber in CTX-injured TA muscles from (A). **(H)** Average number of PAX7+ cells per fiber in contralateral (uninjured) muscle from (A). **(I)** Average number of fibers with centrally located nuclei in uninjured muscles from (A),

n=4 pairs. *p<0.05, **p<0.01, ***p<0.001 by two-tailed paired Student t-test. Data is mean ± SD, using GraphPad Prism 9.4.1 for statistical analysis and graphical representation.

To determine if the observed reduction in PAX7+ numbers impact the regenerative process long-term and the eventual return of MuSCs to quiescence, I repeated the cardiotoxin experiment and assessed regeneration at 28- and 42-days post-injury (dpi). To eliminate effects due to recombination escapers, tamoxifen administration continued weekly until endpoint. Knockout of GR was confirmed by western blot of extracts from isolated satellite cells at necropsy (Fig. 3 A). At 28 dpi, repair is expected to be complete in WT mice with fiber diameters comparable to the uninjured state (Aoki et al., 2013; Fan et al., 2018; Randazzo et al., 2019). Indeed, WT regenerating controls restored their myofiber cross-sectional area to that of the contralateral TA muscle, while the $GR^{MuSC-/-}$ regenerating fibers were ~15% bigger than their WT counterparts (Fig. 3 B, C, D). There were no significant differences in the average CSA of uninjured myofibers between WT and $GR^{MuSC-/-}$ mice (Fig. 3 B, C). The fiber CSA distribution highlights the propensity towards bigger fibers in the regenerating leg in the $GR^{MuSC-/-}$ mice, evidenced as a rightward shift of the curve (~15%) as compared to littermate controls (Fig. 3 D). Interestingly, in the uninjured TA, WT controls had one peak in the fiber CSA frequency curve, whereas two distinct peaks were observed in the $GR^{MuSC-/-}$ TA (Fig. 3 C). Surprisingly the second larger peak observed in the WT uninjured limb at 7 dpi (Fig. 2 C), was essentially gone by 28 days (Fig. 3 C). A peak at 2500 um^2 was only evident in the $GR^{MuSC-/-}$ condition (Fig. 3 C). Further, loss of the GR had no significant effect on fiber number at 28 days post-cardiotoxin injury (Fig. 3 E, F).

Next, I looked at PAX7+ numbers in regenerating muscles of WT and $GR^{MuSC-/-}$ mice 28 days post-injury. I found that the $GR^{MuSC-/-}$ mice had approximately 50% more PAX7+ MuSCs as compared to wild-type controls in CTX-injured muscle at 28 dpi (Fig. 3 G). In the uninjured

(contralateral) limb at 28 days, however, I found that $GR^{MuSC-/-}$ mice had ~33% fewer PAX7+ cells as compared to WT (Fig. 3 H). To understand why there are fewer PAX7+ cells in the contralateral limb, I quantified the number of fibers with centrally located nuclei in the uninjured TA muscle. I found up to 86% increase in newly formed fibers in the $GR^{MuSC-/-}$ mice as compared to WT (Fig. 3 I), suggesting the loss of PAX7+ cells can be attributed to their differentiation in the absence of GR. By contrast, in WT mice, the PAX7+ population in the contralateral limb remained stable between 7- and 28- days post injury (Fig. 3 J). After injury, while both WT and $GR^{MuSC-/-}$ CTX-injured muscles showed a comparable expansion of their MuSC population (fold over contralateral limb) at 7 dpi, in the WT mice the number of activated PAX7+ MuSCs gradually decreased (~66%) over the 3-week period, as expected with the completion of repair (Fig. 3 K). The PAX7+ population in the $GR^{MuSC-/-}$ regenerating mice, however, remained stable from 7 to 28 days post-injury (Fig. 3 K), $GR^{-/-}$ MuSCs failed to terminate the repair process at this time point.

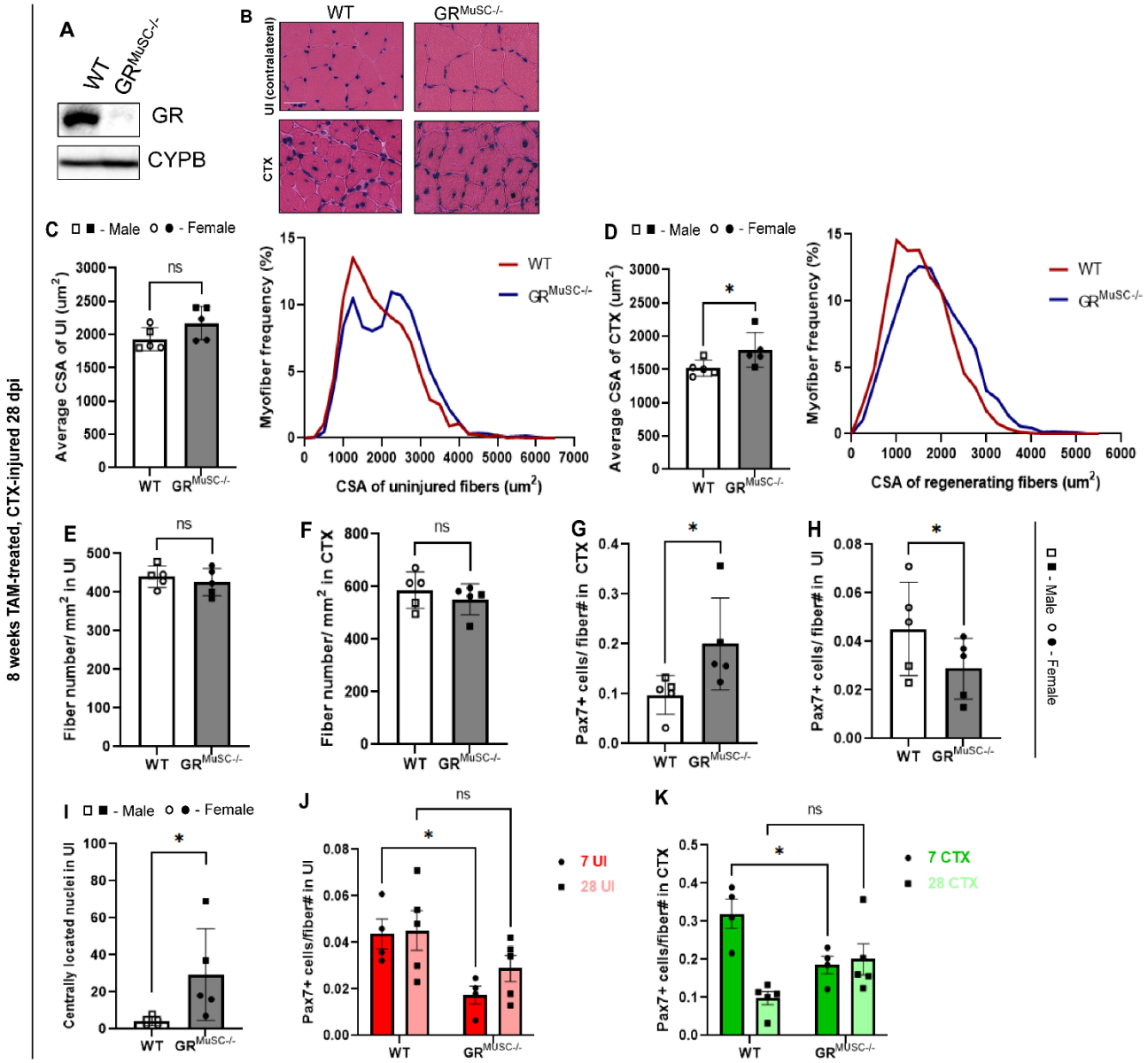

Figure 3: Loss of the glucocorticoid receptor in MuSCs promotes myogenic differentiation in injured and uninjured muscle 28 days post CTX injury.

(A) Western blot to confirm knockdown of the GR expression in primary myoblasts isolated from the *Nr3c1*$^{fl/fl}$; *Pax7*$^{+/CreER}$ (GR$^{MuSC-/-}$) and *Nr3c1*$^{fl/fl}$; *Pax7*$^{+/+}$ (WT) mouse 4 weeks after intraperitoneal (i.p.) tamoxifen administration. Cyclophilin B (CyPB) is a loading control. **(B)** H&E stained cardiotoxin (CTX)-injured TA muscle sections from WT and GR$^{MuSC-/-}$ mice 28 days post injury (28 d.p.i) compared to uninjured muscle. Scale bar = 50 µm. **(C)** Mean fiber cross-sectional area (CSA) and distribution of cross-sectional area of uninjured fibers from the right (contralateral) TA muscle of mice treated as in (A). **(D)** Average cross-sectional area and frequency distribution of CSA of regenerating (CTX) fibers from the injured left TA muscle of mice treated as in (A). **(E)** Average number of fibers per mm^2 in uninjured TA muscles from (A). **(F)** Average number of fibers per mm^2 in CTX-injured TA muscles from (A). **(G)** Average number of PAX7+ MuSCs per fiber in CTX-injured TA muscles from (A). **(H)** Average number

of PAX7+ MuSCs per fiber in contralateral (uninjured) muscle from (A). **(I)** Average number of fibers with centrally located nuclei in uninjured muscles from (A). **(J)** PAX7+ cells/mm^2 from UI (contralateral) muscles at 7- and 28- days post CTX. **(K)** PAX7+ cells/ mm^2 from CTX injured muscles at 7- and 28- days post cardiotoxin injury, n=5 pairs. *p<0.05, **p<0.01, ***p<0.001 by two-tailed paired Student t-test. Ordinary 2-way ANOVA was performed for **(J, K)**. Data is mean ± SD, using GraphPad Prism 9.4.1 for statistical analysis and graphical representation.

To determine if MuSCs lacking GR return to quiescence following repair, I assessed repair and PAX7+ cell numbers at 42 dpi (Fig. 4 A, B). At this time point, I observed that the average myofiber CSA of GR$^{MuSC-/-}$ mice was ~17% bigger in the uninjured muscle (as compared to WT), and the injured GR$^{MuSC-/-}$ muscle was ~14% bigger than the WT-controls (Fig. 4 B, C). Fiber CSA distribution in the uninjured condition showed two distinct peaks for the GR$^{MuSC-/-}$ and WT mice at this time-point (Fig. 4 C). However, the GR$^{MuSC-/-}$ mice had a CSA peak centered at ~3000um^2, suggesting that a proportion of the fibers continue to grow with the loss of GR (Fig. 4 C). In the WT controls the first peak coincided with that of the GR$^{MuSC-/-}$ mice at 1100 um^2 (Fig. 4 C), and the second peak which was less evident at 28-days (Fig. 3 C) re-emerged at 42- days post-injury centered at 2250 um^2 (Fig. 4 C). In the injured leg, the distribution of fibers in the GR$^{MuSC-/-}$ mice shows a 14% rightward shift indicating a higher percentage of myofibers with increased CSA as compared to the WT (Fig. 4 B, D). There were no significant differences in fiber number between the WT and GR$^{MuSC-/-}$ mice in both injured and uninjured states (Fig. 4 E, F). At 42 days post injury, PAX7 numbers are expected to have returned to the uninjured levels (baseline) and be quiescent (Collins et al., 2005; Sacco et al., 2008). In the CTX-injured condition, the PAX7 cell numbers were approximately 50% higher in the GR$^{MuSC-/-}$ mice as compared to the regenerating WT muscle (Fig. 4 G). However, in the uninjured leg, the PAX7 numbers were comparable between the WT and GR$^{MuSC-/-}$ mice (Fig. 4 H).

I also performed an ordinary 2-way ANOVA on PAX7 numbers using Tukey's multiple contrasts test on WT and GR$^{MuSC-/-}$ at 7-, 28- and 42- dpi in UI (contralateral) and CTX

(regenerating) muscles. In the uninjured condition 7 days following injury I noticed a ~50% decrease in the PAX7+ cells in the $GR^{MuSC-/-}$ mice as compared to WT (Fig. 2 H). This difference in PAX7+ cells dropped to ~33% at 28 days between $GR^{MuSC-/-}$ and WT mice (Fig. 3 H), eventually returning to similar levels as that of the WT at 42 dpi (Fig. 4 I). In the presence of injury, even though the PAX7+ population in the $GR^{MuSC-/-}$ mice at 7 dpi expanded like the WT controls (~89% expansion in both populations) the total expanded population was approximately 59% smaller in the $GR^{MuSC-/-}$ mice (Fig. 2 G). The PAX7+ population in $GR^{MuSC-/-}$ remained stable from 7- to 28-days post injury, eventually returning to baseline levels (Fig. 4 J), suggesting a protracted repair period in the absence of GR in MuSCs. However, the number of PAX7+ MuSCs in the $GR^{MuSC-/-}$ mice was (~50%) higher than the WT at 42- days post injury, suggesting that loss of GR leads to long-term activation of PAX7+ cells in the injured limb (Fig. 4 J).

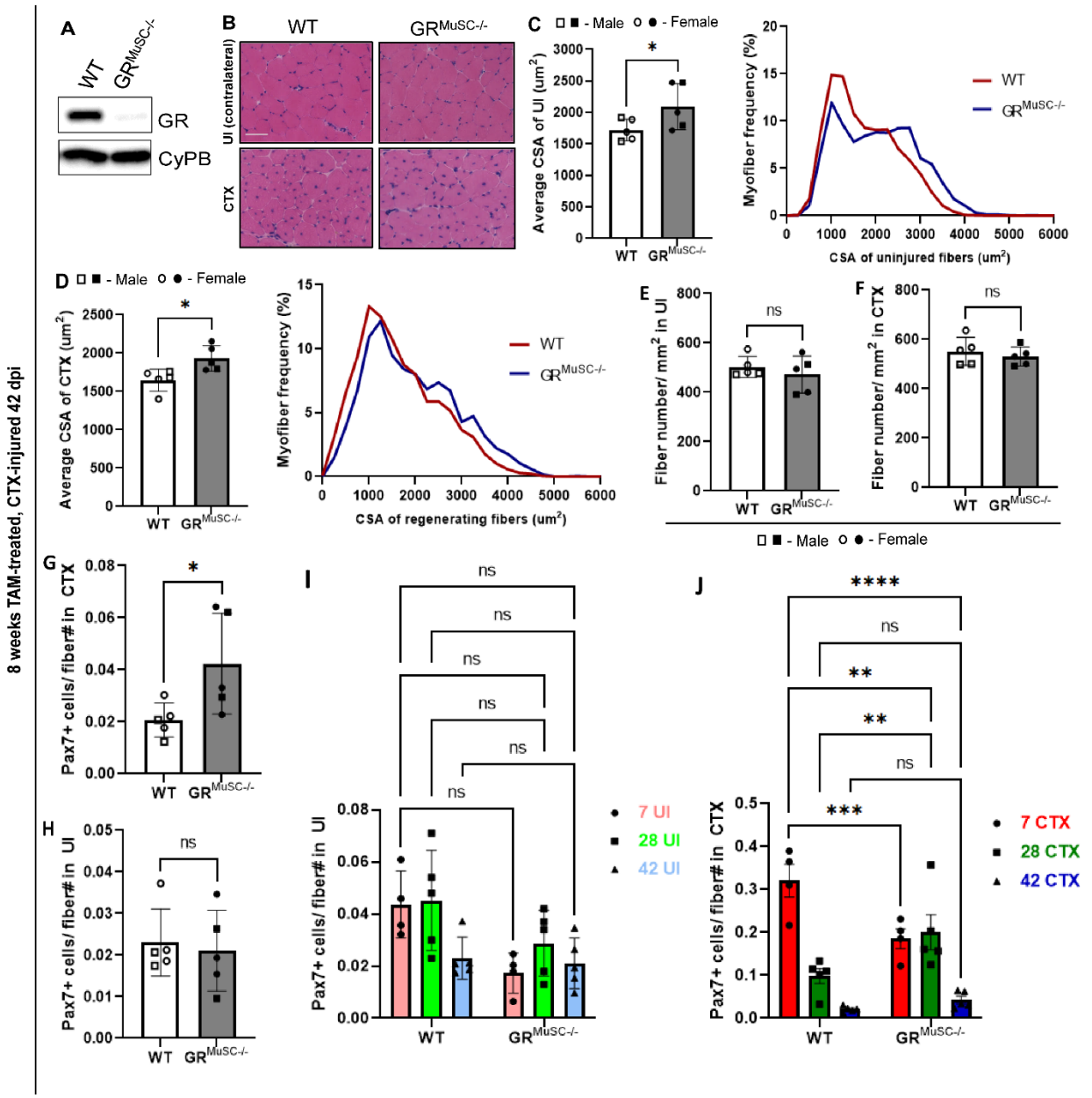

Figure 4: Loss of the glucocorticoid receptor in MuSCs maintains PAX7+ cell numbers elevated at 42 dpi.

(A) Western blot to confirm knockdown of the GR expression in primary myoblasts isolated from the *Nr3c1*$^{fl/fl}$*; Pax7*$^{+/CreER}$ (GR$^{MuSC-/-}$) and *Nr3c1*$^{fl/fl}$*; Pax7*$^{+/+}$ (WT) mice eight weeks after intraperitoneal (i.p.) tamoxifen administration. **(B)** H&E-stained TA muscle sections from cardiotoxin injured and control uninjured muscle were analyzed at 42 days post injury. Scale=50um. **(C)** Average CSA and distribution of cross-sectional areas of uninjured fibers from the right (contralateral) TA muscle of mice treated as in (A). **(D)** CSA and frequency distribution of cross-sectional areas of regenerating (CTX) fibers from the injured left TA muscle of mice treated as in (A). **(E)** Average number of fibers per mm^2 in uninjured TA muscles from (A). **(F)** Average number of fibers per mm^2 in CTX-injured TA muscles from (A). **(G)** Average number of PAX7+ MuSCs per fiber in CTX-injured TA muscles from (A). **(H)** Average number of PAX7+

cells per fiber in contralateral (uninjured) muscle from (A). **(I)** Contrast of PAX7+ cells/mm^2 from uninjured muscles at 7- and 28- days post cardiotoxin injury. **(J)** Contrast of PAX7+ cells/mm^2 from CTX-injured muscles at 7- and 28- days post cardiotoxin injury, n=5 pairs. *p<0.05, **p<0.01, ***p<0.001 by two-tailed paired Student t-test. Ordinary 2-way ANOVA using Tukey's multiple contrast test was performed for **(I)** and **(J)**. Data is mean ± SD, using GraphPad Prism 9.4.1 for statistical analysis and graphical representation.

Given that loss of GR reduced the PAX7+ population at 7- and 28- dpi in the uninjured muscle accompanied by a concomitant increase in fiber number with centrally located nuclei and average fiber cross-sectional area from 7- to 28-days in resting muscle, I sought to examine the fate of MuSCs after loss of GR in the absence of injury. Briefly, 1-week after tamoxifen treatment, the TA muscles were isolated from 8-week-old mice and histology was examined. Knockout of GR was confirmed by western blot of extracts from isolated satellite cells (Fig. 5 A). In the absence of muscle injury, no significant differences in average muscle fiber CSA or fiber number were observed in GR$^{MuSC-/-}$ mice as compared to WT controls (Fig. 5 B-E). No genotype-dependent differences were noted in PAX7 numbers in the absence of injury (Fig. 5 F), however a significant (~42%) increase in fibers with centrally located nuclei in the GR$^{MuSC-/-}$ mice was noted (Fig. 5 G).

Next, I assessed the effect of GR knockdown on the PAX7+ population and muscle histology in mature mice at 18 weeks of age in the absence of injury. Briefly, mice were treated with 5 daily intraperitoneal injections at 1.5-2.0 mg/20 g body weight at 16 weeks of age, and 1-week post tamoxifen treatment, the TA muscles were isolated (at 18 weeks of age). I noted ~41% significant reduction in the number of PAX7+ MuSCs in GR$^{MuSC-/-}$ mice as compared to WT controls (Fig. 5 H). Further, while few centrally located fibers were observed in resting muscle of WT mice, GR$^{MuSC-/-}$ had a significant increase as compared to controls. The proportion of fibers with centrally located nuclei in GR$^{MuSC-/-}$ mice increased by ~40% from young to mature mice (Fig. 5 G, I). Thus, in young mice, the absence of GR did not have impact myofiber size or PAX7+ cell numbers. However, in mature mice, the loss of GR led to a decrease in the PAX7+ MuSC

population and an increase in fibers with centrally located nuclei, in the absence of injury. These findings suggest that loss of GR does not adversely impact myofiber growth in young mice, but later, when stem cell contributions to myofibers are not expected, loss of GR leads to precocious differentiation and consumption of the PAX7+ MuSC pool, suggesting defects in self-renewal.

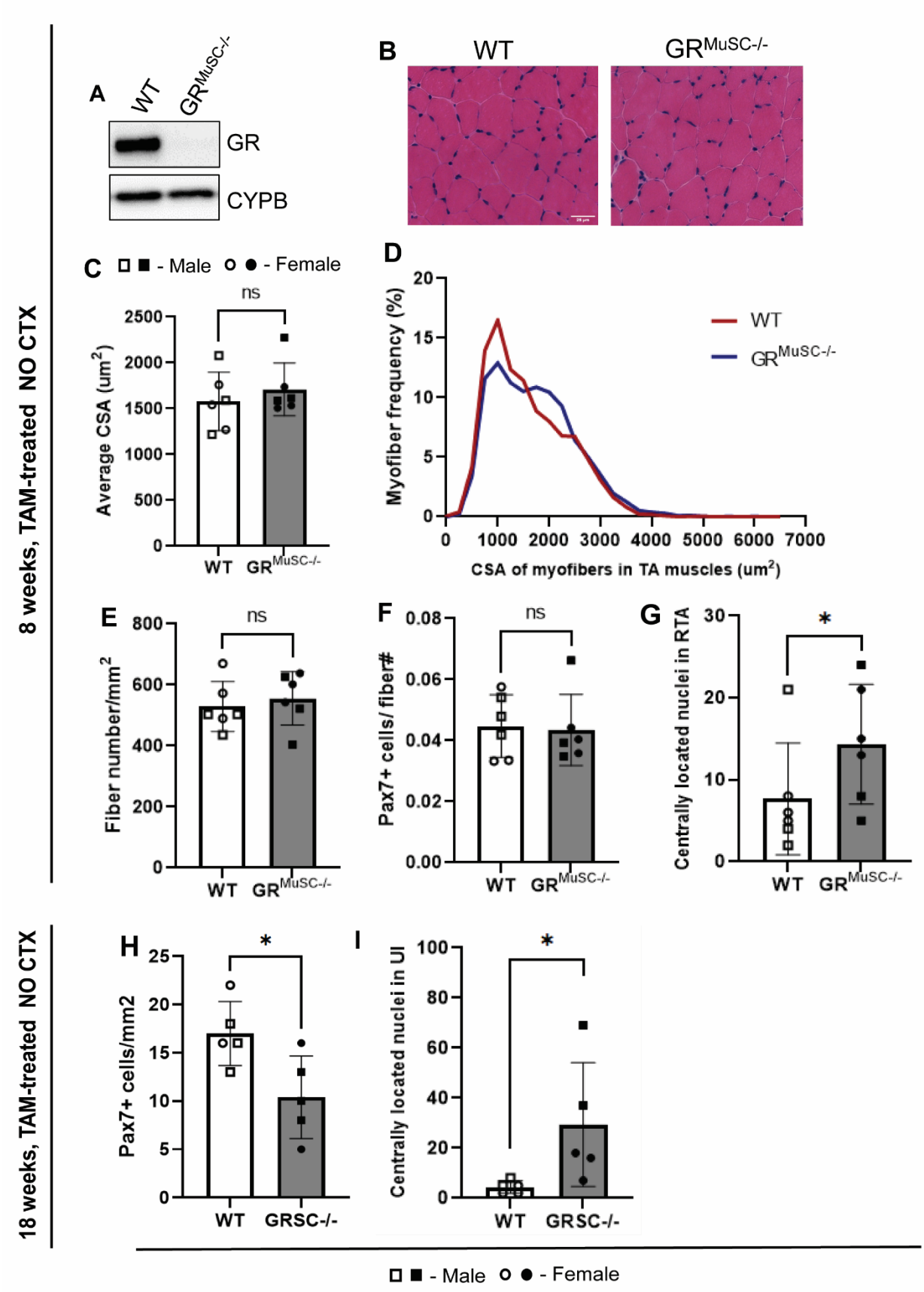
8 weeks, TAM-treated NO CTX
A
WT
GRMuSC-/-
GR
CYPB
B
WT
GRMuSC-/-
C
- Male - Female
ns
Average CSA (um2)
WT
GRMuSC-/-
D
Myofiber frequency (%)
WT
GRMuSC-/-
CSA of myofibers in TA muscles (um2)
E
ns
Fiber number/mm2
F
ns
Pax7+ cells/ fiber#
G
*
Centrally located nuclei in RTA
18 weeks, TAM-treated NO CTX
H
*
Pax7+ cells/mm2
WT
GRSC-/-
I
*
Centrally located nuclei in UI
- Male - Female

Figure 5: Loss of the GR in older mice reduces the PAX7+ pool and drives myogenic differentiation in the absence of injury.
(A) Western blot to confirm knockdown of the GR expression in primary myoblasts isolated from the *Nr3c1*$^{fl/fl}$; *Pax7*$^{+/CreER}$ (GR$^{MuSC-/-}$) and *Nr3c1*$^{fl/fl}$; *Pax7*$^{+/+}$ (WT) mice 2 weeks after first intraperitoneal (i.p.) tamoxifen administration beginning at 6 weeks of age. **(B)** Representative images of H&E-stained TA muscle histology in 8-week-old WT and GR$^{MuSC-/-}$ mice one week after completion of tamoxifen treatments to knock out GR expression. Scale=100 um. **(C)** Average myofiber CSA in mice from (A), (left and right TA average plotted together). (**D)** Distribution of cross-sectional areas of myofibers fibers from mice treated as in (A). **(E)** Average number of fibers per mm^2 of TA muscles from (A). **(F)** Average number of PAX7+ MuSCs per fiber in TA muscles from (A). **(G)** Average number of fibers with centrally located nuclei in uninjured muscles from (A) n=6 pairs. **(H)** Concurrently, GR$^{MuSC-/-}$ and WT mice were intraperitoneally (i.p.) administered tamoxifen beginning at 16 weeks of age to excise GR in mature mice. Average number of PAX7+ MuSCs per fiber in TA muscles from (H). **(I)** Average number of fibers with centrally located nuclei in uninjured muscles from (H) n=5 pairs *p<0.05, **p<0.01, ***p<0.001 by two-tailed paired Student t-test. Data is mean ± SD, using GraphPad Prism 9.4.1 for statistical analysis and graphical representation.

In separate experiments at 6- and 8- weeks of age I confirmed that both WT and GR$^{MuSC-/-}$ mice had similar average muscle CSA (Fig. 6 A, B, E, F) and distribution (Fig. 6 C, G) prior to tamoxifen treatment (in the presence of GR) and in the absence of injury. I also assessed Feret diameter as a secondary measure of myofiber size and found that there were no significant changes recorded between the two genotypes (Fig. 6 D, H). These data taken together show that there are no inherent genotype differences in myofiber size or distribution.

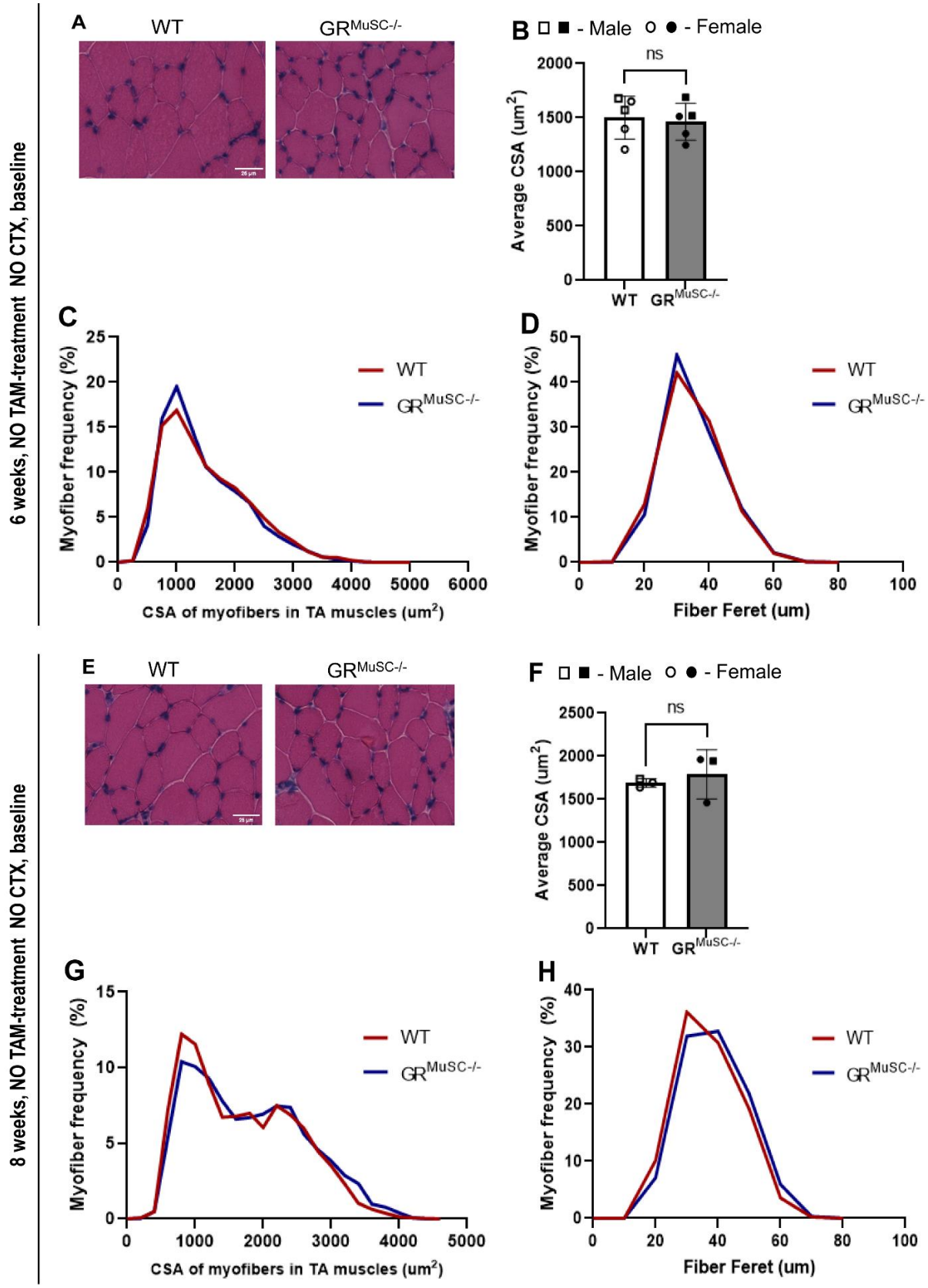
6 weeks, NO TAM-treatment NO CTX, baseline
A
WT
GRMuSC-/-
B
□ ■ - Male ○ ● - Female
ns
Average CSA (um2)
2000
1500
1000
500
0
WT
GRMuSC-/-
C
Myofiber frequency (%)
25
20
15
10
5
0
0
1000
2000
3000
4000
5000
6000
CSA of myofibers in TA muscles (um2)
WT
GRMuSC-/-
D
Myofiber frequency (%)
50
40
30
20
10
0
0
20
40
60
80
100
Fiber Feret (um)
WT
GRMuSC-/-
8 weeks, NO TAM-treatment NO CTX, baseline
E
WT
GRMuSC-/-
F
□ ■ - Male ○ ● - Female
ns
Average CSA (um2)
2500
2000
1500
1000
500
0
WT
GRMuSC-/-
G
Myofiber frequency (%)
15
10
5
0
0
1000
2000
3000
4000
5000
CSA of myofibers in TA muscles (um2)
WT
GRMuSC-/-
H
Myofiber frequency (%)
40
30
20
10
0
0
20
40
60
80
100
Fiber Feret (um)
WT
GRMuSC-/-

Figure 6: Muscle histology is unperturbed in both genotypes in the presence of GR and in the absence of injury at baseline (at 6 – and 8- weeks).

(A) Representative images of H&E-stained TA muscle histology in both genotypes at 6-week-old mice, in the absence of tamoxifen-treatment and cardiotoxin injury. Scale=100 um. **(B)** Average myofiber CSA in mice from (A), left and right TA plotted together. **(C)** Frequency distribution of CSA of myofibers from both TA muscle as in (A). **(D)** Fiber Feret (um) measurement in both TA sections from (A), n=5 pairs. **(E)** Representative images of H&E-stained TA muscle histology of both genotypes at 8 weeks of age, without tamoxifen-treatment and cardiotoxin injury. Scale=100 um. **(F)** Average myofiber CSA in mice from (A), n=3 pairs (left and right TA plotted together). **(G)** Frequency distribution CSA of myofibers from both TA muscle as in (A). **(H)** Fiber Feret (um) measurement in both TA sections from (A), n=3 pairs. Scale=100 um. *$p<0.05$, **$p<0.01$, ***$p<0.001$ by two-tailed paired Student t-test. Data is mean ± SD using GraphPad Prism 9.4.1 for statistical analysis and graphical representation.

Chapter 2: GR is required for the maintenance of MuSC quiescence.

To examine the role for the GR during *in vivo* muscle stem cell activation, I injected 6-week-old mice for 5 consecutive days with tamoxifen to knock out glucocorticoid receptor expression. Two weeks following the last injection, $GR^{MuSC-/-}$ and WT mice were intraperitoneally injected once with 100 mg/kg of body weight of BrdU for 24 hours. TA muscles and hindlimbs were collected a day later. Loss of GR expression was confirmed by immunoblot (Fig. 7 A). I then performed immunostaining for PAX7 and BrdU on TA muscle cross sections from WT and $GR^{MuSC-/-}$ mice (Fig. 7 B). I observed that loss of the GR *in vivo* leads to a 68% increase in BrdU+ incorporation in MuSCs (Fig. 7 B, C). In a parallel cohort, I immunostained TA muscle sections to quantify the number of PAX7+ MuSCs that were activated/cycling, using anti-Ki67 antibody (MKi67 – marker of proliferation 67). Given that there is no myotrauma, I did not expect to see any cycling cells at this stage. Consistent with previous observations (Fig. 5 F), even though there were no significant changes in the number of PAX7+ MuSCs between WT and $GR^{MuSC-/-}$ mice, there was a significant increase (~52%) in the number of PAX7+/Ki67+ double positive cycling cells in $GR^{MuSC-/-}$ mice (Fig. 7 D -F).

Concurrently I immunostained TA muscle sections obtained from 7- to 42 days post injury from WT and $GR^{MuSC-/-}$ mice, to quantify the number of PAX7+/Ki67+ cycling cells. The percentage of Ki67+ cycling cells was not significantly different between the two genotypes at 7-days post injury (Fig. 7 G). However, at 42dpi, PAX7+ MuSCs are expected to have returned to quiescence, and accordingly I found only ~2% of PAX7+ cells were also Ki67+ in WT mice (Fig. 7 H). Interestingly loss of the GR led to a significant increase in the percentage of PAX7+Ki67+ cycling cells in $GR^{MuSC-/-}$ mice (as compared to controls) at this time point (Fig. 7 H). Taken

together, this data suggests that loss of GR in PAX7+ MuSCs leads to a break in quiescence and precocious activation of these stem cells.

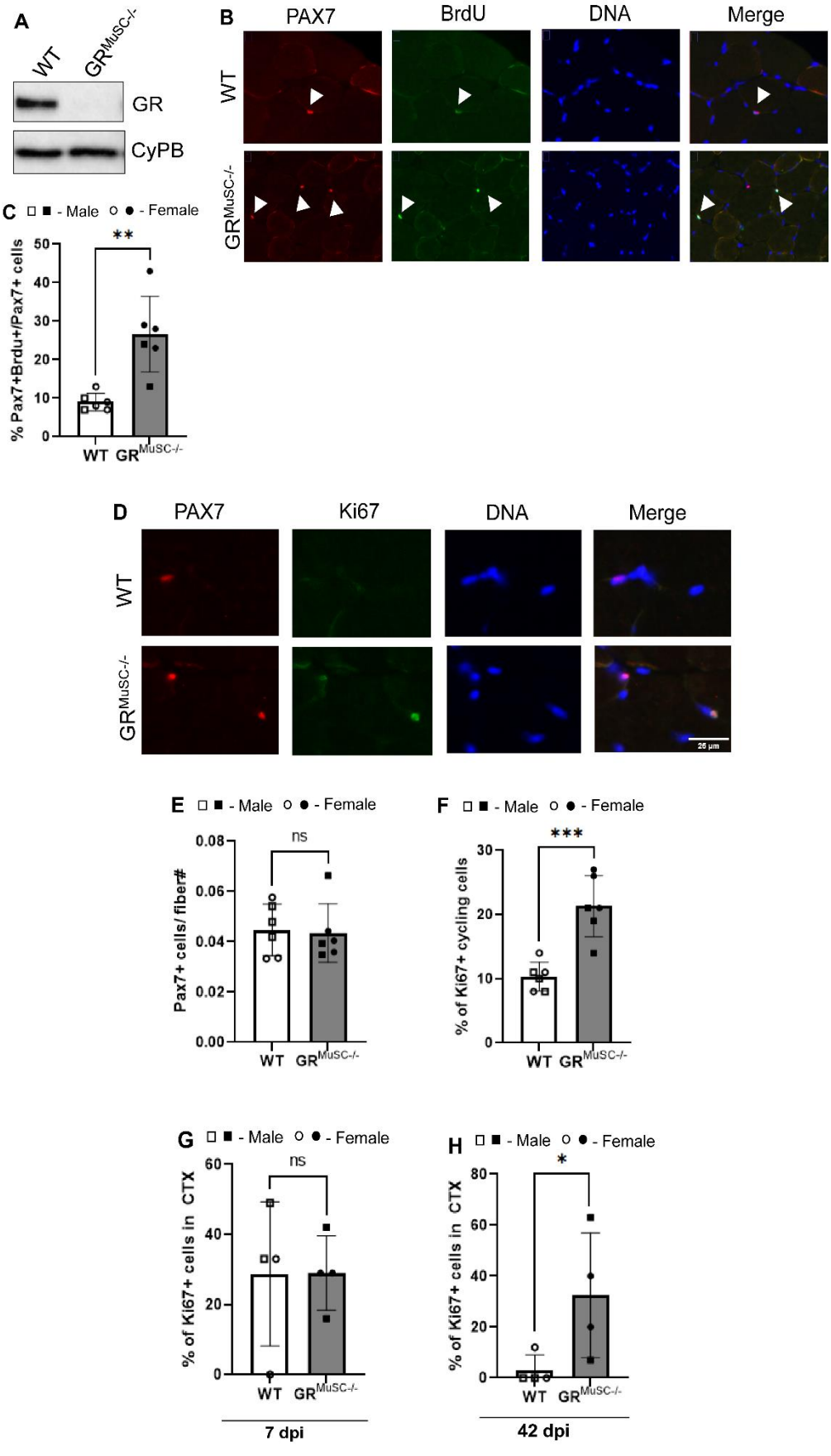
A
WT
GRMuSC-/-
GR
CyPB
B
PAX7
BrdU
DNA
Merge
WT
GRMuSC-/-
C
□ ■ - Male ○ ● - Female
**
% Pax7+Brdu+/Pax7+ cells
WT GRMuSC-/-
D
PAX7
Ki67
DNA
Merge
WT
GRMuSC-/-
26 µm
E
□ ■ - Male ○ ● - Female
ns
Pax7+ cells/ fiber#
WT GRMuSC-/-
F
□ ■ - Male ○ ● - Female
***
% of Ki67+ cycling cells
WT GRMuSC-/-
G
□ ■ - Male ○ ● - Female
ns
% of Ki67+ cells in CTX
WT GRMuSC-/-
7 dpi
H
□ ■ - Male ○ ● - Female
*
% of Ki67+ cells in CTX
WT GRMuSC-/-
42 dpi

Figure 7: Loss of the GR in vivo increases the percentage of BrdU and Ki67+ cycling cells in the TA muscles of mice.
(A) *Nr3c1$^{fl/fl}$; Pax7$^{+/+}$* (wild-type, WT) and conditional null *Nr3c1$^{fl/fl}$; Pax7$^{+/CreER}$* (GR$^{MuSC-/-}$) mice aged 6 weeks were injected daily with tamoxifen for 5 days. Two weeks following the last injection, TA muscles and hindlimbs were collected and GR expression was verified by western blot in these mice. **(B)** Representative images of TA muscle sections stained for PAX7 (red) and BrdU (green) from (A). Nuclei were counterstained with DAPI (blue). Scale bar = 50 μm. **(C)** Percentage of BrdU+ cells from (A), n= 6 pairs. **(D)** Representative images of TA muscle sections stained for PAX7 (red) and Ki67 (green) from mice that were tamoxifen-treated and uninjured at the same age as (A). Nuclei were counterstained with DAPI (blue). Scale bar = 25 μm. **(E)** Quantification of Pax7+ cell per mm^2 on mouse TA section from (D). **(F)** Percentage of Ki67+ cycling cells from (D), n=6 pairs. **(G)** Percentage of PAX7+Ki67+ cycling cells from WT and GR$^{MuSC-/-}$ CTX-injured mice 7 days post cardiotoxin insult, n= 4 pairs. **(H)** Percentage of Ki67+ cycling cells 42 days post cardiotoxin insult in WT and GR$^{MuSC-/-}$ mice, n= 4 pairs. Data is represented as mean ± SD, *p < 0.05, **p < 0.01, ***p <0.001, ns = not significant by two-tailed paired Student t-test using GraphPad Prism 9.4.1 for statistical analysis and graphical representation.

Single myofiber isolations from either the extensor digitorum longus (EDL) or the flexor digitorum brevis (FDB) have been widely used to investigate MuSC functions such as quiescence, self-renewal, activation, and differentiation in their microenvironment. PAX7 and MYOD are used to mark the different myogenic cell populations, where PAX7+MYOD- cells are the self-renewing population, PAX7+MYOD+ are the activated (proliferating) cells and PAX7-MYOD+ marks differentiating cells (Zammit et al., 2006). To study the role of GR in the regulation of myogenic cell fate in resting muscle, I excised the receptor from PAX7+ cells of GR$^{MuSC-/-}$ and WT mice. Loss of GR was confirmed via western analysis from isolated satellite cells from WT and GR$^{MuSC-/-}$ mice respectively (Fig. 8 A). The immunoblot also showed increased expression of MYOD in the GR$^{MuSC-/-}$ cultures as compared to the WT, consistent with increased MuSC activation (Fig. 8 A). Two weeks following the last intraperitoneal tamoxifen injection, myofibers were isolated from the EDL muscle of each mouse and immunostained for the myogenic cell populations 2 hours post dissociation using anti-PAX7 and anti-MYOD antibodies (Fig. 8 B). To achieve single EDL myofiber cultures, the fibers were left suspended in wash media for ~2 hours prior to fixing and as such, should produce fibers with largely quiescent MuSCs. Accordingly, ~70% of MuSCs from

WT myofiber were PAX7+MYOD- (quiescent) as compared to only about 40% on the GR $^{MuSC-/-}$ myofibers (Fig. 8 C). Concomitantly, the PAX7+MYOD+ (activated) MuSC populations was larger in the GR$^{MuSC-/-}$ as compared to WT myofibers 2 hours post-dissociation (Fig. 8 D, E). However, there were no significant differences in the PAX7-MYOD+ group between the two genotypes (Fig. 8 E). Myofiber width was also quantified and consistent with the *in vivo* findings, GR$^{MuSC-/-}$ fibers has a significant (up to 10%) rightward shift in the distribution curve, suggesting that the EDL myofibers increase in size with loss of GR in MuSCs (Fig. 8 F). When fibers were instead stained for PAX7 and Ki67, the PAX7+Ki67+ (cycling) population was ~30% greater on GR$^{MuSC-/-}$ myofibers as compared to WT controls (Fig. 8 G, H), consistent with increased activation of MuSC cells. Hence, our data suggests that loss of GR leads to an increase in the percentage of Ki67+ cycling cells and PAX7+MYOD+ activated MuSCs population.

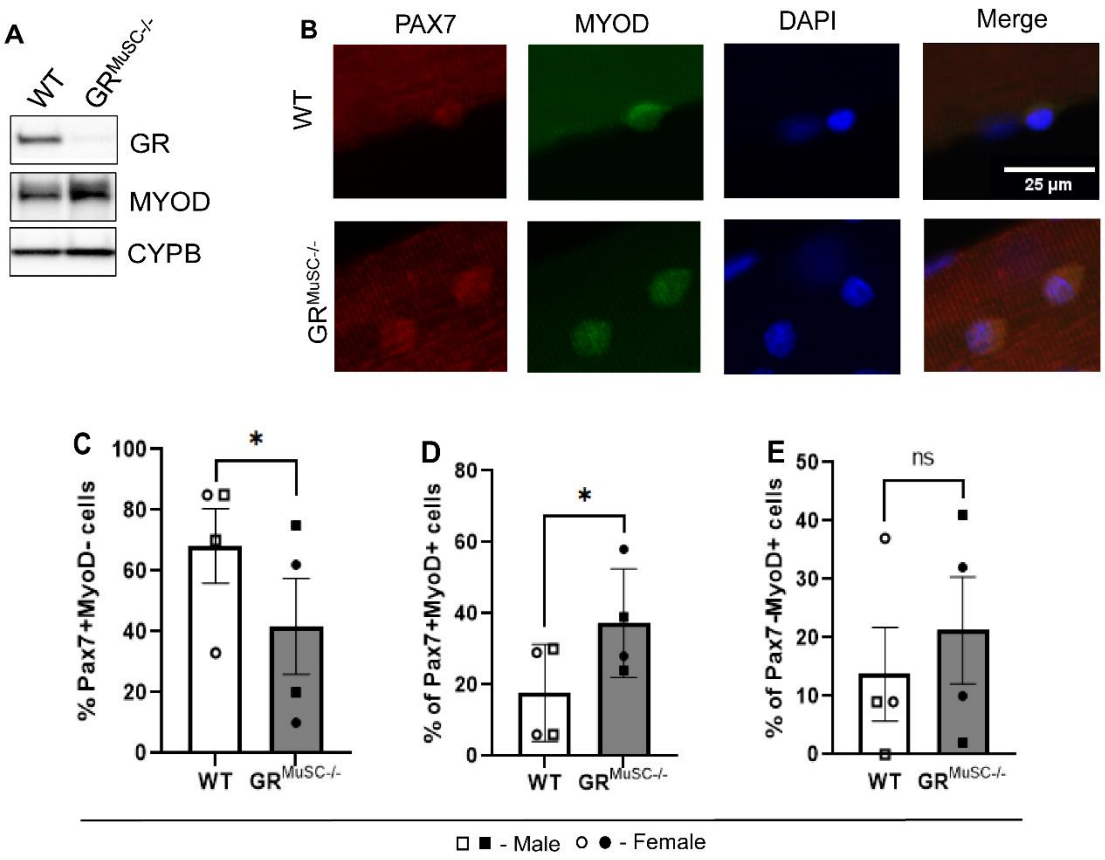
A
WT
GRMuSC-/-
GR
MYOD
CYPB
B
PAX7
MYOD
DAPI
Merge
WT
GRMuSC-/-
25 µm
C
% Pax7+MyoD- cells
*
WT
GRMuSC-/-
D
% of Pax7+MyoD+ cells
*
WT
GRMuSC-/-
E
% of Pax7-MyoD+ cells
ns
WT
GRMuSC-/-
□ ■ - Male ○ ● - Female
F
Myofiber frequency (%)
Myofiber width (um)
WT
GRMuSC-/-
G
PAX7
KI67
DAPI
Merge
WT
GRMuSC-/-
25 µm
H
□ ■ - Male ○ ● - Female
% Ki67+ cycling MuSCs
*
WT
GRMuSC-/-

Figure 8: Loss of GR leads to increased cell proliferation post activation in ex-vivo single EDL myofibers.

Nr3c1$^{fl/fl}$*; Pax7+/*^{CreER} (GR$^{MuSC-/-}$) and *Nr3c1*$^{fl/fl}$*l; Pax7*$^{+/+}$ (WT) mice were treated with tamoxifen for 5 days. Two weeks following the last injection, myofibers were isolated from the extensor digitorum longus (EDL) of each mouse and left in suspension for 2h before immunostaining. **(A)** Western analysis of GR and MYOD protein expression in MuSCs isolated from the hind limb of WT and GR$^{MuSC-/-}$ mice injected with tamoxifen for 5 days. **(B)** Representative images of myofibers stained for PAX7 (red) and MYOD (green). Nuclei were counterstained with DAPI (blue). Scale bar = 25 μm. **(C)** Percentage of quiescent/self-renewing (PAX7+MYOD−) MuSCs on single myofibers at T2h from dissociation as in (A). **(D)** Percentage of activated/proliferating (PAX7+MYOD+) myoblasts on single myofibers as in (A). **(E)** Percentage of differentiating (PAX7−MYOD+) myoblasts on single EDL myofibers at time-point T2h from (A). **(F)** Distribution of width (um) of single myofibers at time-point T2h from (B). **(G)** Representative images of myofibers stained for PAX7 (red) and Ki67 (green). Nuclei were counterstained with DAPI (blue) in mice from (A). Scale bar = 25 μm. **(H)** Percentage of Ki67+ cycling MuSCs from (A). n= 4 pairs. Data is represented as mean ± SD, *p < 0.05, **p < 0.01, ***p <0.001, ns = not significant by two-tailed paired Student t-test using GraphPad Prism 9.4.1 for statistical analysis and graphical representation

Given that loss of the glucocorticoid receptor in MuSCs leads to increased Ki67+ cycling cells on single fiber cultures (~43% higher) and *in vivo* (~52% higher), and a concomitant increase (as much as 64%) in BrdU+ incorporation in MuSCs, I predicted that GR is required for MuSC quiescence. Prior to 2017, the majority of MuSC isolation protocols involved extensive dissociation steps using enzymatic and mechanical stresses which disrupt the physiological niche and MuSC morphology. MuSCs are present in a highly specified niche which consists of multiple components such as the vasculature, neural networks, extracellular matrix (ECM), endothelial and immune cells working together in synergy (Yin et al., 2013). The anatomical niche is central for non-MuSC dependent regulation and is important in the maintenance of quiescence, self-renewal, proliferation, and differentiation of MuSCs (F. Relaix et al., 2021). To understand how GR regulates the MuSC transcriptome and discover novel targets during quiescence and MuSC activation, I performed a high throughput mRNA sequencing (mRNA-seq) experiment on truly quiescent MuSCs isolated from their physiological niche following *in situ* fixation (Machado et al., 2017). Briefly, I treated *Nr3c1*$^{fl/fl}$*; Pax7*$^{+/+}$ (wild-type, WT) and conditional null *Nr3c1*$^{fl/fl}$*;*

Pax7$^{+/CreER}$ (GR$^{MuSC-/-}$) mice aged 6 weeks with 5 daily injections of tamoxifen as previously performed. Two weeks following the last injection, mice were sacrificed and their MuSCs were harvested *in situ*, by fixing the muscle immediately after dissection in 0.5% cold PFA as described by Machado and others (Machado et al., 2017). MuSCs were isolated via fluorescence activated cell sorting (FACS), using α-mCD106^{+} (Vcam) as a positive marker and Sca1^{+}, CD31^{+}, CD45^{+} as negative markers to obtain a highly purified population (Maesner et al., 2016). The RNA isolated from these sorted samples was sent to the Donnelly Sequencing Center at the University of Toronto for library preparation and consecutive PCR amplification and sequencing. A fraction of the sorted (cell) events from WT and GR$^{MuSC-/-}$ mice were subject to anti-PAX7 immunostaining post-sorting to verify *in situ* fixed MuSCs sample purity (Supp Fig. 1 A).

Quality check and preprocessing of the raw sequence files was done using MultiQC, a tool that aggregates results from bioinformatics analyses across multiple samples into a single report (Ewels et al., 2016). Using FastQC, a good overall sequence read quality of ~40 million uniquely mapped reads, producing ~20 million read pairs per sample (Supp Fig. 1 B) was observed. It is noteworthy that the two female WT samples had ~37% lower than average read numbers when compared to the rest of the fixed samples. The data was then aligned on the mm10 genome using STAR, an ultrafast universal RNA-seq aligner (Dobin et al., 2013) (Supp Fig. 1 C). The overall alignment score was ~45-75% for all reads that aligned with the genome and ~7-30% of those aligned reads mapped to exons. Although the duplication rate was as high as 55%, which is expected from low input samples such as ours, it was comparable to other less challenging RNA sequencing projects that do not include the use of formalin-fixed paraffin-embedded (FFPE) samples (Supp Fig. 1 B). Using Picard to analyze RNA-seq metrics, I found that the average percentage of non-exonic (intronic and intergenic) reads was as high as 80% (Supp Fig. 1 D).

Overall samples had ~40% rate of intergenic reads (Supp Fig. 1 D). Overall, I had an approximate 40% rate of intronic reads, which was expected from similar studies done in the past using FFPE samples, like ours. It is thought that the increased distribution of intronic reads could be due to the capture of recently transcribed pre-mRNA molecules that may not have been fully spliced (Esteve-Codina et al., 2017). For all further analyses, I chose to use data (read counts) only from the mature RNA (coding + UTR) transcripts (Supp Fig. 1 D). I removed duplicates introduced by PCR using the unique molecular identifiers (UMIs) that were incorporated in the SMART-Seq® Stranded Kit during library preparation. The criteria for two read pairs to be marked as a duplicate was based on, first, both read pairs having the exact chromosomal coordinates for each mate of the pair, and second, the random UMI barcode generated for each read pair being the exact same for both set of reads (Supp Fig. 1 E). One read pair was used and all other duplicates of it were rejected from the analysis pipeline. The principal component analysis (PCA) plot shows a variance of 38.64% on PC1 post normalization and distinctly highlights the clusters first by genotype and then by sex (Supp Fig. 1 F).

As the *in vivo* BrdU pulse experiments showed a stronger phenotype in $GR^{MuSC-/-}$ females as compared to males with loss of GR, I first looked at differentially expressed genes (DEGs) in $GR^{MuSC-/-}$ versus WT female mice. The Bland-Altman (MA) plot revealed that there were 83 differentially expressed genes in $GR^{MuSC-/-}$ females (51 up- and 32 down- regulated) (Fig. 9 A, B) using a log2 fold-change cut-off of 1 and FDR cut-off of 0.05. Heatmaps with the top 300 genes, sorted based on their FDR values and regardless of logFC and FDR cut-off criteria were generated (Fig. 9 C). A median-centered log2 normalized expression pattern of the top 300 DEG in females shows diversity between $GR^{MuSC-/-}$ and WT mice (Fig. 9 C). The downregulation of *Nr3c1* (GR)

in $GR^{MuSC-/-}$ mice as compared to WT controls confirms the validity of the differential expression analysis. The top enriched biological processes (GOBP) in the down-regulated gene list in $GR^{MuSC-/-}$ females highlighted processes such as translation, peptide metabolite processes, peptide, and amide biosynthetic process and organonitrogen compound biosynthetic process (Fig. 9 D). The top enriched GOBP terms for up-regulated genes revealed association with processes such as extracellular matrix (ECM) and structure organization, cell substrate-adhesion, regulation of cell division, cell cycle process and mitotic cell cycle process all consistent with MuSCs that are considered "activated" upon loss of GR (Fig. 9 E). Pathway analysis revealed that 16 genes were implicated in cell cycle regulation and phase transition [*Uhrf1, Kif20a, Nes, Cdc6, Racgap1, Pkmyt1, Plk4, Cenpf, Rbl1, Ccna2, Iqgap3, Aspm, Dtl, Ckap2, Ncapd2, Cenpe*], which ranked first (Fig. 9 E). Extracellular matrix and structure organization had 7 genes [*Col1a1, Lamb1, Fn1, Col15a1, Dmp1, Col1a2, Olfml2b*] that were differentially expressed (Fig. 9 F). Performing network analysis revealed that there were 2 upregulated clusters: one related to the extracellular matrix (with ECM organization and extracellular structure organization) and the other grouped terms related to cell cycle and cell division (such as cell division, mitotic cell cycle, cytokinesis, regulation of cell division and cell cycle, cell cycle G2/M phase transition and cytokinesis) (Fig. 9 G). The third cluster related to membrane attack complex was downregulated, and included the two genes namely, Complement C3 (*C3*) and Complement Factor H (*Cfh*), components of the innate immune response (Fig. 9 G). Gene set enrichment analysis (GSEA) was performed to rank all the ~15,000 filtered genes in our dataset first using the genotype contrast ($GR^{MuSC-/-}$ vs WT) in female mice. GSEA showed a strong enrichment in females, (green curve shows a left-ward accumulation of 610 genes) with a highly significant p-value (1.2e-13) and a normalized enrichment score (NES) of 2.03, for genes belonging to the "Reactome cell cycle" gene set,

implying that cell cycle genes are enriched in the female $GR^{-/-}$ MuSCs as compared to WT (Fig. 9 H). In the Reactome Extracellular Matrix organization gene set I found 159 core enriched genes in female $GR^{MuSC-/-}$ MuSCs as seen in the running enrichment score (ES) plot (Fig. 9 H). These data taken together demonstrate that RNA sequenced from $GR^{MuSC-/-}$ *in situ* fixed females are associated with genes and pathways that support a role for GR in the maintenance of the quiescent "G_0" state.

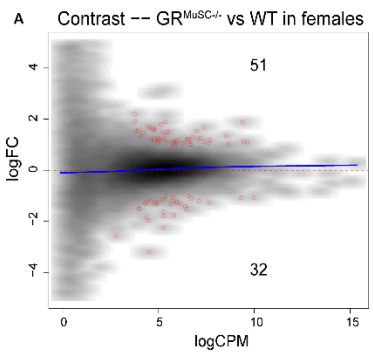

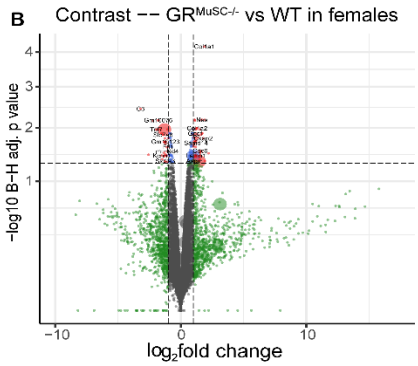

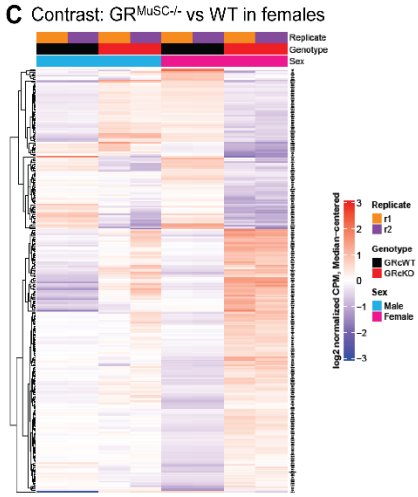

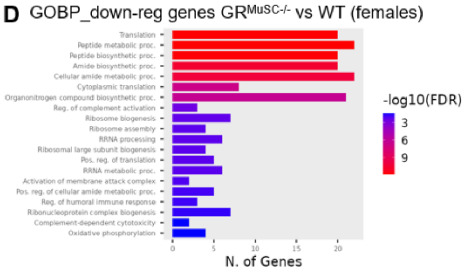

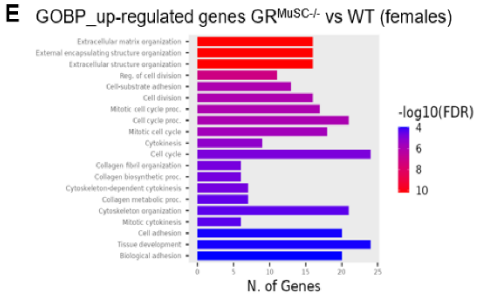

F

Enriched pathways in DEGs for the selected comparison:

Direction	adj.Pval	nGenes	Pathways
Down regulated	6.5e-03	2	Activation of membrane attack complex
Up regulated	3.6e-06	12	Mitotic cell cycle process
	3.6e-06	13	Mitotic cell cycle
	8.0e-06	14	Cell cycle process
	8.6e-06	7	Regulation of cell division
	2.3e-05	16	Cell cycle
	3.5e-05	10	Cell division
	9.6e-05	8	Mitotic cell cycle phase transition
	1.5e-04	7	Extracellular matrix organization
	1.5e-04	7	Extracellular structure organization
	1.5e-04	7	External encapsulating structure organization
	2.7e-04	8	Cell cycle phase transition
	2.9e-04	5	G2/M transition of mitotic cell cycle
	4.4e-04	5	Cell cycle G2/M phase transition
	7.0e-04	10	Regulation of cell cycle
	8.8e-04	5	Cytokinesis

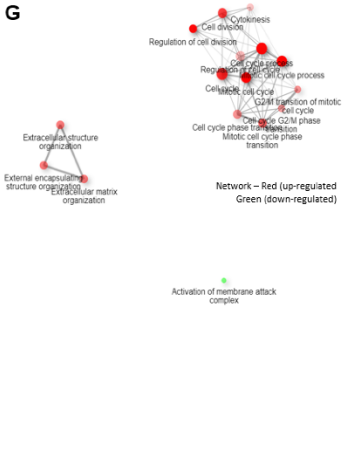

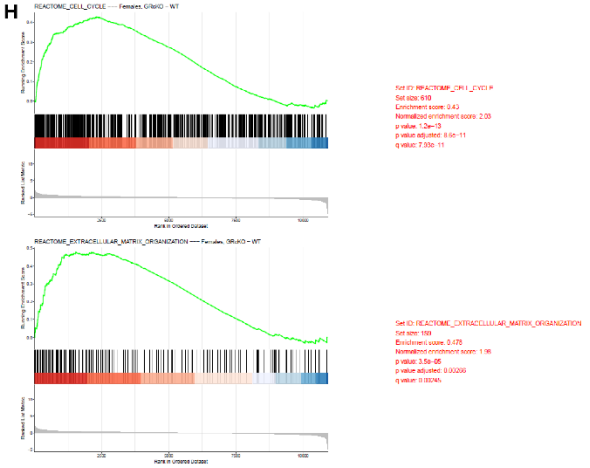

Figure 9: RNA sequenced from GR$^{-/-}$ in situ fixed female MuSCs are associated with genes and pathways involved in actively cycling cells.
(A) DEG contrasts in RNA sequenced from WT and GR$^{MuSC-/-}$ FFPE (in situ) fixed MuSCs from n=2 (multiple pooled mice) female mice. MA plot showing logCPM values on the X axis and logFC values on the Y axis in fixed MuSCs. (**B)** Volcano plot representing log_2FC on X-axis and -log10 adjusted P- value on the Y axis of DEGs in fixed muscle from (A). **(C)** A median-centered log2 normalized expression heatmap of the top 300 genes most differentially expressed, ranked by FDR without imposed cut-off in fixed MuSCs from (A). **(D)** Bar plot showing significantly down-regulated Gene Ontology (GO) terms from female mice (contrast GR$^{MuSC-/-}$ vs WT). **(E)** Bar plot showing the most significantly up-regulated GO terms from female (contrast GR$^{MuSC-/-}$ vs WT) mice. **(F)** Gene number and adjusted P-values for enriched pathways. **(G)** Pathway analysis of upregulated genes from female mice (contrast GR$^{MuSC-/-}$ vs WT) connected by nodes. Color key: Red-dots are up-regulated and green dots are down-regulated. **(H)** Running enrichment score (ES) plot of all genes processed for the sets "Reactome Cell Cycle" and "Reactome regulation of extracellular matrix organization" from female mice (contrast GR$^{MuSC-/-}$ vs WT).

Next, I analyzed the list of significant differentially expressed genes (DEGs) with an FDR of 0.05 or less in male mice. The MA plot for this comparison indicated that there were 93 up-regulated and 49 down-regulated genes (total 142 genes) in GR$^{MuSC-/-}$ male MuSCs as compared to WT (Fig. 10 A, B). A heat map of the top 300 differentially expressed genes by FDR without an imposed cut-off in male mice show distinct gene expression patterns between genotypes (Fig. 10 C). Gene ontology analysis for biological processes (GOBP) on up- and down-regulated genes in GR$^{MuSC-/-}$ males revealed that the top enriched terms are associated with processes such as oxidative phosphorylation, ATP metabolism, ribonucleoprotein complex biogenesis, aerobic respiration, and chromatin organization, all consistent with MuSCs that are considered "primed for activation" (Rodgers et al., 2014), in the absence of GR (Fig. 10 D). Enriched pathways (direction, upregulated) revealed that the top pathway includes genes implicated in the generation of precursor metabolites and energy [*Cox6c, Prelid1, UqcRb, Atp5j, Ndufa4, Cox7b, Atp5h, Atp5k, Gm10053, Hmgb1, Chchd2*] (Fig. 10 E). Placed second with 10 genes each was the ATP metabolic process [*Cox6c, UqcRb, Atp5j, Cox7b, Atp5h, Atp5k, Atpif1, Gm10053, Chchd2, Atp5o*] followed by energy derivation by oxidation of organic compounds [*Cox6c, Prelid1, UqcRb, Atp5j, Cox7b,*

Atp5h, Atp5k, Gm10053, Hmgb1, Chchd2] (Fig. 10 E). Cellular and aerobic respiration were the next most enriched categories in terms of number of genes. Network analysis revealed that there were 2 distinct clusters seen; one with chromatin assembly & disassembly, DNA conformation change, and DNA packaging grouped together (Fig. 10 F) and a second cluster regrouping terms such as electron transport chain (ETC), oxidative phosphorylation (OXPHOS), ATP metabolic processes synthesis, cellular respiration and generation of precursor metabolites and energy (Fig. 10 F).

GSEA ranked all the ~15,000 filtered genes in our dataset first using the genotype contrast ($GR^{MuSC-/-}$ vs WT) in male mice. When compared to "Cell cycle" in the Reactome database, the running enrichment score (ES) graphs showed an accumulation of 611 enriched genes towards the left with a highly significant p-value (8.3e-35) and a normalized enrichment score (NES) of 2.57 (Fig. 10 G), indicating that these genes are significantly enriched in the genes upregulated in $GR^{MuSC-/-}$ cells. The analysis also revealed strong enrichment for genes (162 genes) belonging to the Citric Acid Cycle (TCA) and Respiratory Electron Transport Chain gene sets (Fig. 10 G). These data taken together show that RNA sequenced from *in situ* fixed $GR^{MuSC-/-}$ males are associated with genes and pathways involved in cells being primed for activation.

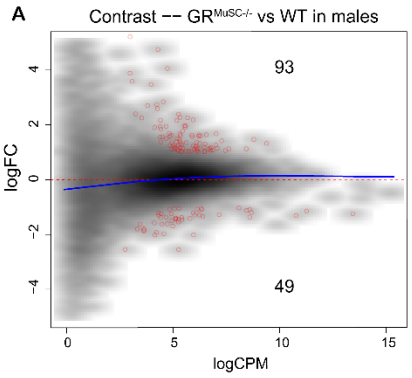

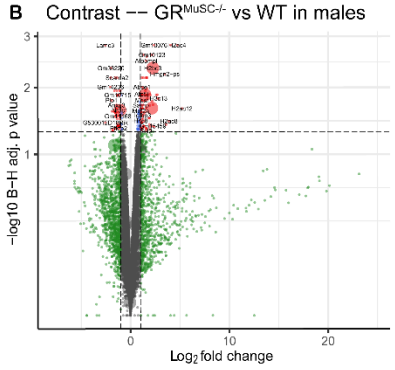

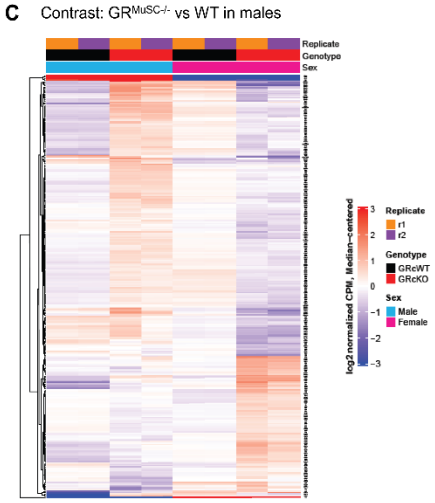

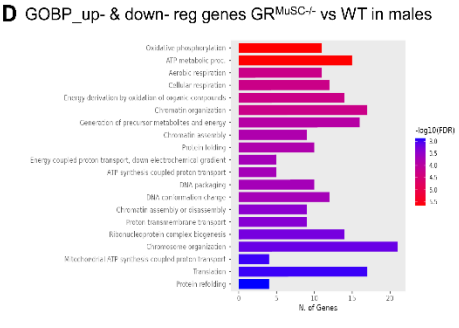

E Enriched pathways in DEGs for the selected comparison:

Direction	adj.Pval	nGenes	Pathways
Up regulated	4.4e-06	8	Oxidative phosphorylation
	6.1e-06	10	ATP metabolic process
	1.0e-05	9	Cellular respiration
	1.1e-05	10	Energy derivation by oxidation of organic compounds
	1.6e-05	8	Aerobic respiration
	3.3e-05	11	Generation of precursor metabolites and energy
	7.6e-05	7	Proton transmembrane transport
	9.9e-05	4	Energy coupled proton transport, down electrochemical gradient
	9.9e-05	4	ATP synthesis coupled proton transport
	1.5e-04	7	DNA packaging
	1.8e-04	8	DNA conformation change
	2.5e-04	6	Chromatin assembly
	4.0e-04	6	Electron transport chain
	5.4e-04	6	Chromatin assembly or disassembly
	1.2e-03	3	Mitochondrial ATP synthesis coupled proton transport

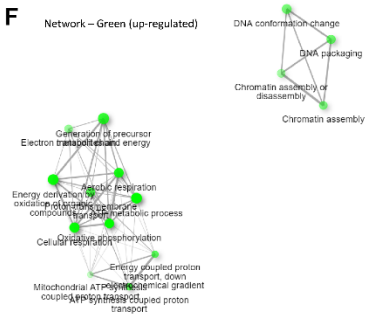

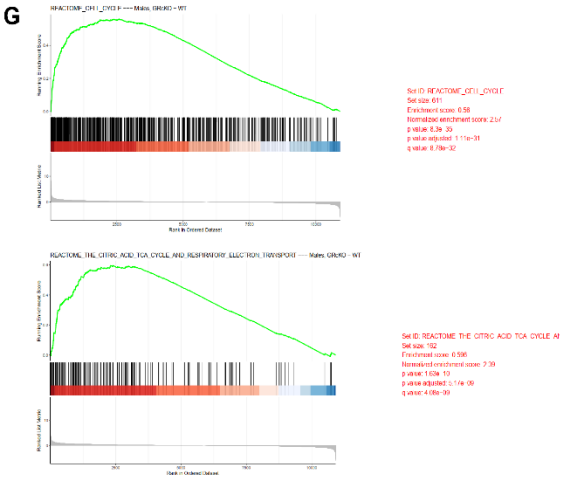

Figure 10: $GR^{MuSC-/-}$ in situ fixed male MuSCs are associated with genes and pathways involved in cells being primed for activation.
(A) Differentially expressed gene (DEG) contrast in RNA sequenced from WT and $GR^{MuSC-/-}$ FFPE (in situ) fixed MuSCs from n=2 (multiple pooled mice) male mice. MA plot showing the sum of expression values in all samples (in logCPM) on the X axis and logFC values ($GR^{MuSC-/-}$ vs WT) on the Y axis. The circles in red represent the significant differentially expressed genes that have a logFC bigger than 1 or smaller than -1 and an FDR significance value of 0.05 or less. **(B)** Volcano plot representing log_2FC on X-axis and -log10 adjusted p-value of all genes on the Y axis. Red dots have an absolute log2FC greater than 1 and adjusted p-value lower than 0.05 in fixed muscle from (A). **(C)** A heatmap of median-centered log2 normalized expression showing the top 300 DEGs (by FDR, regardless of logFC and FDR cut-off criteria) in fixed MuSCs from (A). **(D)** Bar plot showing the most significantly up-and-down regulated Gene Ontology (GO) terms fro m male mice (contrast $GR^{MuSC-/-}$ vs WT). **(E)** Number of genes and their adjusted p-values for enriched pathways. **(F)** Network of pathways in upregulated genes from male mice (contrast $GR^{MuSC-/-}$ vs WT) connected by nodes. Color key: Green is significantly up regulated. **(G)** Running enrichment score (ES) plot of ~15,000 genes processed for the gene sets "Reactome Cell Cycle" and "Reactome Citric Acid Cycle and Respiratory Electron Transport Chain" from male mice (contrast $GR^{MuSC-/-}$ vs WT).

To determine if loss of GR results in a more activated MuSC population, I compared our DE gene sets to publicly available datasets from early activated MuSCs. In 2014, Rando *et al* observed that MuSCs in the leg contralateral to the muscle in which an injury was induced (contralateral satellite cells, CSCs) possessed cycling properties in response to the distant injury, and these characteristics were different from those in non-injured (quiescent MuSCs, QSCs) and from injured tissue (activated MuSC, ASCs) (Rodgers et al., 2014). Rando *et al.*, demonstrated that the rather elusive state of muscle stem cell quiescence is composed of at least two distinct functional phases, G_0 and an 'alert' or "primed" phase that they term as G_{alert}. Using their published microarray dataset from FACS purified hindlimb MuSCs harvested immediately after isolation from uninjured {quiescent satellite cells (QSCs)} or muscles contralateral to a $BaCl_2$ injury {contralateral satellite cells (CSCs)} (GSE55490) (Rodgers et al., 2014), I performed Gene Set Enrichment Analysis to determine if the genes signature of CSC MuSCs (G_{alert}) were significantly enriched in our *in situ* fixed $GR^{MuSC-/-}$ samples. I found that genes upregulated by at least two-fold

in CSCs (compared to quiescent cells) are also largely up-regulated in $GR^{MuSC-/-}$ cells (compared to wild-type controls). In males, 51 G_{alert} genes (~49%) are enriched in *in situ* fixed $GR^{MuSc-/-}$ MuSCs (Fig. 11 A, B). To examine how the core genes are overrepresented within specific functional categories of genes, Gene Ontology for Biological Processes (GOBP) was performed and the analysis of the 51 genes revealed the top 5 enriched terms in males were cell cycle, cell cycle division, mitotic cell cycle process and chromosome organization, of which 31 (~60%) genes were found under the GOBP term "cell cycle" (Fig 11 C). In females, 65 core genes were enriched in the Rando dataset (Fig. 11 D, E) of which 42 (~64%) were related to cell cycle (Fig. 11 F). The following 39 genes were upregulated in both sexes upon loss of GR (*Mcm3, Mcm6, Sgo2a, Nek2, Tnnt2, Tpx2, Ube2c, Ccna2, Ect2, Ccne2, Smc2, Stmn1, Kif2c, Ncapg, Tyms, Cdca3, Prc1, Cdk1, Asf1b, Mcm5, Wdhd1, Pbk, Esco2, Nt5dc2, Diaph3, H1f1, Top2a, Birc5, Spag5, Aurkb, Kif15, Ccnb1, Uhrf1, Racgap1, Kif20a, Hells, Fam111a, Cdca5 and Kif11*) and upregulated two-fold in CSC compared to QSC, and thus form a core signature of cell cycle regulation by the GR.

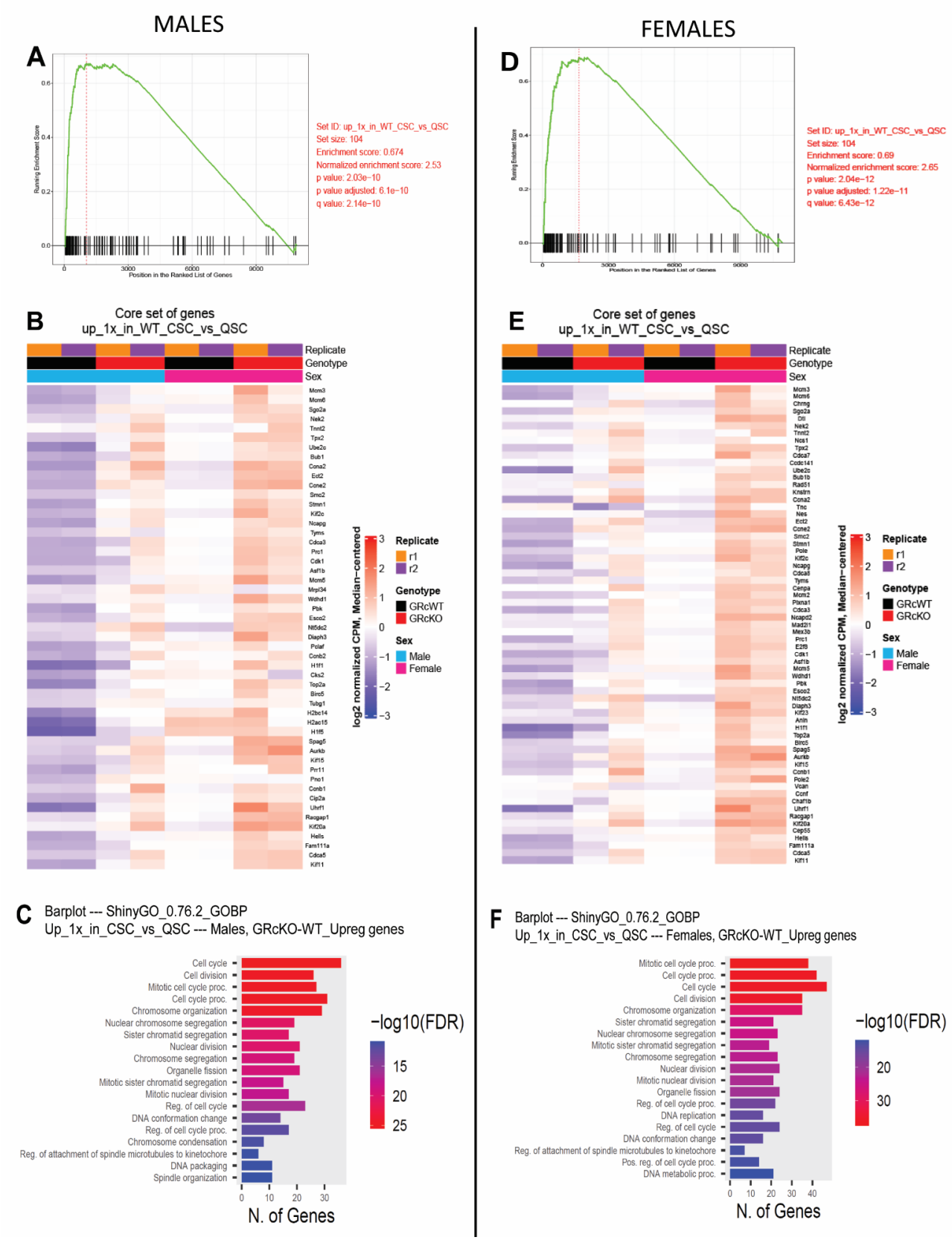
MALES
A
Running Enrichment Score
Position in the Ranked List of Genes
Set ID: up_1x_in_WT_CSC_vs_QSC
Set size: 104
Enrichment score: 0.674
Normalized enrichment score: 2.53
p value: 2.03e−10
p value adjusted: 6.1e−10
q value: 2.14e−10
B
Core set of genes
up_1x_in_WT_CSC_vs_QSC
Replicate
Genotype
Sex
log2 normalized CPM, Median−centered
Replicate
r1
r2
Genotype
GRcWT
GRcKO
Sex
Male
Female
C
Barplot --- ShinyGO_0.76.2_GOBP
Up_1x_in_CSC_vs_QSC --- Males, GRcKO-WT_Upreg genes
Cell cycle
Cell division
Mitotic cell cycle proc.
Cell cycle proc.
Chromosome organization
Nuclear chromosome segregation
Sister chromatid segregation
Nuclear division
Chromosome segregation
Organelle fission
Mitotic sister chromatid segregation
Mitotic nuclear division
Reg. of cell cycle
DNA conformation change
Reg. of cell cycle proc.
Chromosome condensation
Reg. of attachment of spindle microtubules to kinetochore
DNA packaging
Spindle organization
N. of Genes
−log10(FDR)
FEMALES
D
Running Enrichment Score
Position in the Ranked List of Genes
Set ID: up_1x_in_WT_CSC_vs_QSC
Set size: 104
Enrichment score: 0.69
Normalized enrichment score: 2.65
p value: 2.04e−12
p value adjusted: 1.22e−11
q value: 6.43e−12
E
Core set of genes
up_1x_in_WT_CSC_vs_QSC
Replicate
Genotype
Sex
log2 normalized CPM, Median−centered
Replicate
r1
r2
Genotype
GRcWT
GRcKO
Sex
Male
Female
F
Barplot --- ShinyGO_0.76.2_GOBP
Up_1x_in_CSC_vs_QSC --- Females, GRcKO-WT_Upreg genes
Mitotic cell cycle proc.
Cell cycle proc.
Cell cycle
Cell division
Chromosome organization
Sister chromatid segregation
Nuclear chromosome segregation
Mitotic sister chromatid segregation
Chromosome segregation
Nuclear division
Mitotic nuclear division
Organelle fission
Reg. of cell cycle proc.
DNA replication
Reg. of cell cycle
DNA conformation change
Reg. of attachment of spindle microtubules to kinetochore
Pos. reg. of cell cycle proc.
DNA metabolic proc.
N. of Genes
−log10(FDR)

Figure 11: Loss of GR in MuSCs induces expression of early in vivo activation genes.
(A) Running ES plot using contrast ($GR^{MuSC-/-}$ vs WT) in mice processed for the "Up_1x_in_CSC_vs_QSC" gene set from GSE55490 (Galert_microarray data). **(B)** A heatmap of the (median-centered) log2 normalized expression of the core genes enriched from (A). **(C)** Bar plot showing the most significantly up-regulated GO terms in males (contrast $GR^{MuSC-/-}$ vs WT) from (B). **(D)** GSEA in females, (contrast $GR^{MuSC-/-}$ vs WT) processed for the gene set "Up_1x_in_CSC_vs_QSC" from published microarray data. **(E)** A heatmap of core enriched genes from (D). **(F)** Bar plot showing Gene Ontology terms in female mice (contrast $GR^{MuSC-/-}$ vs WT) from (E).

To evaluate the degree of activation in MuSCs lacking GR, I compared our DEG list to publicly available RNA-seq datasets from *in situ* fixed (true quiescent, T0) and unfixed muscle after standard isolation (unfixed) (at 3 hours (T3) or 5 hours (T5) post-isolation) published by Machado *et al* (GSE103164) (Machado et al., 2017). GSEA revealed that genes induced in wild-type MuSCs during their early activation (between 3 and 5 hours of *in vitro* activation) are enriched in the upregulated genes from $GR^{MuSC-/-}$ cells, with 157 genes forming the core enriched gene set (Fig. 12 A). Of these, 35 (~22%) were upregulated two-fold in the most activated (T5 vs T3 hours post activation) cells using the contrast ($GR^{MuSC-/-}$ vs WT) (Fig. 12 B). To observe the enrichment of core genes in certain gene functional categories, I next performed Gene Ontology for Biological Processes (GOBP) analysis on the 35 core genes and found that ~42% of these genes were classified as "cell cycle" and included the following genes: *Kif11, Birc5, Cdk1, Igf1, Top2a, Esco2, Cenpf, Nek2, Nuf2, Knl1, Tpx2, Mki67, Aspm, Prc1 and Cenpe.* Nuclear division, organelle fission and mitotic nuclear division, chromosome segregation, and the mitotic cell cycle were also identified in this analysis (Fig. 12 C). Gene Set Enrichment Analysis (GSEA) in females also revealed a similar number (157) of core enriched genes (Fig. 12 D), of which 57 genes were upregulated two-fold in common between the most activated gene set in the $GR^{MuSC-/-}$ mice (Fig. 12 E). I found ~31% of these were associated in the cell cycle process and included the following genes: *Kif11, Birc5, Cdk1, Top2a, Esco2, Cenpf, Nek2, Nuf2, Knl1, Tpx2, Mki67, Aspm, Anln,*

Prc1, Bub1b, Cenpe, Kif18b and Ccnd1. Thus, the upregulation of these genes suggests a role for GR in maintaining quiescence.

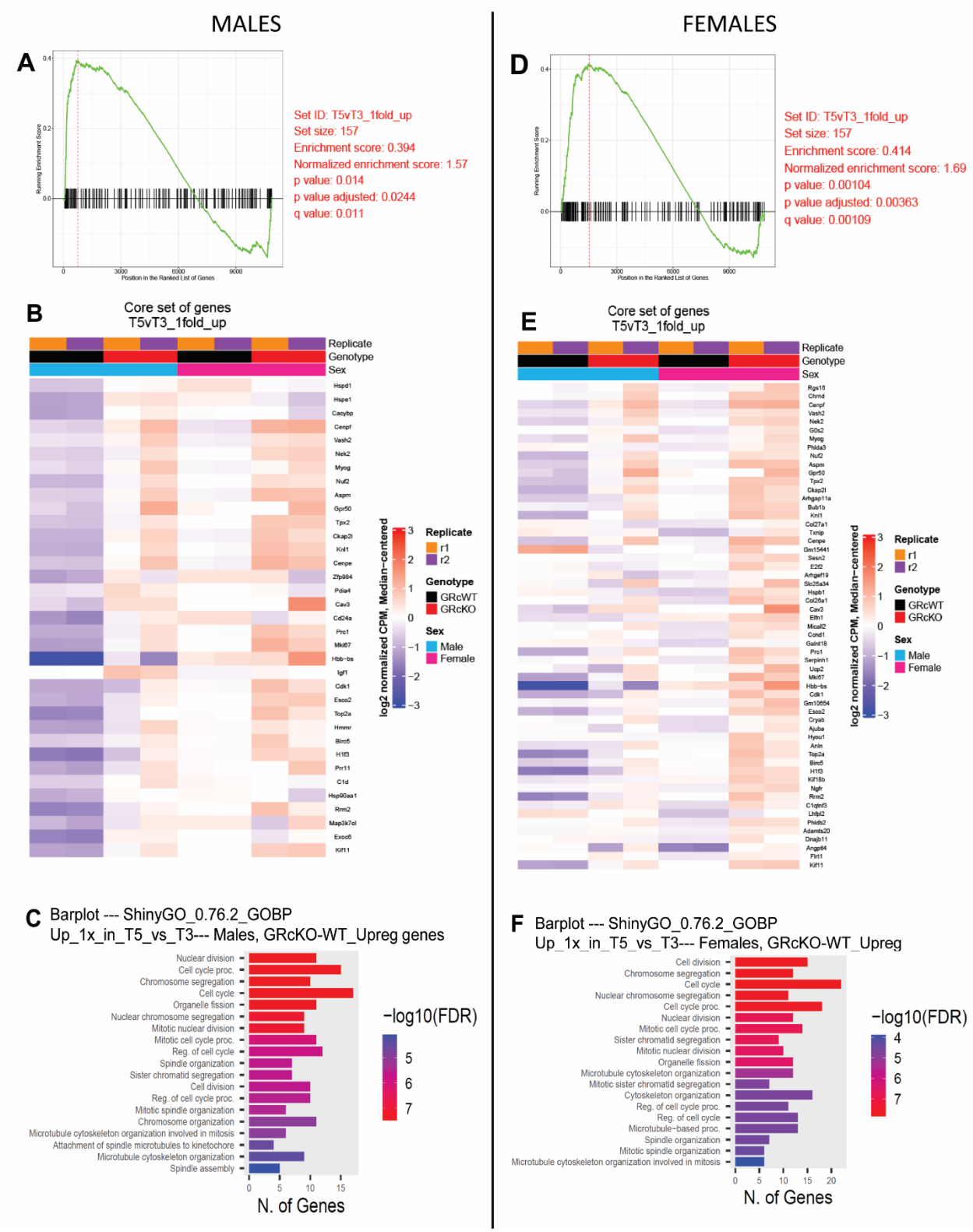
MALES
A
Set ID: T5vT3_1fold_up
Set size: 157
Enrichment score: 0.394
Normalized enrichment score: 1.57
p value: 0.014
p value adjusted: 0.0244
q value: 0.011
Running Enrichment Score
Position in the Ranked List of Genes
B
Core set of genes
T5vT3_1fold_up
Replicate
Genotype
Sex
log2 normalized CPM, Median−centered
Replicate
r1
r2
Genotype
GRcWT
GRcKO
Sex
Male
Female
C
Barplot --- ShinyGO_0.76.2_GOBP
Up_1x_in_T5_vs_T3--- Males, GRcKO-WT_Upreg genes
Nuclear division
Cell cycle proc.
Chromosome segregation
Cell cycle
Organelle fission
Nuclear chromosome segregation
Mitotic nuclear division
Mitotic cell cycle proc.
Reg. of cell cycle
Spindle organization
Sister chromatid segregation
Cell division
Reg. of cell cycle proc.
Mitotic spindle organization
Chromosome organization
Microtubule cytoskeleton organization involved in mitosis
Attachment of spindle microtubules to kinetochore
Microtubule cytoskeleton organization
Spindle assembly
N. of Genes
−log10(FDR)
FEMALES
D
Set ID: T5vT3_1fold_up
Set size: 157
Enrichment score: 0.414
Normalized enrichment score: 1.69
p value: 0.00104
p value adjusted: 0.00363
q value: 0.00109
Running Enrichment Score
Position in the Ranked List of Genes
E
Core set of genes
T5vT3_1fold_up
Replicate
Genotype
Sex
log2 normalized CPM, Median−centered
Replicate
r1
r2
Genotype
GRcWT
GRcKO
Sex
Male
Female
F
Barplot --- ShinyGO_0.76.2_GOBP
Up_1x_in_T5_vs_T3--- Females, GRcKO-WT_Upreg
Cell division
Chromosome segregation
Cell cycle
Nuclear chromosome segregation
Cell cycle proc.
Nuclear division
Mitotic cell cycle proc.
Sister chromatid segregation
Mitotic nuclear division
Organelle fission
Microtubule cytoskeleton organization
Mitotic sister chromatid segregation
Cytoskeleton organization
Reg. of cell cycle proc.
Reg. of cell cycle
Microtubule−based proc.
Spindle organization
Mitotic spindle organization
Microtubule cytoskeleton organization involved in mitosis
N. of Genes
−log10(FDR)

Figure 12: Loss of GR in MuSCs induces expression of early in vitro activation genes.
(A) Running ES plot of genes in males (contrast $GR^{MuSC-/-}$ vs WT) processed through the "most activation" (Up_1x_in_T5_vs_T3) dataset from GSE103164 (Machado T0_vs_T3_vs_T5 RNA-seq data). **(B)** A heatmap of the median-centered log2 normalized expression of the core gene set from (A). **(C)**. Bar plot showing the most significantly up-regulated Gene Ontology (GO) terms from male mice from (B). **(D)** GSEA in females (contrast $GR^{MuSC-/-}$ vs WT) processed through the gene set Up_1x_in_T5_vs_T3 from the Machado *et al* RNA-seq dataset. **(E)** A heatmap of the core gene set from (D). **(F)** Bar plot showing the most significantly up-regulated GO terms from female mice from (F).

Chapter 3: The GR and regulation of nuclear movements during myoblast fusion.

While regeneration was not adversely affected in $GR^{MuSC-/-}$ mice, I did observe histological differences in the regenerated muscle. Specifically, at 28 days post-CTX injury, $GR^{MuSC-/-}$ had significantly more regenerating fibers with greater than or equal to 3 centrally positioned nuclei, (Fig. 13 A-E). The increase in myonuclear number could represent an increase in myonuclear accretion due to precocious activation and differentiation or represent cytoskeletal defects that impair alignment and distribution of myonuclei in regenerating fibers. To explore potential defects in nuclear alignment, longitudinal sections through uninjured and injured muscle that was left to repair for 28 days were examined. In the WT uninjured muscle, the majority of the myonuclei were localized to the periphery under the sarcolemma as expected (Fig. 13 F). The injury of WT TA produced a single chain of myonuclei in a central location parallel to the long axis of the myofiber (Fig. 13 F). However, in regenerating $GR^{MuSC-/-}$ muscle, multiple parallel chains of nuclei were observed, suggesting defects in centration (Fig. 13 F). Taken together, these results suggest that there are nuclear alignment defects in the $GR^{MuSC-/-}$ mouse model suggesting a role for this receptor in nuclear movements during myoblast fusion.

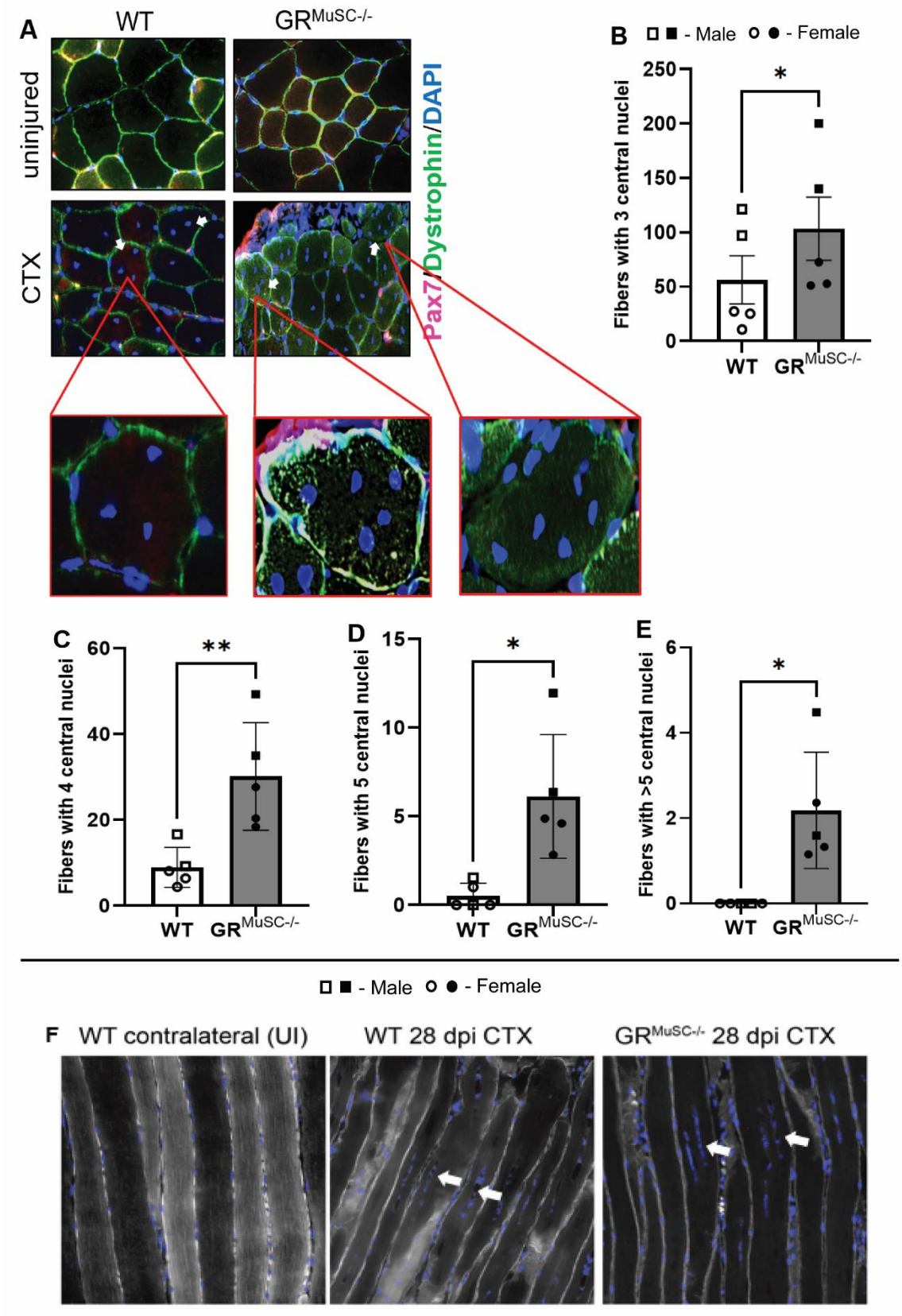
A
WT
GRMuSC-/-
uninjured
CTX
Pax7/Dystrophin/DAPI
B
□ ■ - Male ○ ● - Female
Fibers with 3 central nuclei
250
200
150
100
50
0
*
WT
GRMuSC-/-
C
Fibers with 4 central nuclei
60
40
20
0
**
WT
GRMuSC-/-
D
Fibers with 5 central nuclei
15
10
5
0
*
WT
GRMuSC-/-
E
Fibers with >5 central nuclei
6
4
2
0
*
WT
GRMuSC-/-
□ ■ - Male ○ ● - Female
F
WT contralateral (UI)
WT 28 dpi CTX
GRMuSC-/- 28 dpi CTX

Figure 13: Loss of the GR increases the number of centrally located myonuclei in regenerating muscle fibers.
(A) Uninjured and regenerating TA muscle cross- sections from *Nr3c1$^{fl/fl}$; Pax7$^{+/CreER}$* (GR$^{MuSC-/-}$) and *Nr3c1$^{fl/fl}$; Pax7$^{+/+}$* (WT) mouse 5 weeks after intraperitoneal (i.p.) tamoxifen administration stained with anti-PAX7 and anti-Dystrophin antibodies and DAPI to stain nuclei. **(B-E)** The average number of myofibers in WT and GR$^{MuSC-/-}$ mice with 3 **(B)**, 4 **(C)**, 5 **(D)** and >5 **(E)** centrally located nuclei from (G). **(F)** Position of nuclei stained with DAPI in longitudinal sections from WT, contralateral (UI) TA muscle, 28 days post injury with cardiotoxin (WT, CTX-injured) and TA muscle from GR$^{MuSC-/-}$ mice 28 days after injury with cardiotoxin (GR$^{MuSC-/-}$, CTX-injured). Scale bar= 10um, n=5 pairs. Data is represented as ± SD, *p < 0.05, **p < 0.01, ***p <0.001, ****p <0.0001, ns = not significant by two-tailed paired Student t-test using GraphPad Prism 9.4.1 for statistical analysis and graphical representation.

Nuclear movements and placement during myogenic differentiation are regulated by microtubules and defects in the cytoskeleton, such as what is observed in DMD results in abnormal nuclear positioning. To explore a potential role for GR in the regulation of the cytoskeleton, I isolated primary myoblasts from WT and GR$^{MuSC-/-}$ mice. Isolated myoblasts were treated in culture with 4-OH tamoxifen to generate a non-functional GR protein (GR$^{MuSC-/-}$), or to create WT controls (Fig. 14 A). WT and GR$^{MuSC-/-}$ myoblasts were differentiated for two days under low serum conditions (Fig. 14 B-D). While there were no significant differences between the differentiation (% nuclei in myosin heavy chain (MyHC) positive cells) and fusion (average number of nuclei per MyHC+ myotube) indices between the WT and GR$^{MuSC-/-}$ cultures, consistent with our findings *in vivo*, the myotubes produced from GR$^{MuSC-/-}$ cells had a pronounced rounded morphology in contrast to the elongated myotube shape produced by WT cells (Fig. 14 B). Further, the nuclei in GR$^{MuSC-/-}$ myotubes clustered at the center of the myotube without evidence of alignment or spreading (Fig. 14 B). To quantify cell shape, I measured the circularity index. I observed a 2-fold increase (~50% higher) in the circularity index in the GR$^{MuSC-/-}$ myotubes as compared to wild-type litter mate controls (Fig. 14 E), indicating that GR regulates myotube morphology *in vitro*. The average length of the myotubes was also significantly decreased (as much as a 40% reduction) in myotubes lacking GR (Fig. 14 F).

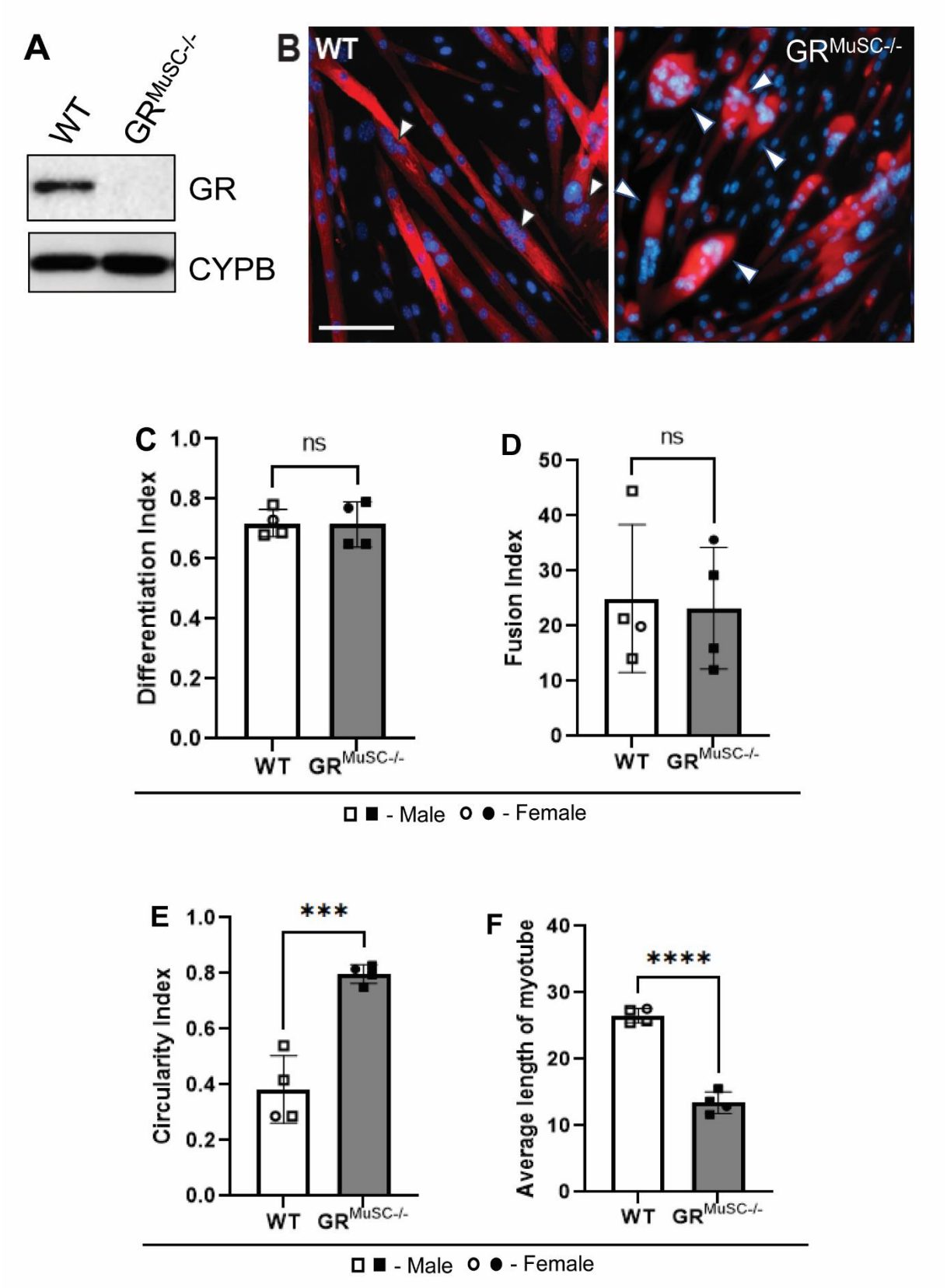
A
WT
GRMuSC-/-
GR
CYPB
B
WT
GRMuSC-/-
C
Differentiation Index
ns
WT
GRMuSC-/-
D
Fusion Index
ns
WT
GRMuSC-/-
□ ■ - Male ○ ● - Female
E
Circularity Index
***
WT
GRMuSC-/-
F
Average length of myotube
****
WT
GRMuSC-/-
□ ■ - Male ○ ● - Female

Figure 14: Loss of GR expression in differentiating myoblasts results in abnormal myotube morphology.

(A) Isolated satellite cells from *Nr3c1*$^{fl/fl}$; *Pax7*$^{+/CreER}$ (GR$^{MuSC-/-}$) and *Nr3c1*$^{fl/fl}$; *Pax7*$^{+/+}$ (wild-type, WT) mice were treated with tamoxifen for 3 days and GR expression was verified by western blot. **(B)** Cells from (A) were differentiated for 2 days and immunostained for myosin heavy chain (MyHC, red) and counterstained for nuclei with DAPI (blue). Scale bar = 100 um. **(C)** Differentiation index (% nuclei in MyHC+ cells compared to total nuclei) from (B). **(D)** Fusion index (average # nuclei per MyHC+ cell) from (B). **(E)** Circularity index of cells in (B) calculated using thresholding on FIJI, where 1= a perfect circle and 0= a straight line. **(F)** Average length of myotube from (B). Arrowheads indicate abnormally rounded myotubes in GR$^{MuSC-/-}$ cultures as compared to indicating normal elongated myotubes in WT cultures n=4 pairs. Data is represented as ± SD, *p < 0.05, **p < 0.01, ***p <0.001, ****p <0.0001, ns = not significant by two-tailed paired Student t-test using GraphPad Prism 9.4.1 for statistical analysis and graphical representation.

Given the morphological defects seen in GR$^{MuSC-/-}$ myotubes and myofibers (Fig. 14 B), I assessed the effect of the synthetic GR ligand dexamethasone (DEX) on primary myoblast cell morphology. To this end, I differentiated primary myoblasts from C57BL/6 mice, in the continuous presence of 10 nM, 100 nM and 1 uM DEX for 2 days. After 48 hours in DM, I fixed the cells and performed immunostaining for anti-MyHC (Myosin heavy chain) to stain the contractile apparatus in multinucleated myotubes. I observed an overall increase in myogenic differentiation and myotube size as quantified by the differentiation and fusion indices (Fig. 15 A, B). However, while WT cultures had elongated myotubes with evenly spaced nuclei as expected, the 48 hours DEX treatment resulted in abnormally large stellate myotubes at all concentrations tested (Fig. 15 C). I observed that the average angle of branches in vehicle-treated myotubes was approximately 157°, which agrees with the observation that the majority of myotubes without treatment were largely straight and elongated. However, DEX treatment reduced the branch angle of myotubes to an average of 138° giving them a stellate appearance (Fig. 15 D). These data suggests that DEX treatment as well alters cell morphology in culture.

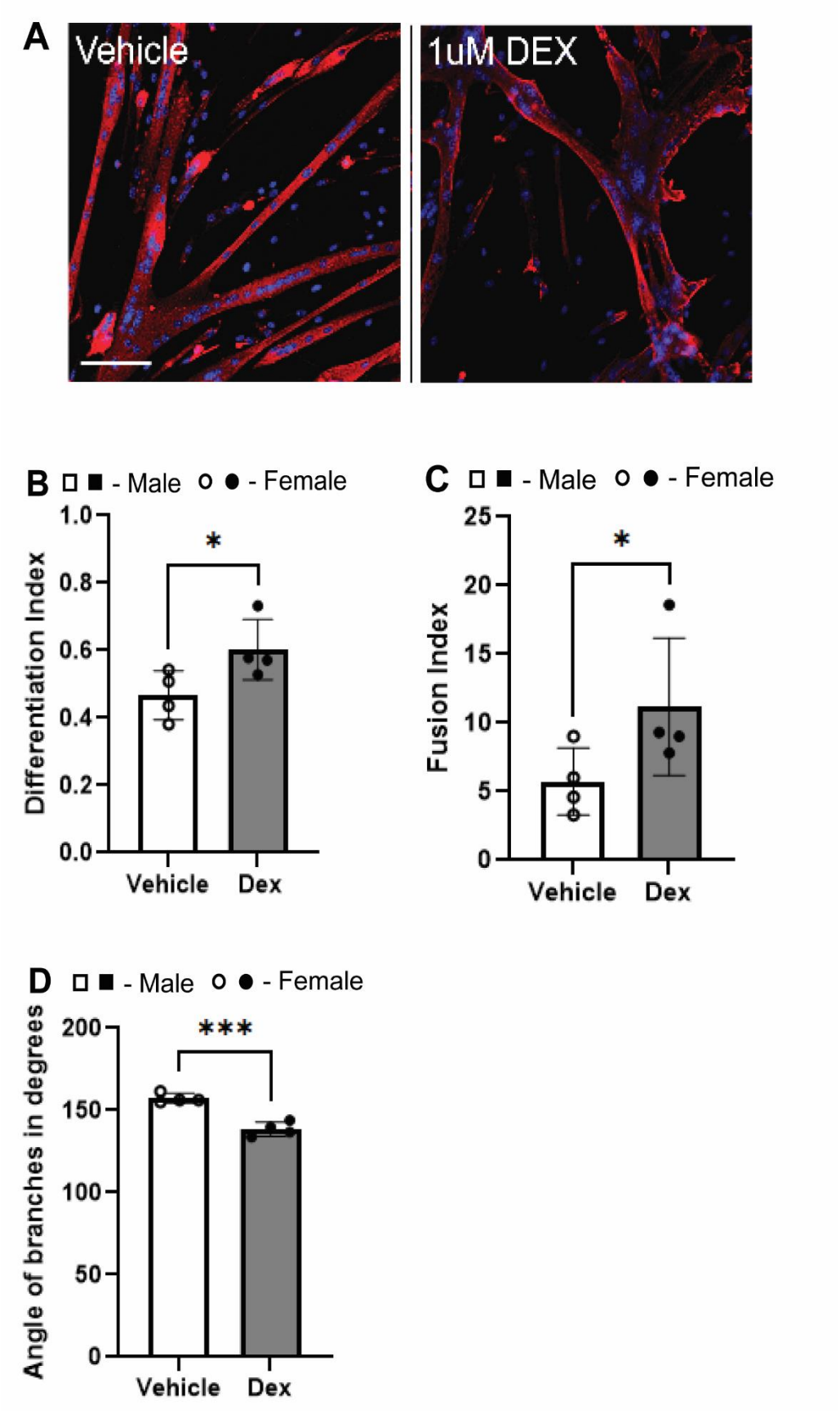
A
Vehicle
1uM DEX
B
- Male
- Female
Differentiation Index
1.0
0.8
0.6
0.4
0.2
0.0
*
Vehicle
Dex
C
- Male
- Female
Fusion Index
25
20
15
10
5
0
*
Vehicle
Dex
D
- Male
- Female
Angle of branches in degrees
200
150
100
50
0
***
Vehicle
Dex

Figure 15: Dexamethasone treatment increases myoblast fusion but impairs normal elongation of myotubes in culture.
(A) Primary myoblasts form C57BL/6 mice were differentiated for 48 hours in the presence of 100% ethanol (vehicle) or dexamethasone (DEX) and immunostained for Myosin Heavy chain expression (red) and counterstained with DAPI. The differentiation index (# nuclei in myosin heavy chain+ cells/total nuclei) was calculated. **(B)** Fusion index (average number of nuclei per myotube) in cells cultured as in (A). **(C)** Representative images from (A) immunostained for MyHC (red) and DAPI (blue). **(D)** Angle of branches (in °C). Scale = 50um, n=4 pairs. Data is represented as ± SD, *p < 0.05, **p < 0.01, ***p <0.001, ****p <0.0001, ns = not significant by two-tailed paired Student t-test using GraphPad Prism 9.4.1 for statistical analysis and graphical representation.

I next assessed nuclear positioning in GR deficient ($GR^{MuSC-/-}$) myotubes. WT and $GR^{MuSC-/-}$ myoblasts were differentiated for two days under low serum conditions post excision of GR *in vitro* (Fig. 16 A). Myotubes were immunostained for MyHC to visualize myotubes and the percentage of nuclei that were not placed along the central axis of the cell were quantified. I found that there was an ~50% increase in the percentage of nuclei that were not located on the long axis of $GR^{MuSC-/-}$ myotubes as compared to WT-controls (Fig. 16 B). This suggests that loss of GR impairs the cell's ability to align nuclei along the central longitudinal axis resulting in a defect in alignment. Next, I looked at the step of "spreading" in WT and $GR^{MuSC-/-}$ myoblasts (Fig. 16 C). Using the line tool in FIJI, I analyzed the inter-nuclear distance (μm) between nuclei present in myotubes in both genotypes to assess spreading (Fig. 16 D). I found that there was an ~54% decrease in the average inter-nuclear distance between myonuclei lacking GR as compared to the controls, resulting in the clustering of nuclei (Fig. 16 A, C, D) and the rounded morphology seen earlier (Fig. 14 B, E, F).

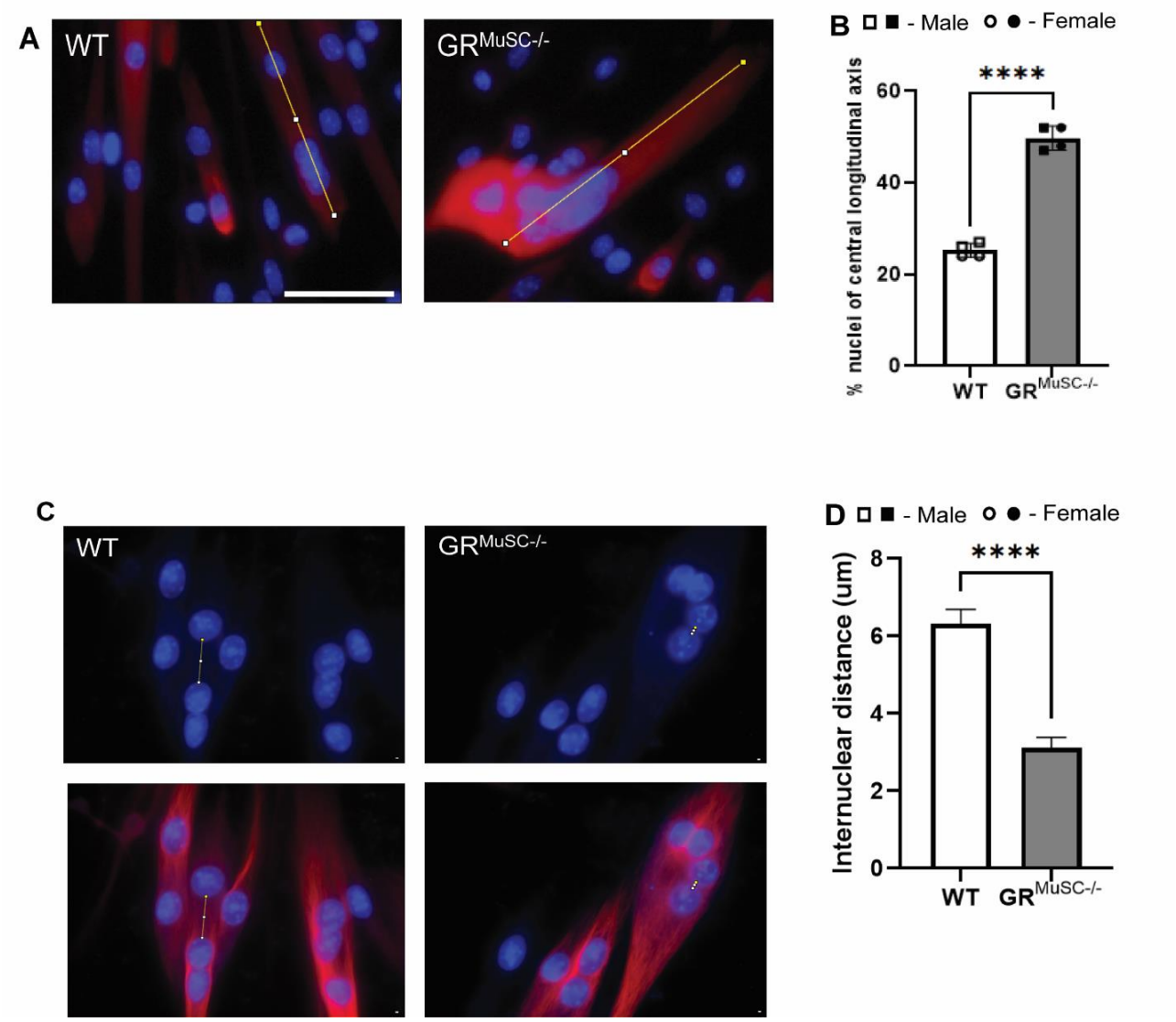

Figure 16: Loss of the GR increases nuclear alignment defects in primary myotubes.
(A) MACS-isolated primary myoblasts from $GR^{MuSC-/-}$ and WT mice differentiated in DM for 48 hours and immunostained with anti-MyHC and DAPI to quantify alignment defects in myotubes from both mice. **(B)** Nuclei off the central longitudinal axis (as a percentage) in myotubes from (A), n=4 pairs. **(C)** MACS-isolated myoblasts from $GR^{MuSC-/-}$ and WT mice differentiated in DM for 48 hours and immune-stained with anti-alpha-tubulin and DAPI to quantify spreading defects in myotubes from both mice. **(D)** Inter-nuclear distance (in microns) between myonuclei along myotubes from (A). Scale bar = 10um, n=4 pairs. Data is represented as ± SD, *p < 0.05, **p < 0.01, ***p <0.001, ****p <0.0001, ns = not significant by two-tailed paired Student t-test using GraphPad Prism 9.4.1 for statistical analysis and graphical representation.

Given the defect in microtubule dependent nuclear movement and the lack of studies regarding the regulation of these MT networks by glucocorticoids in skeletal muscle, I wanted to assess the effect of DEX treatment on MT networks. Microtubules and Golgi elements in the *mdx* are disordered and have been linked to the dystrophic pathology seen in these mice (Oddoux et al., 2019). For this purpose, I isolated myofibers from the extensor digitorum longus (EDL) muscle of *mdx* mice (aged 8 weeks) and age-matched controls (C57BL/10J). I treated these mice with nocodazole (4ug/ml for 4h, a MT depolymerizing agent) and vehicle and let them recover for 4 hours before fixing and immunostaining for α-tubulin to mark the microtubule network. In accordance with data from the literature (Oddoux et al., 2013a, 2019), I observed that control myofibers had a highly organized MT network with longitudinal bundles and thinner attachments at perpendicular angles (Fig. 17 A). After nocodazole treatment, which caused the entire MT network to depolymerize, the regrowth was mostly found around myonuclei in the myofiber, and the microtubules re-emerged parallel to the long axis of the fiber or at 90° angles. This intense network of bundles seen in the WT were found to be more diffuse in the *mdx* mouse, with numerous random connections projecting at all angles, without preference for orthogonal MT growth. Nocodazole treatment highlighted this lack of organization in the *mdx* mouse, with new MTs emerging in multiple directions, producing a random network (Fig. 17 A). To determine if glucocorticoids influence MT organization, I isolated myofibers from WT and *mdx* mice and cultured them in the presence of 100 nM DEX for 48 hours before immunostaining with alpha-tubulin. I noticed that DEX treatment promoted the bundling of MTs along the long axis of the myofiber in WT cells as seen earlier, producing denser networks of parallel MTs as compared to untreated WT fibers (Fig. 17 B). DEX- treatment of *mdx* fibers resulted in a regularization of the MT network, with reduced global MT density and enhanced parallel bundling (Fig. 17 B). Further,

$GR^{MuSC-/-}$ myotubes in culture also demonstrate highly disorganized MT networks (Fig.17 C). These data taken together suggest that glucocorticoids promote microtubule bundling and network organization.

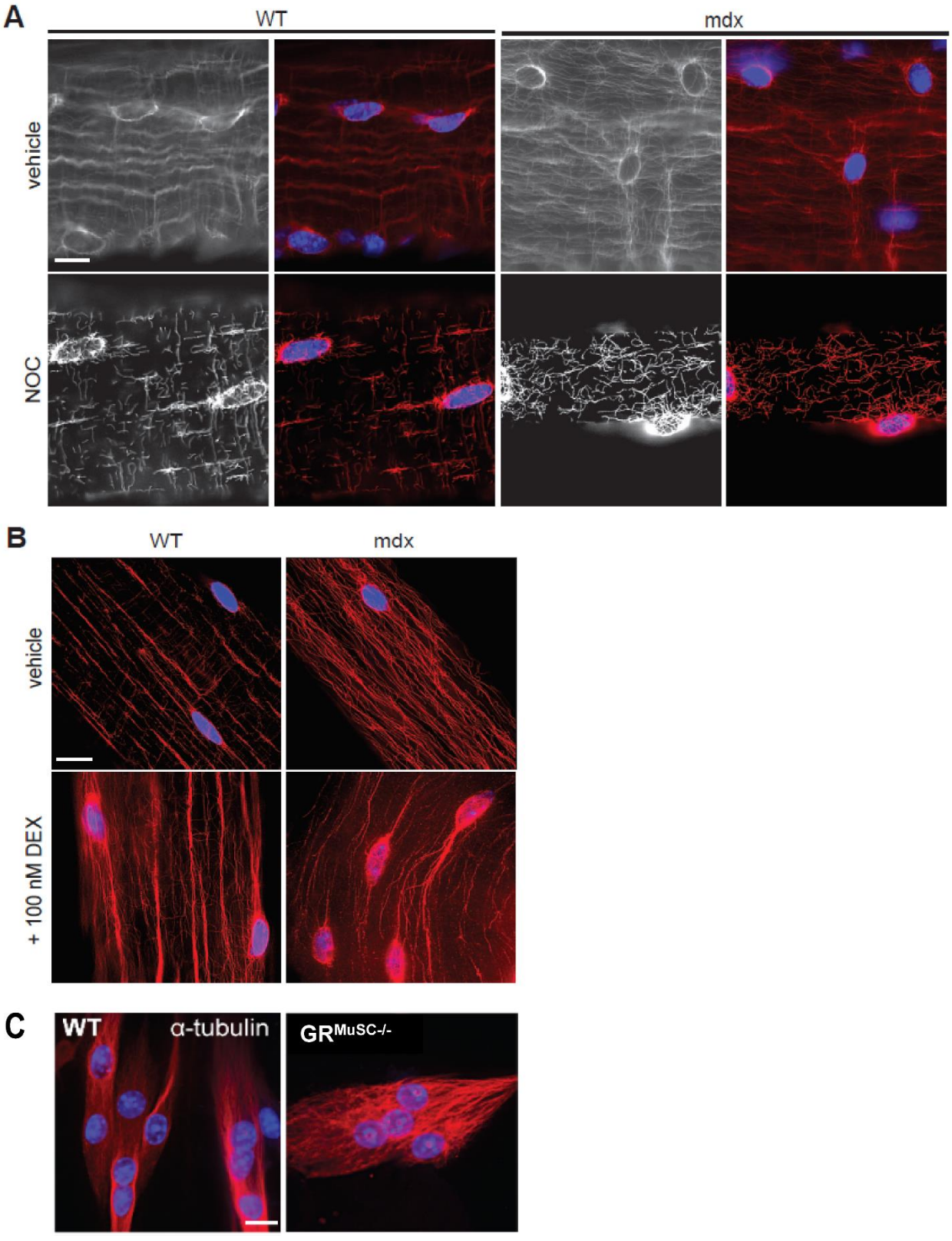
A
WT
mdx
vehicle
NOC
B
WT
mdx
vehicle
+ 100 nM DEX
C
WT
α-tubulin
GRMuSC-/-

Figure 17: Glucocorticoids promote microtubule bundling and organization.
(A) Myofibers isolated from the EDL muscle of WT and *mdx* mice, aged 8 weeks, were treated with nocodazole (NOC) for 4 hrs or with vehicle to depolymerize microtubule networks and allowed to recover for 4 hours before immunostaining for α-tubulin. Nuclei are counterstained with DAPI. Scale bar = 10 um. **(B)** Myofibers from WT and *mdx* mice, aged 8 weeks, were treated with vehicle or 100 nM dexamethasone (DEX) for 48 hours before immunostaining for α-tubulin. **(C)** Immunostaining for alpha-tubulin in myotubes derived from WT and $GR^{MuSC-/-}$ mice. Scale bar = 10 um.

Changes in morphology are manifestations of changes in the cell's cytoskeleton, which comprises of microtubules, actin filaments, and intermediate filaments. To elucidate the role of GR in the regulation of the cytoskeleton, I performed bulk RNA sequencing on WT and $GR^{MuSC-/-}$ (conditional GR knockouts) proliferating myoblasts cultured in the presence or absence of Dexamethasone (DEX) for 24 hours. Knockdown of GR was confirmed by western blot (Fig. 18 A). In the vehicle and DEX-treated samples from $GR^{MuSC-/-}$ myoblasts, GR expression was decreased. DEX treatment of WT myoblasts also resulted in decreased GR expression (as compared to the DMSO control), which is consistent with the autoregulation of receptor protein turnover, in part through the ubiquitin-proteasome pathway that has been described (Wallace & Cidlowski, 2001). The differentially expressed gene statistics revealed that 261 genes were upregulated, and 301 genes were downregulated in DMSO (vehicle) treated $GR^{MuSC-/-}$ myoblasts as compared to WT (Fig. 18 B, C). A DEG heat map of DMSO-treated $GR^{MuSC-/-}$ myoblasts (as one of the comparisons) shows good concordance between both replicates of the same condition in terms of their significant differentially expressed genes (Fig. 18 D).

To observe the enrichment of core genes in certain gene functional categories, I next performed Gene Ontology for Biological Processes (GOBP) analysis on the differentially expressed genes in DMSO-treated $GR^{MuSC-/-}$ myoblasts. The top enriched GOBP terms in up-regulated genes from DMSO-treated GR^{MuSC} myoblasts highlighted processes such as anatomical structure formation in morphogenesis, circulatory system development, cellular locomotion, and

vasculature development. (Fig. 18 E). The down-regulated genes in DMSO-treated $GR^{MuSC-/-}$ myoblasts were enriched for GO terms being associated with processes such as muscle system process, muscle structure development, muscle cell differentiation, muscle contraction and muscle organ development, all consistent with loss of GR in proliferating myoblasts affecting muscle morphology (Fig. 18 F). I further explored the gene set related to muscle adaptation process and found a significant downregulation of important skeletal muscle specific genes such as *Mef2c, Actn3, Tcap, Mymk, Tnni1, Myog and Acta1* (Fig. 18 D, F). The role of *Mef2c*, *Myog* and *Mymk* have been extensively studied during skeletal muscle development and function. Further we also see the downregulation of *Tcap* (titin-cap) that binds to the titin Z1-Z2 domains and is a substrate of titin kinase interactions which are thought to be critical for sarcomere assembly of the contractile apparatus. We also see the downregulation of *Acta1* another major constituent of the contractile apparatus, suggesting a role for GR during muscle contraction process. Further, there is downregulation of skeletal specific actinin *Actn3*, that functions as a structural component of the sarcomeric Z line involved in crosslinking actin containing thin filaments and is important in sarcomere assembly. *Tnni1,* is the inhibitory subunit of the troponin complex, blocking actin-myosin interactions and thereby mediating striated muscle relaxation. Data generated from this RNA seq agrees with our previous in culture data (Fig. 14 B) for GR being required for proper muscle structure development and contraction. These results taken together suggest that loss of GR in proliferating myoblasts down-regulates genes associated with skeletal muscle development and contraction assembly.

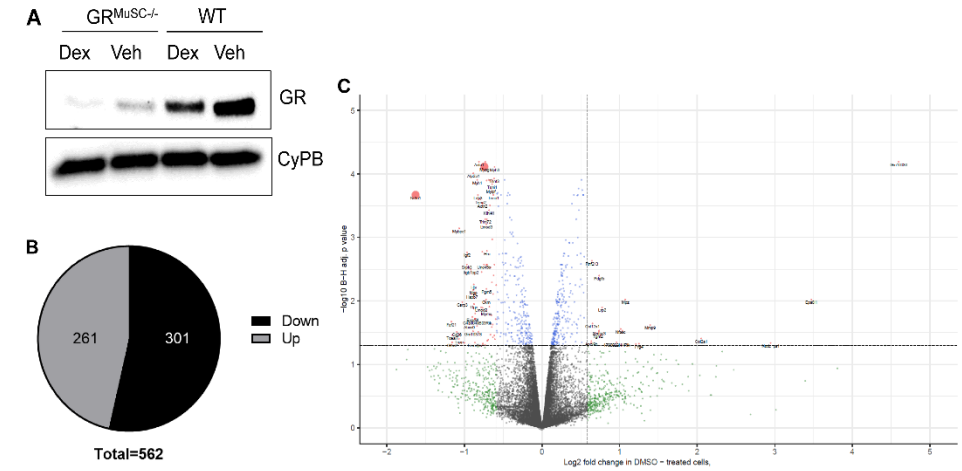

D Effect of GR$^{MuSC-/-}$ and/or DEX treatment

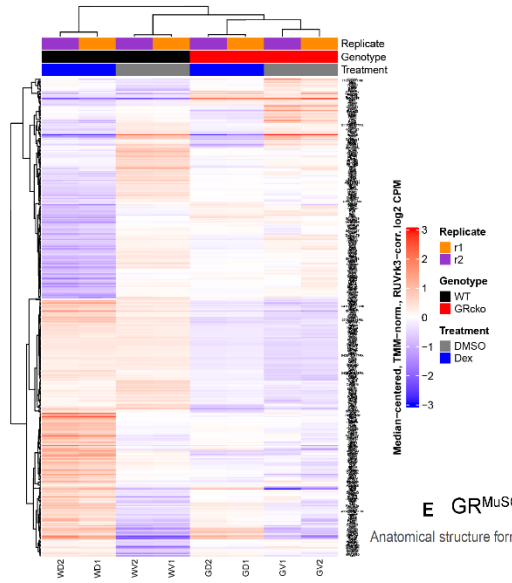

E GR$^{MuSC-/-}$ effect in DMSO -- Males, -- Up reg

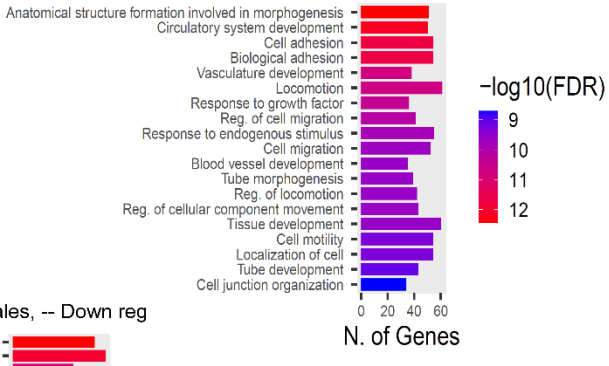

F GR$^{MuSC-/-}$ effect in DMSO -- Males, -- Down reg

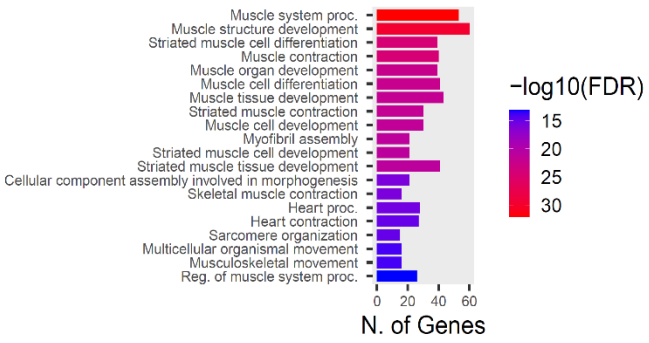

Figure 18: Loss of GR in proliferating myoblasts downregulates the skeletal muscle structure and development process.
(A) Proliferating primary myoblasts treated ± DEX for 24h from male *Nr3c1$^{fl/fl}$; Pax7$^{+/CreER}$* (GR$^{MuSC-/-}$) and *Nr3c1$^{fl/fl}$; Pax7$^{+/+}$* (WT) mice treated with i.p. tamoxifen for 5 days and GR expression was then verified by Western blot. **(B)** Differentially expressed gene (DEG) regulation (up- or down- regulated) contrasts in males on RNA sequenced from WT and GR$^{MuSC-/-}$ proliferating myoblasts treated with DEX for 24h from (A) **(C)** A volcano plot representing log2FC on X-axis and -log10 adjusted p-value of all genes on the Y axis. Red dots have an absolute log2FC greater than 1 and adjusted p-value lower than 0.05 in fixed muscle from (A). **(D)** A heatmap of log FC values plotted showing the DEGs from proliferating myoblasts in WT and GR$^{MuSC-/-}$ male mice as in (A). **(E)** Bar plot showing the most significantly up-regulated Gene Ontology (GO) terms from DMSO-treated GR$^{MuSC-/-}$myoblasts. **(F)** Bar plot showing the most significantly down-regulated Gene Ontology (GO) terms DMSO-treated GR$^{MuSC-/-}$myoblasts, n=3 male pairs.

Given the morphology changes seen with DEX treatment on WT primary myoblasts (Fig. 15 B), I examined the effect of DEX treatment on the cytoskeleton of WT proliferating cells in our RNA seq data. DEX treatment of WT myoblasts resulted in 948 upregulated and 722 downregulated genes from a total of 1670 DE genes (Fig. 19 A). The volcano plot shows the most significantly expressed genes in comparison to their fold-change values (Fig. 19 B). Comparing the effect of DEX on WT and GR$^{MuSC-/-}$ proliferating myoblasts, the heat map shows the highest number of DE genes in this contrast, and a similar trend between both replicates of the significant differentially expressed genes in WT myoblasts ± DEX (Fig. 19 C). The top enriched GOBP terms in the up-regulated genes in DEX-treated WT myoblasts highlighted processes such as ribonucleoprotein complex and ribosome biosynthesis, rRNA processing and rRNA metabolic process and translation (Fig. 19 D). GOBP terms in the down-regulated genes in WT myoblasts treated with DEX showed the top enriched terms being associated with processes such as, circulatory system development, negative regulation of multicellular organismal processes, tube development and morphogenesis, regulation of cell migration, adhesion, and tissue development (Fig. 19 E). Given that morphological changes result from adaptations in the cytoskeleton as seen previously in GR$^{MuSC-/-}$ treated myoblasts, we decided to use a biased approach to observe remodelling of the cytoskeleton in our DEX-treated WT myoblasts. Surprisingly, I found that DEX

treatment significantly up-regulated certain smooth-muscle specific genes such as *Myh11, Lmod1 and Cnn1. Myh11 and Lmod1* function as major contractile proteins of smooth muscle specific cells. *Cnn1* (actin-binding protein), a negative regulator of vascular associated smooth muscle cell proliferation is upregulated with DEX treatment in our cultures. Additionally, there is upregulation of the troponin proteins, specifically *Tnnt1* (slow skeletal type) and *Tnnt2* (cardiac type) in our DEX-treated WT myoblasts. These results taken together suggest that DEX treatment in WT myoblasts appears to up-regulate certain genes associated with a non-skeletal specific phenotype potentially leading to the subsequent remodelling of the cytoskeleton.

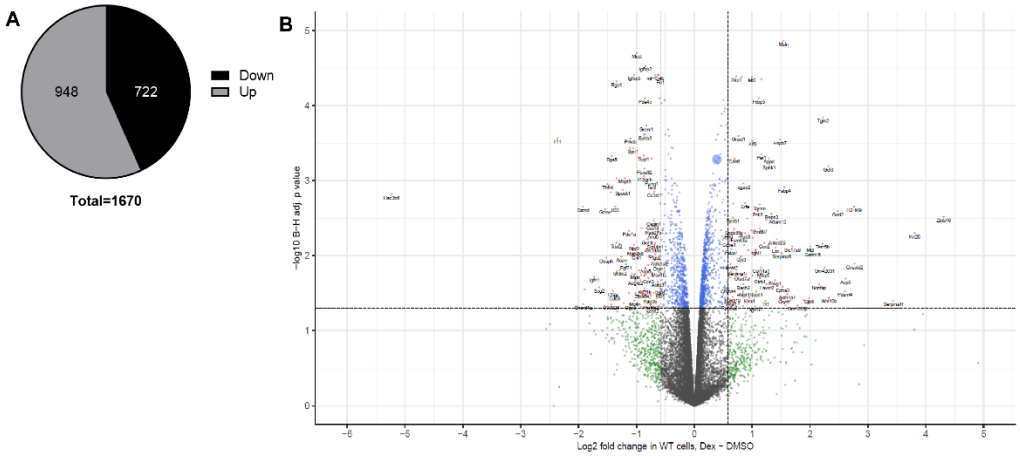

C Effect of GR$^{MuSC-/-}$ and/or DEX treatment

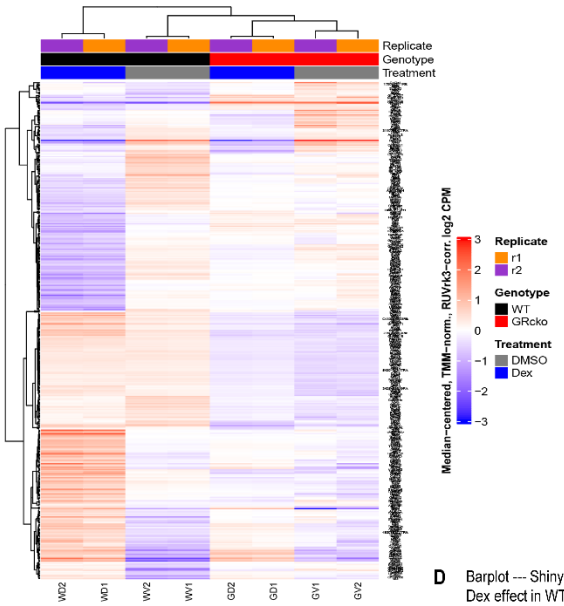

D Barplot --- ShinyGO_0.76.2_GOBP
Dex effect in WT-- Males, --Up reg genes

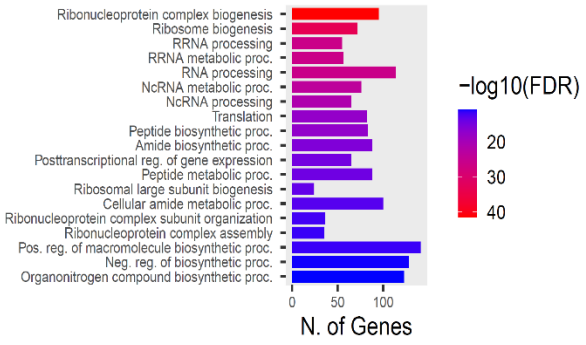

E Barplot --- ShinyGO_0.76.2_GOBP
Dex effect in WT-- Males, --Down reg genes

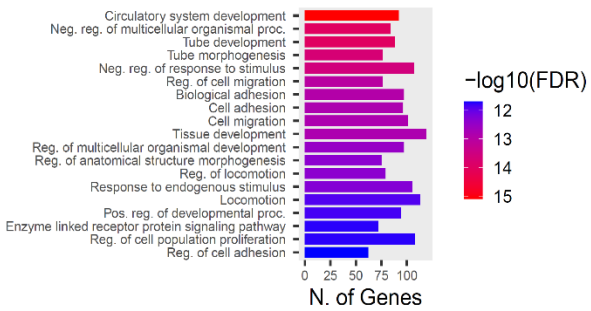

Figure 19: DEX treatment in WT proliferating myoblasts induces expression of cytoskeletal and sarcomeric components.

(A) Proliferating primary myoblasts treated ± DEX for 24h from male *Nr3c1*$^{fl/fl}$*; Pax7*$^{+/CreER}$ (GR$^{MuSC-/-}$) and *Nr3c1*$^{fl/fl}$*; Pax7*$^{+/+}$ (WT) mice treated with i.p. tamoxifen for 5 days and GR expression was then verified by Western blot. **(B)** A volcano plot representing log2FC on X-axis and -log10 adjusted p-value of all genes on the Y axis. **(C)** A heatmap of logFC values plotted showing the differentially expressed gene (DEG) regulation (up- or down- regulated) contrasts in males on RNA sequenced from WT and GR$^{MuSC-/-}$ proliferating myoblasts treated with DEX for 24h from (A). **(D)** Bar plot showing the most significantly up-regulated Gene Ontology (GO) terms from DEX-treated WT myoblasts. **(E)** Bar plot showing the most significantly down-regulated Gene Ontology (GO) terms from DEX-treated myoblasts, n= 3 male pairs.

DISCUSSION

Using the Human Protein Atlas (Uhlén et al., 2015), *Pax7* expression, while enriched in skeletal muscle, is also found in the brain particularly the midbrain and brainstem regions and to a lesser extent in the hypothalamus. The hypothalamus is part of the hypothalamic-pituitary-adrenal (HPA) axis that regulates the production of glucocorticoids in the adrenal cortex under conditions of stress (Chrousos, 1995) (https://www.proteinatlas.org/ENSG00000009709-PAX7/brain). Cortisol is a key negative regulator of the HPA axis through feedback loops to the anterior pituitary and hypothalamus where it suppresses the release of corticotropin-releasing hormone (CRH). While it is unclear if PAX7+ cells in the hypothalamus are also those that respond to cortisol, one potential limitation of my model is that loss of the GR in the PAX7+ cells in the hypothalamic region could impair the negative feedback loop that detects glucocorticoids in blood. Therefore, reduced glucocorticoid sensitivity in the brain could result in higher levels of glucocorticoids in $GR^{MuSC-/-}$ animals than in the wild types. While the MuSCs of $GR^{MuSC-/-}$ mice would be insensitive to increased cortisol, other cells that are glucocorticoid responsive may impact stem cell function locally in the muscle niche or via changes to whole body metabolism. However, no evidence of myofiber wasting is observed in $GR^{MuSC-/-}$ mice in resting conditions, suggesting that hypercortisolemia is unlikely to impact muscle homeostasis. This can be verified by measuring urine cortisol levels in the $GR^{MuSC-/-}$ and WT mice in resting and injured muscle.

The glucocorticoid receptor (GR) is closely related to the mineralocorticoid receptor (MR) which responds to aldosterone and regulates blood pressure. Although the primary receptor for glucocorticoids is GR, MR can also bind to low cortisol levels with high affinity (Reul et al., 1990). In tissues that express both GR and MR, endogenous cortisol occupies MR preferentially, with GR ligand binding seen only at supraphysiological levels (Rimmele et al., 2012) underlying a role for

cortisol as a stress hormone. While both GR and MR are expressed in C2C12 cells, MR mRNA is only weakly expressed in skeletal muscle making GR the predominant receptor for glucocorticoid action. Despite this, in the *mdx* mouse model genetic inactivation of myofiber MR has shown to improve skeletal muscle force and reduce fibrosis (Hauck et al., 2019a; Lowe et al., 2016; Rafael-Fortney et al., 2011). Additional findings have also indicated that MR antagonist treatment improves muscle membrane integrity in muscular dystrophy (Chadwick et al., 2016; Hauck et al., 2019b).

i. A role for the glucocorticoid receptor in the regulation of quiescence

My results show a role for GR in the maintenance of quiescence in resting muscle. I find that 7 days after acute injury, the PAX7+ population in the muscle of $GR^{MuSC-/-}$ mice expands (10-fold increase) to a similar extent as the population in WT mice (7.5-fold increase), in comparison to their respective baseline levels in non-injury conditions. However, despite the comparable expansion, the total number of PAX7+ cells in the muscle of $GR^{MuSC-/-}$ mice were ~59% smaller compared to WT mice at 7 dpi (Fig. 2 G), due to fewer PAX7+ cells in the muscle to begin with. Despite fewer PAX7+ cells, regeneration was equally effective in the $GR^{MuSC-/-}$ mice. This activated PAX7+ population in $GR^{MuSC-/-}$ remained stable from 7- to 28- days post injury. At 42 dpi, the number of PAX7+ MuSCs in the $GR^{MuSC-/-}$ mice was ~50% higher than the WT at 42-days post injury and more proliferative (%Ki67+ cycling cells), suggesting that loss of GR leads to long-term activation of PAX7+ cells in the injured limb and supports a role for the GR in the return of MuSCs to quiescence after injury (Fig. 4 K). As such, my findings place GR as an important regulator of MuSC quiescence.

In a broader sense, it is interesting to intersect the role of glucocorticoids in the stress response in the context of myotrauma and their role in the regulation of quiescence in muscle stem

cells. We find that *Nr3c1(GR)* expression in MuSCs is highest in resting MuSCs and late in regeneration, coincident with self-renewal and consistent with a role in quiescence. The receptor, however, appears to be downregulated in early regeneration and myogenic differentiation, suggesting that decreased sensitivity to glucocorticoids is required to allow for MuSC activation and differentiation despite high levels of cortisol following injury. Thus, in chronic inflammation treated with glucocorticoids (such as DMD), or in illnesses that feature high levels of cortisol such as cachexia, stem cell defects may be expected, for example, precocious differentiation initially followed by repair defects and wasting due to dwindling stem cell populations. This prediction is consistent with the observed effects of glucocorticoid treatment for DMD, where only a narrow three-year therapeutic window exists, followed by accelerated muscle wasting.

Based on the observed role for glucocorticoids in the maintenance of MuSC quiescence, we predict that self-renewal of MuSCs will be impaired. Indeed, we find that myofibers produced in $GR^{MuSC-/-}$ mice are larger than WT and that at 42 dpi, loss of GR results in the persistence of cycling cells when WT counterparts are largely quiescent (Ki67-). However, my experiments do not specifically investigate self-renewal in this model. To address this, serial injuries could be performed to determine if MuSCs become depleted with repeated injury and whether, ultimately regeneration fails. Myofiber culture experiments are also a useful model to examine cell fate. At 72 hours post isolation, all the three myogenic cell fates (proliferating, differentiating and self-renewing) could be quantified by immunostaining PAX7, MYOD and Ki67 to confirm if they are (PAX7+MYOD-) self-renewing or back to a PAX7+Ki67- state quiescent state.

While my findings support a role for the GR in quiescence, the exact mechanism by which GR-dependent quiescence is established remains unknown. The Retinoblastoma (*Rb*) protein is a major substrate of cyclinD-CDK4/6 phosphorylation (Cheung & Rando, 2013; Yao et al., 2008).

In quiescent cells, *Rb* is hypophosphorylated and inhibits proliferation by binding to and inactivating E2F1, a key transcriptional activator for cell-cycle and cell-division genes (Cheung & Rando, 2013; Yao et al., 2008). The phosphorylation of *Rb* by cyclin D-Cdk4 (upon exposure to mitogenic signals) prevents its repression of E2F, thus allowing for cell-cycle entry (Yao et al., 2008). E2F activity is sufficient to induce quiescent cells to enter S phase, whereas preventing E2F activation inhibits cell-cycle re-entry (Yao et al., 2008). The functional relationship between *Rb* and GR was studied using a combination of co-immunoprecipitation and reporter assays. Hong *et al* found that not only do *Rb* and GR co-localize in the nucleus of cells, but *Rb* interacts with GR in a ligand-dependent manner, and this interaction is required for GR-mediated transcriptional activation (Paramjeet Singh et al., 2001). In contrast, *Rb* homologues (p107 and p130) do not interact with GR in a similar manner, indicating a functional difference between these proteins. Furthermore, Singh *et al* also explored the role of *Rb* in regulating GR-mediated apoptosis, showing that the loss of *Rb* sensitizes cells to glucocorticoid-induced apoptosis, indicating that *Rb* plays a critical role in regulating this process (Paramjeet Singh et al., 2001). The impact of GR on *Rb*-mediated action has not been fully explored.

ii. ECM remodelling in $GR^{MuSC-/-}$ MuSCs

My RNA-seq data from $GR^{MuSC-/-}$ female mice indicates that *Lamb1* is down-regulated, while the collagens (*Col2a1* and *Col12a1*) are upregulated. Laminin is a major component of the basement membrane, a specialized ECM structure that separates epithelial and endothelial cells from surrounding connective tissue. Laminin plays a critical role in maintaining tissue integrity and regulating cell behavior, including c ell adhesion, migration, proliferation, and differentiation. Interaction between β1-integrin and laminin in the extracellular matrix can alter the fate choices of muscle stem cells (MuSCs), leading to increased differentiation (Rozo et al., 2016). Specifically,

decreased laminin interactions resulted in a higher probability of MuSCs that are no longer in contact with the basement membrane differentiating, rather than self-renewing during asymmetric cell division (Rozo et al., 2016). In contrast, fibronectin and collagen are major components of the interstitial ECM, which surrounds and supports cells in most tissues. Increased interactions between stem cells and fibronectin and collagen can promote stem cell differentiation into specific cell types, such as osteoblasts (Purva Singh & Schwarzbauer, 2012). Both reduced laminin and increased fibronectin and collagen are expected to stimulate the differentiation of muscle stem cells into myoblasts (Sanes, 2003) and as such, changes in the composition of the MuSC niche ECM may underly the precocious differentiation of $GR^{MuSC-/-}$ satellite cells.

iii. Planar Cell Polarity Proteins regulation with loss of GR and/or DEX treatment

Planar cell polarity (PCP) refers to the coordinated orientation of cells within a tissue plane, which is a fundamental process that is critical for the development and function of various tissues and organs in multicellular organisms (Goodrich & Strutt, 2011) . In this process, cells align their structures and behaviors in a specific direction relative to the tissue plane, and this orientation is regulated by a group of evolutionarily conserved proteins known as planar cell polarity proteins (Bayly & Axelrod, 2011). PCP proteins can regulate cell division and this has been shown to impact MuSC function (Le Grand et al., 2009). I explored the expression of planar cell polarity genes in $GR^{MuSC-/-}$ myoblasts and DEX-treated cells and found two members of the Prickle (Pk) family (*Pk1* and *Pk2*), LDL Receptor Related Protein 8 (*Lrp8*), and *Fat1* as putative GR targets. Interestingly, *Ror1* is upregulated by DEX treatment in WT primary myoblasts and downregulated with loss of GR. ROR1 is an orphan nuclear receptor that plays a crucial role in both embryonic development (Matsuda et al., 2001; Nomi et al., 2001; Takeuchi et al., 2000) and cancer progression (Barna et al., 2011; Baskar et al., 2008; Daneshmanesh et al., 2013; Zhang, Chen, Cui,

et al., 2012; Zhang, Chen, Wang-Rodriguez, et al., 2012). In cancer, glucocorticoids increase ROR1 expression, which in turn enhances its interaction with the transcription factor SOX2 (Karvonen et al., 2020). This interaction activates stem cell genes, ultimately resulting in the acquisition of chemoresistance in ovarian cancer cells and reduced cell proliferation. In skeletal muscle, Kamizaki *et al* showed that *Ror1* and *Ror2* expression is induced by the inflammatory cytokines TNF-α and IL-1β after injury, and that *Ror1* expression is induced primarily in PAX7+ cells after muscle injury (Kamizaki et al., 2017). Given that muscle inflammation is known to inhibit MuSC activation through the expression of the transcription factor C/EBPβ, a known quiescence inducer in satellite cells, it is intriguing to speculate that GR induces quiescence through ROR1 expression.

iv. Regulation of the Cytoskeleton by GCs and loss of the GR

Molecularly, Quattrocelli *et al* demonstrate that the membrane repair process involves the recruitment of an annexin-containing protein complex to the injury site, which leads to the formation of a patch that seals the plasma membrane in DMD (Quattrocelli et al., 2017b). This repair process is shown to be dependent on actin polymerization and the presence of calcium ions. However, my findings suggest that glucocorticoids may also enhance mechanical resistance by rebundling microtubules in *mdx* mice. As such, it would be particularly interesting to cross my conditional knockout model into the *mdx* background to directly explore the role of MuSC responsiveness to glucocorticoids in DMD to therapeutic benefit.

Both $GR^{-/-}$ myotubes and *mdx* myofibers have defects in nuclear positioning which is thought to be regulated by microtubules. To understand how GR regulates the microtubule network, it would be interesting to examine microtubule stability by immunostaining for detyrosinated and acetylated tubulin. Further, differences in cell migration, cell movement and fusion can be

examined by live cell imaging, and microtubule networks can be visualized after treatment with depolymerizing agents such as nocodazole and using fluorescent tubulin end binding proteins. A careful examination of the RNA-seq data set may provide critical information about the expression of genes involved in the regulation of the cytoskeleton. Given that defects in nuclear placement may impact contractile fiber organization and force generation, it would be interesting to investigate sarcomere structure by immunofluorescence and electron microscopy and to perform *ex vivo* force experiments in regenerated WT and $GR^{MuSC-/-}$ EDL muscles.

Several signaling pathways play a role in the regulation of the cytoskeleton, including Rho GTPases (*RhoA*, *Rac1*, and *Cdc42*), the phosphoinositide 3-kinase (PI3K)-Akt pathway, the extracellular signal-regulated kinase (ERK) branch of the mitogen-activated protein kinase (MAPK) pathway and the c-Jun N-terminal kinase (JNK) pathway which collectively regulate actin polymerization and microtubule stabilization. These signaling pathways are interconnected and can regulate the cytoskeleton in a coordinated manner to regulate various cellular processes such as muscle stem cell function, among others. Therefore, an analysis of the kinome of WT and $GR^{MuSC-/-}$ myoblasts could identify differentially activated signalling pathways which influence cytoskeleton dynamics regulated by the GR.

Changes in the cell's cytoskeleton result in alterations in its morphology. *Tcap* and *Actn3* are critical for sarcomere assembly of the contractile apparatus. Decreased expression of *Tcap* and *Actn3* in $GR^{MuSC-/-}$ proliferating myoblasts could indicate a potential impairment in muscle development and contraction resulting in the altered morphology we notice in our primary cultures. Specifically, *Tcap* is involved in maintaining the structural integrity of the Z-disk which is important in the proper functioning of muscle fibers and during contraction, decreased expression of which could lead to a decrease in force generated or dysregulation of muscle contraction in mice

with loss of the GR. *Actn3* is important for the proper alignment of actin filaments in fast-twitch muscle fibers, a decrease in which could result in impaired contraction and activities (high-intensity and strength based) that require fast-twitch muscle fiber function in our $GR^{MuSC-/-}$ myoblasts. The downregulation of *Tnni1* in our GR-/- proliferating cells could suggest the inability of this troponin in blocking actin-myosin interactions thus unable to facilitate muscle relaxation and maintains $GR^{-/-}$ myotubes in a hypercontracted rounded morphology as seen in our $GR^{-/-}$ primary myotubes.

v. Conclusion

In summary, I have demonstrated that glucocorticoid receptor expression loss during muscle regeneration leads to a reduction in the PAX7+ MuSC population 7 days post cardiotoxin injury without affecting myofiber size. Long-term loss of GR causes a defect in exit from the differentiation process leading to continual repair and enhanced fibers 28- and 42- days post CTX injury. *In vivo* loss of GR showed an increase in the percentage of BrdU and KI67+ cycling cells in resting TA muscles of C57BL/6 mice. Similarly increased MuSC activation was observed on *ex-vivo* single EDL myofibers lacking GR. Transcriptome profiling of GR-deficient *in situ* fixed MuSCs ($GR^{MuSC-/-}$) revealed distinct clustering between genotypes and sex. Loss of GR was also shown to upregulate pathways such as oxidative phosphorylation and ribosomal RNA biogenesis in $GR^{MuSC-/-}$ male mice, while cell cycle and extracellular and matrix-receptor interactions were found to be upregulated in females. $GR^{MuSC-/-}$ *in situ* fixed male MuSCs have a gene expression profile consistent with cells that are primed for activation, whereas female MuSCs had exited the quiescent G_0 state and were actively cycling (seen by the upregulation of multiple components of the cell cycle as compared to only CyclinA in males). Gene ontology analysis of differentially expressed genes from GR-deficient proliferating myoblasts ($GR^{MuSC-/-}$) as compared the WT

showed downregulation of genes related to muscle structure development, differentiation, and contraction, suggesting defects in cell morphology. I found that *in vitro* loss of GR expression did not affect the differentiation or fusion indices of differentiating myoblasts but did result in abnormal myotube morphology. GR loss also increased the number of centrally located myonuclei in regenerating muscle fibers in mice 28 days post myotrauma. *In vitro* loss of GR leads to an increase in the number of alignment and spreading defects in GR-deficient myotubes suggesting defects in the cytoskeleton that are microtubule dependent. Lastly, glucocorticoids promote microtubule bundling and organization in WT and *mdx* myofibers *ex-vivo*. The results of this study indicate that the glucocorticoid receptor is a positive regulator of muscle stem cell quiescence and is essential for the morphological maturation of myotubes.

REFRENCES

Aartsma-Rus, A., Janson, A. A. M., Kaman, W. E., Bremmer-Bout, M., Van Ommen, G. J. B., Den Dunnen, J. T., & Van Deutekom, J. C. T. (2004). Antisense-induced multiexon skipping for Duchenne muscular dystrophy makes more sense. *American Journal of Human Genetics*, *74*(1), 83–92. https://doi.org/10.1086/381039

Abou-Khalil, R., Le Grand, F., Pallafacchina, G., Valable, S., Authier, F. J., Rudnicki, M. A., Gherardi, R. K., Germain, S., Chretien, F., Sotiropoulos, A., Lafuste, P., Montarras, D., & Chazaud, B. (2009). Autocrine and Paracrine Angiopoietin 1/Tie-2 Signaling Promotes Muscle Satellite Cell Self-Renewal. *Cell Stem Cell*, *5*(3), 298–309. https://doi.org/10.1016/j.stem.2009.06.001

Akhmanova, A., & Steinmetz, M. O. (2019). Microtubule minus-end regulation at a glance. *Journal of Cell Science*, *132*(11), jcs227850. https://doi.org/10.1242/jcs.227850

Aktas, H., Cai, H., & Cooper, G. M. (1997). Ras links growth factor signaling to the cell cycle machinery via regulation of cyclin D1 and the Cdk inhibitor p27KIP1. *Molecular and Cellular Biology*, *17*(7), 3850–3857. https://doi.org/10.1128/MCB.17.7.3850

Aoki, Y., Nagata, T., Yokota, T., Nakamura, A., Wood, M. J. A., Partridge, T., & Takeda, S. (2013). Highly efficient in vivo delivery of PMO into regenerating myotubes and rescue in laminin-α2 chain-null congenital muscular dystrophy mice. *Human Molecular Genetics*, *22*(24), 4914–4928. https://doi.org/10.1093/HMG/DDT341

Aoki, Y., Nakamura, A., Yokota, T., Saito, T., Okazawa, H., Nagata, T., & Takeda, S. (2010). In-frame dystrophin following exon 51-skipping improves muscle pathology and function in the exon 52-deficient mdx mouse. *Molecular Therapy : The Journal of the American Society of*

Gene Therapy, *18*(11), 1995–2005. https://doi.org/10.1038/MT.2010.186

Arai, F., Hirao, A., Ohmura, M., Sato, H., Matsuoka, S., Takubo, K., Ito, K., Koh, G. Y., & Suda, T. (2004). Tie2/angiopoietin-1 signaling regulates hematopoietic stem cell quiescence in the bone marrow niche. *Cell*, *118*(2), 149–161. https://doi.org/10.1016/j.cell.2004.07.004

Arora, M., Moser, J., Phadke, H., Basha, A. A., & Spencer, S. L. (2017). Endogenous Replication Stress in Mother Cells Leads to Quiescence of Daughter Cells. *Cell Reports*, *19*(7), 1351–1364. https://doi.org/10.1016/J.CELREP.2017.04.055

Baehr, L. M., Furlow, J. D., & Bodine, S. C. (2011). Muscle sparing in muscle RING finger 1 null mice: response to synthetic glucocorticoids. *The Journal of Physiology*, *589*(Pt 19), 4759. https://doi.org/10.1113/JPHYSIOL.2011.212845

Barna, G., Mihalik, R., Timár, B., Tömböl, J., Csende, Z., Sebestyén, A., Bödör, C., Csernus, B., Reiniger, L., Peták, I., & Matolcsy, A. (2011). ROR1 expression is not a unique marker of CLL. *Hematological Oncology*, *29*(1), 17–21. https://doi.org/10.1002/HON.948

Barr, A. R., Cooper, S., Heldt, F. S., Butera, F., Stoy, H., Mansfeld, J., Novák, B., & Bakal, C. (2017). DNA damage during S-phase mediates the proliferation-quiescence decision in the subsequent G1 via p21 expression. *Nature Communications*, *8*. https://doi.org/10.1038/NCOMMS14728

Baskar, S., Ka, Y. K., Hofer, T., Levy, J. M., Kennedy, M. G., Lee, E., Staudt, L. M., Wilson, W. H., Wiestner, A., & Rader, C. (2008). Unique cell surface expression of receptor tyrosine kinase ROR1 in human B-cell chronic lymphocytic leukemia. *Clinical Cancer Research : An Official Journal of the American Association for Cancer Research*, *14*(2), 396–404. https://doi.org/10.1158/1078-0432.CCR-07-1823

Bayly, R., & Axelrod, J. D. (2011). Pointing in the right direction: new developments in the field of planar cell polarity. *Nature Reviews Genetics 2011 12:6*, *12*(6), 385–391. https://doi.org/10.1038/nrg2956

Belanto, J. J., Mader, T. L., Eckhoff, M. D., Strandjord, D. M., Banks, G. B., Gardner, M. K., Lowe, D. A., & Ervasti, J. M. (2014). Microtubule binding distinguishes dystrophin from utrophin. *Proceedings of the National Academy of Sciences of the United States of America*, *111*(15), 5723–5728. https://doi.org/10.1073/PNAS.1323842111

Bischoff, R. (1990). Interaction between satellite cells and skeletal muscle fibers. *Development (Cambridge, England)*, *109*(4), 943–952. https://doi.org/10.1242/DEV.109.4.943

Bischoff, Richard. (1975). Regeneration of single skeletal muscle fibers in vitro. *The Anatomical Record*, *182*(2), 215–235. https://doi.org/10.1002/AR.1091820207

Bischoff, Richard. (1986). A satellite cell mitogen from crushed adult muscle. *Developmental Biology*, *115*(1), 140–147. https://doi.org/10.1016/0012-1606(86)90235-6

Blighe K, Rana S, L. M. (2022). *EnhancedVolcano: Publication-ready volcano plots with enhanced colouring and labeling.*

Bodine, S. C., & Furlow, J. D. (2015). Glucocorticoids and Skeletal Muscle. *Advances in Experimental Medicine and Biology*, *872*, 145–176. https://doi.org/10.1007/978-1-4939-2895-8_7

Bothe, I., & Baylies, M. K. (2016). Drosophila myogenesis. *Current Biology : CB*, *26*(17), R786–R791. https://doi.org/10.1016/J.CUB.2016.07.062

Bowles, D. E., McPhee, S. W. J., Li, C., Gray, S. J., Samulski, J. J., Camp, A. S., Li, J., Wang, B.,

Monahan, P. E., Rabinowitz, J. E., Grieger, J. C., Govindasamy, L., Agbandje-Mckenna, M., Xiao, X., & Samulski, R. J. (2012). Phase 1 gene therapy for Duchenne muscular dystrophy using a translational optimized AAV vector. *Molecular Therapy : The Journal of the American Society of Gene Therapy*, *20*(2), 443–455. https://doi.org/10.1038/MT.2011.237

Bremmer-Bout, M., Aartsma-Rus, A., de Meijer, E. J., Kaman, W. E., Janson, A. A. M., Vossen, R. H. A. M., van Ommen, G. J. B., den Dunnen, J. T., & van Deutekom, J. C. T. (2004). Targeted exon skipping in transgenic hDMD mice: A model for direct preclinical screening of human-specific antisense oligonucleotides. *Molecular Therapy : The Journal of the American Society of Gene Therapy*, *10*(2), 232–240. https://doi.org/10.1016/J.YMTHE.2004.05.031

Britto, F. A., Begue, G., Rossano, B., Docquier, A., Vernus, B., Sar, C., Ferry, A., Bonnieu, A., Ollendorff, V., & Favier, F. B. (2014). REDD1 deletion prevents dexamethasone-induced skeletal muscle atrophy. *American Journal of Physiology. Endocrinology and Metabolism*, *307*(11), E983–E993. https://doi.org/10.1152/AJPENDO.00234.2014

Brouhard, G. J., & Rice, L. M. (2018). Microtubule dynamics: an interplay of biochemistry and mechanics. *Nature Reviews. Molecular Cell Biology*, *19*(7), 451–463. https://doi.org/10.1038/S41580-018-0009-Y

Buckingham, M. (2001). Skeletal muscle formation in vertebrates. *Current Opinion in Genetics & Development*, *11*(4), 440–448. https://doi.org/10.1016/S0959-437X(00)00215-X

Buckingham, Margaret, & Relaix, F. (2007). The role of Pax genes in the development of tissues and organs: Pax3 and Pax7 regulate muscle progenitor cell functions. *Annual Review of Cell and Developmental Biology*, *23*, 645–673.

https://doi.org/10.1146/ANNUREV.CELLBIO.23.090506.123438

Cadot, B., Gache, V., & Gomes, E. R. (2015). Moving and positioning the nucleus in skeletal muscle - one step at a time. *Nucleus (Austin, Tex.)*, *6*(5), 373–381. https://doi.org/10.1080/19491034.2015.1090073

Cadot, B., Gache, V., Vasyutina, E., Falcone, S., Birchmeier, C., & Gomes, E. R. (2012). Nuclear movement during myotube formation is microtubule and dynein dependent and is regulated by Cdc42, Par6 and Par3. *EMBO Reports*, *13*(8), 741–749. https://doi.org/10.1038/EMBOR.2012.89

Capetanaki, Y., Milner, D. J., & Weitzer, G. (1997). Desmin in muscle formation and maintenance: knockouts and consequences. *Cell Structure and Function*, *22*(1), 103–116. https://doi.org/10.1247/CSF.22.103

Carlsson, L., Li, Z., Paulin, D., & Thornell, L. E. (1999). Nestin is expressed during development and in myotendinous and neuromuscular junctions in wild type and desmin knock-out mice. *Experimental Cell Research*, *251*(1), 213–223. https://doi.org/10.1006/EXCR.1999.4569

Chadwick, J. A., Bhattacharya, S., Lowe, J., & Rafael-Fortney, J. A. (2016). Renin-angiotensin-aldosterone system inhibitors improve membrane stability and change gene expression profiles in dystrophic skeletal muscles. *Am J Physiol Cell Physiol*. https://doi.org/10.1152/ajpcell.00269.2016

Chakkalakal, J. V., Jones, K. M., Basson, M. A., & Brack, A. S. (2012). The aged niche disrupts muscle stem cell quiescence. *Nature*, *490*(7420), 355–360. https://doi.org/10.1038/NATURE11438

Chen, J. C. J., & Goldhamer, D. J. (1999). Transcriptional mechanisms regulating MyoD expression in the mouse. *Cell and Tissue Research*, *296*(1), 213–219. https://doi.org/10.1007/S004410051282

Chen, M., Gos, A., Morris, M. A., & Antonarakis, S. E. (1996). Localization of a human homolog of the mouse pericentrin gene (PCNT) to chromosome 21qter. *Genomics*, *35*(3), 620–624. https://doi.org/10.1006/GENO.1996.0411

Chen, S., Zhou, Y., Chen, Y., & Gu, J. (2018). fastp: an ultra-fast all-in-one FASTQ preprocessor. *Bioinformatics (Oxford, England)*, *34*(17), i884–i890. https://doi.org/10.1093/BIOINFORMATICS/BTY560

Cheung, T. H., & Rando, T. A. (2013). Molecular regulation of stem cell quiescence. *Nature Reviews. Molecular Cell Biology*, *14*(6), 329–340. https://doi.org/10.1038/NRM3591

Chiristov, C., Chrétien, F., Abou-Khalil, R., Bassez, G., Vallet, G., Authier, F. J., Bassaglia, Y., Shinin, V., Tajbakhsh, S., Chazaud, B., & Gherardi, R. K. (2007). Muscle Satellite Cells and Endothelial Cells: Close Neighbors and Privileged Partners. *Molecular Biology of the Cell*, *18*(4), 1397. https://doi.org/10.1091/MBC.E06-08-0693

Chrousos, G. P. (1995). The Hypothalamic–Pituitary–Adrenal Axis and Immune-Mediated Inflammation. *Https://Doi.Org/10.1056/NEJM199505183322008*, *332*(20), 1351–1363. https://doi.org/10.1056/NEJM199505183322008

Cole, T. J., Blendy, J. A., Monaghan, A. P., Krieglstein, K., Schmid, W., Aguzzi, A., Fantuzzi, G., Hummler, E., Unsicker, K., & Schütz, G. (1995). Targeted disruption of the glucocorticoid receptor gene blocks adrenergic chromaffin cell development and severely retards lung maturation. *Genes & Development*, *9*(13), 1608–1621.

https://doi.org/10.1101/GAD.9.13.1608

Collins, C. A., Olsen, I., Zammit, P. S., Heslop, L., Petrie, A., Partridge, T. A., & Morgan, J. E. (2005). Stem cell function, self-renewal, and behavioral heterogeneity of cells from the adult muscle satellite cell niche. *Cell*, *122*(2), 289–301. https://doi.org/10.1016/J.CELL.2005.05.010

Cooper, R. N., Tajbakhsh, S., Mouly, V., Cossu, G., Buckingham, M., & Butler-Browne, G. S. (1999). In vivo satellite cell activation via Myf5 and MyoD in regenerating mouse skeletal muscle. *Journal of Cell Science*, *112 (Pt 17)*(17), 2895–2901. https://doi.org/10.1242/JCS.112.17.2895

Cornelison, D. D. W., & Wold, B. J. (1997). Single-cell analysis of regulatory gene expression in quiescent and activated mouse skeletal muscle satellite cells. *Developmental Biology*, *191*(2), 270–283. https://doi.org/10.1006/dbio.1997.8721

Cotsarelis, G., Sun, T. T., & Lavker, R. M. (1990). Label-retaining cells reside in the bulge area of pilosebaceous unit: Implications for follicular stem cells, hair cycle, and skin carcinogenesis. *Cell*, *61*(7), 1329–1337. https://doi.org/10.1016/0092-8674(90)90696-C

Daneshmanesh, A. H., Porwit, A., Hojjat-Farsangi, M., Jeddi-Tehrani, M., Tamm, K. P., Grandér, D., Lehmann, S., Norin, S., Shokri, F., Rabbani, H., Mellstedt, H., & Österborg, A. (2013). Orphan receptor tyrosine kinases ROR1 and ROR2 in hematological malignancies. *Leukemia & Lymphoma*, *54*(4), 843–850. https://doi.org/10.3109/10428194.2012.731599

Desai, A., & Mitchison, T. J. (1997). Microtubule polymerization dynamics. *Annual Review of Cell and Developmental Biology*, *13*, 83–117. https://doi.org/10.1146/ANNUREV.CELLBIO.13.1.83

Dobin, A., Davis, C. A., Schlesinger, F., Drenkow, J., Zaleski, C., Jha, S., Batut, P., Chaisson, M., & Gingeras, T. R. (2013). STAR: ultrafast universal RNA-seq aligner. *Bioinformatics*, *29*(1), 15. https://doi.org/10.1093/BIOINFORMATICS/BTS635

Dumont, N. A., Wang, Y. X., Von Maltzahn, J., Pasut, A., Bentzinger, C. F., Brun, C. E., & Rudnicki, M. A. (2015). Dystrophin expression in muscle stem cells regulates their polarity and asymmetric division. *Nature Medicine*, *21*(12), 1455–1463. https://doi.org/10.1038/nm.3990

Eliazer, S., Sun, X., & Brack, A. S. (2020). Spatial Heterogeneity of Delta-like 4 Within a Multinucleated Niche Cell Maintains Muscle Stem Cell Diversity. *BioRxiv*, 2020.10.20.347484. https://doi.org/10.1101/2020.10.20.347484

Emery, A. E. H. (2002). The muscular dystrophies. *Lancet (London, England)*, *359*(9307), 687–695. https://doi.org/10.1016/S0140-6736(02)07815-7

Espigat-Georger, A., Dyachuk, V., Chemin, C., Emorine, L., & Merdes, A. (2016). Nuclear alignment in myotubes requires centrosome proteins recruited by nesprin-1. *Journal of Cell Science*, *129*(22), 4227–4237. https://doi.org/10.1242/JCS.191767

Esteve-Codina, A., Arpi, O., Martinez-García, M., Pineda, E., Mallo, M., Gut, M., Carrato, C., Rovira, A., Lopez, R., Tortosa, A., Dabad, M., Barco, S. Del, Heath, S., Bagué, S., Ribalta, T., Alameda, F., Iglesia, N. La, & Balaña, C. (2017). A Comparison of RNA-Seq Results from Paired Formalin-Fixed Paraffin-Embedded and Fresh-Frozen Glioblastoma Tissue Samples. *PLoS ONE*, *12*(1). https://doi.org/10.1371/JOURNAL.PONE.0170632

Ewels, P., Magnusson, M., Lundin, S., & Käller, M. (2016). MultiQC: summarize analysis results for multiple tools and samples in a single report. *Bioinformatics (Oxford, England)*, *32*(19),

3047–3048. https://doi.org/10.1093/BIOINFORMATICS/BTW354

Falcone, S., Roman, W., Hnia, K., Gache, V., Didier, N., Lainé, J., Auradé, F., Marty, I., Nishino, I., Charlet-Berguerand, N., Romero, N. B., Marazzi, G., Sassoon, D., Laporte, J., & Gomes, E. R. (2014). N-WASP is required for Amphiphysin-2/BIN1-dependent nuclear positioning and triad organization in skeletal muscle and is involved in the pathophysiology of centronuclear myopathy. *EMBO Molecular Medicine*, *6*(11), 1455–1475. https://doi.org/10.15252/EMMM.201404436

Fan, W., Gao, X. K., Rao, X. S., Shi, Y. P., Liu, X. C., Wang, F. Y., Liu, Y. F., Cong, X. X., He, M. Y., Xu, S. B., Shen, W. L., Shen, Y., Yan, S. G., Luo, Y., Low, B. C., Ouyang, H., Bao, Z., Zheng, L. L., & Zhou, Y. T. (2018). Hsp70 Interacts with Mitogen-Activated Protein Kinase (MAPK)-Activated Protein Kinase 2 To Regulate p38MAPK Stability and Myoblast Differentiation during Skeletal Muscle Regeneration. *Molecular and Cellular Biology*, *38*(24). https://doi.org/10.1128/MCB.00211-18

Fujimaki, K., Li, R., Chen, H., Croce, K. Della, Zhang, H. H., Xing, J., Bai, F., & Yao, G. (2019). Graded regulation of cellular quiescence depth between proliferation and senescence by a lysosomal dimmer switch. *Proceedings of the National Academy of Sciences of the United States of America*, *116*(45), 22624–22634. https://doi.org/10.1073/PNAS.1915905116/-/DCSUPPLEMENTAL

Gao, Q. Q., & McNally, E. M. (2015). The Dystrophin Complex: Structure, Function, and Implications for Therapy. *Comprehensive Physiology*, *5*(3), 1223–1239. https://doi.org/10.1002/CPHY.C140048

Giouchon-Mantel, A., Loosfelt, H., Lescop, P., Christin-Maitre, S., Perrot-Applanat, M., &

Milgrom, E. (1992). Mechanisms of nuclear localization of the progesterone receptor. *The Journal of Steroid Biochemistry and Molecular Biology*, *41*(3–8), 209–215. https://doi.org/10.1016/0960-0760(92)90346-K

Gnocchi, V. F., White, R. B., Ono, Y., Ellis, J. A., & Zammit, P. S. (2009). Further characterisation of the molecular signature of quiescent and activated mouse muscle satellite cells. *PloS One*, *4*(4). https://doi.org/10.1371/JOURNAL.PONE.0005205

Goodrich, L. V., & Strutt, D. (2011). Principles of planar polarity in animal development. *Development*, *138*(10), 1877–1892. https://doi.org/10.1242/DEV.054080

Goodson, H. V, & Jonasson, E. M. (2018). Microtubules and Microtubule-Associated Proteins. *Cold Spring Harb Perspect Biol*, *10*(6), :a022608. https://doi.org/10.1101/cshperspect.a022608

Grad, I., & Picard, D. (2007). The glucocorticoid responses are shaped by molecular chaperones. *Molecular and Cellular Endocrinology*, *275*(1–2), 2–12. https://doi.org/10.1016/J.MCE.2007.05.018

Grounds, M. D., Garrett, K. L., Lai, M. C., Wright, W. E., & Beilharz, M. W. (1992). Identification of skeletal muscle precursor cells in vivo by use of MyoD1 and myogenin probes. *Cell and Tissue Research*, *267*(1), 99–104. https://doi.org/10.1007/BF00318695

Gu, Z., Eils, R., & Schlesner, M. (2016). Complex heatmaps reveal patterns and correlations in multidimensional genomic data. *Bioinformatics (Oxford, England)*, *32*(18), 2847–2849. https://doi.org/10.1093/BIOINFORMATICS/BTW313

Gundersen, K., & Bruusgaard, J. C. (2008). Nuclear domains during muscle atrophy: nuclei lost

or paradigm lost? *The Journal of Physiology*, *586*(11), 2675–2681. https://doi.org/10.1113/JPHYSIOL.2008.154369

Gussoni, E., Soneoka, Y., Strickland, C. D., Buzney, E. A., Khan, M. K., Flint, A. F., Kunkel, L. M., & Mulligan, R. C. (1999). Dystrophin expression in the mdx mouse restored by stem cell transplantation. *Nature*, *401*(6751), 390–394. https://doi.org/10.1038/43919

Harper, S. Q., Hauser, M. A., DelloRusso, C., Duan, D., Crawford, R. W., Phelps, S. F., Harper, H. A., Robinson, A. S., Engelhardt, J. F., Brooks, S. V., & Chamberlain, J. S. (2002). Modular flexibility of dystrophin: implications for gene therapy of Duchenne muscular dystrophy. *Nature Medicine*, *8*(3), 253–261. https://doi.org/10.1038/NM0302-253

Hasty, P., Bradley, A., Morris, J. H., Edmondson, D. G., Venuti, J. M., Olson, E. N., & Klein, W. H. (1993). Muscle deficiency and neonatal death in mice with a targeted mutation in the myogenin gene. *Nature*, *364*(6437), 501–506. https://doi.org/10.1038/364501A0

Hauck, J. S., Lowe, J., Rastogi, N., McElhanon, K. E., Petrosino, J. M., Peczkowski, K. K., Chadwick, A. N., Zins, J. G., Accornero, F., Janssen, P. M. L., Weisleder, N. L., & Rafael-Fortney, J. A. (2019a). Mineralocorticoid receptor antagonists improve membrane integrity independent of muscle force in muscular dystrophy. *Human Molecular Genetics*, *28*(12), 2030–2045. https://doi.org/10.1093/hmg/ddz039

Hauck, J. S., Lowe, J., Rastogi, N., McElhanon, K. E., Petrosino, J. M., Peczkowski, K. K., Chadwick, A. N., Zins, J. G., Accornero, F., Janssen, P. M. L., Weisleder, N. L., & Rafael-Fortney, J. A. (2019b). Mineralocorticoid receptor antagonists improve membrane integrity independent of muscle force in muscular dystrophy. *Human Molecular Genetics*, *28*(12), 2030–2045. https://doi.org/10.1093/HMG/DDZ039

Heck, S., Bender, K., Kullmann, M., Göttlicher, M., Herrlich, P., & Cato, A. C. B. (1997). I kappaB alpha-independent downregulation of NF-kappaB activity by glucocorticoid receptor. *The EMBO Journal*, *16*(15), 4698–4707. https://doi.org/10.1093/EMBOJ/16.15.4698

Hoffman, E. P., Brown, R. H., & Kunkel, L. M. (1987). Dystrophin: the protein product of the Duchenne muscular dystrophy locus. *Cell*, *51*(6), 919–928. https://doi.org/10.1016/0092-8674(87)90579-4

Holland, A., Carberry, S., & Ohlendieck, K. (2013). Proteomics of the dystrophin-glycoprotein complex and dystrophinopathy. *Current Protein & Peptide Science*, *14*(8), 680–697. https://doi.org/10.2174/13892037113146660083

Hu, Z., Wang, H., In, H. L., Du, J., & Mitch, W. E. (2009). Endogenous glucocorticoids and impaired insulin signaling are both required to stimulate muscle wasting under pathophysiological conditions in mice. *The Journal of Clinical Investigation*, *119*(10), 3059–3069. https://doi.org/10.1172/JCI38770

Huard, J., Roy, R., Bouchard, J. P., Malouin, F., Richards, C. L., & Tremblay, J. P. (1992). Human myoblast transplantation between immunohistocompatible donors and recipients produces immune reactions. *Transplantation Proceedings*, *24*(6), 3049–3051.

Jankowski, R. J., Deasy, B. M., & Huard, J. (2002). Muscle-derived stem cells. *Gene Therapy*, *9*(10), 642–647. https://doi.org/10.1038/SJ.GT.3301719

Kamizaki, K., Doi, R., Hayashi, M., Saji, T., Kanagawa, M., Toda, T., Fukada, S. ichiro, Ho, H. Y. H., Greenberg, M. E., Endo, M., & Minami, Y. (2017). The Ror1 receptor tyrosine kinase plays a critical role in regulating satellite cell proliferation during regeneration of injured muscle. *The Journal of Biological Chemistry*, *292*(38), 15939–15951.

https://doi.org/10.1074/JBC.M117.785709

Karvonen, H., Arjama, M., Kaleva, L., Niininen, W., Barker, H., Koivisto-Korander, R., Tapper, J., Pakarinen, P., Lassus, H., Loukovaara, M., Bützow, R., Kallioniemi, O., Murumägi, A., & Ungureanu, D. (2020). Glucocorticoids induce differentiation and chemoresistance in ovarian cancer by promoting ROR1-mediated stemness. *Cell Death & Disease*, *11*(9). https://doi.org/10.1038/S41419-020-03009-4

Kerr, J. P., Robison, P., Shi, G., Bogush, A. I., Kempema, A. M., Hexum, J. K., Becerra, N., Harki, D. A., Martin, S. S., Raiteri, R., Prosser, B. L., & Ward, C. W. (2015). Detyrosinated microtubules modulate mechanotransduction in heart and skeletal muscle. *Nature Communications 2015 6:1*, *6*(1), 1–14. https://doi.org/10.1038/ncomms9526

Khairallah, R. J., Shi, G., Sbrana, F., Prosser, B. L., Borroto, C., Mazaitis, M. J., Hoffman, E. P., Mahurkar, A., Sachs, F., Sun, Y., Chen, Y. W., Raiteri, R., Lederer, W. J., Dorsey, S. G., & Ward, C. W. (2012). Microtubules underlie dysfunction in duchenne muscular dystrophy. *Science Signaling*, *5*(236). https://doi.org/10.1126/SCISIGNAL.2002829

Koenig, M., Hoffman, E. P., Bertelson, C. J., Monaco, A. P., Feener, C., & Kunkel, L. M. (1987). Complete cloning of the Duchenne muscular dystrophy (DMD) cDNA and preliminary genomic organization of the DMD gene in normal and affected individuals. *Cell*, *50*(3), 509–517. https://doi.org/10.1016/0092-8674(87)90504-6

Kollman, J. M., Merdes, A., Mourey, L., & Agard, D. A. (2011). Microtubule nucleation by γ-tubulin complexes. *Nature Reviews. Molecular Cell Biology*, *12*(11), 709–721. https://doi.org/10.1038/NRM3209

Kuang, S., Kuroda, K., Le Grand, F., & Michael, and R. (1967). Asymmetric Self-Renewal and

Commitment of Satellite Stem Cells in Muscle. *The Journal of Biological Chemistry*, *242*(9), 2278–2282. https://doi.org/10.1016/j.cell.2007.03.044.Asymmetric

Kuang, S., Kuroda, K., Le Grand, F., & Rudnicki, M. A. (2007). Asymmetric self-renewal and commitment of satellite stem cells in muscle. *Cell*, *129*(5), 999–1010. https://doi.org/10.1016/J.CELL.2007.03.044

Kumar, R., & Thompson, E. B. (2005). Gene regulation by the glucocorticoid receptor: structure:function relationship. *The Journal of Steroid Biochemistry and Molecular Biology*, *94*(5), 383–394. https://doi.org/10.1016/J.JSBMB.2004.12.046

Kunkel, L. M., Monaco, A. P., Middlesworth, W., Ochs, H. D., & Latt, S. A. (1985). Specific cloning of DNA fragments absent from the DNA of a male patient with an X chromosome deletion. *Proceedings of the National Academy of Sciences of the United States of America*, *82*(14), 4778–4782. https://doi.org/10.1073/PNAS.82.14.4778

Kuo, T., Harris, C. A., & Wang, J. C. (2013). Metabolic functions of glucocorticoid receptor in skeletal muscle. *Molecular and Cellular Endocrinology*, *380*(1–2), 79–88. https://doi.org/10.1016/j.mce.2013.03.003

Le Grand, F., Jones, A. E., Seale, V., Scimè, A., & Rudnicki, M. A. (2009). Wnt7a Activates the Planar Cell Polarity Pathway to Drive the Symmetric Expansion of Satellite Stem Cells. *Cell Stem Cell*, *4*(6), 535–547. https://doi.org/10.1016/j.stem.2009.03.013

Lepper, C., Partridge, T. A., & Fan, C. M. (2011). An absolute requirement for pax7-positive satellite cells in acute injury-induced skeletal muscle regeneration. *Development*, *138*(17), 3639–3646. https://doi.org/10.1242/DEV.067595/-/DC1

Li, B., Sun, C., Sun, J., Yang, M. H., Zuo, R., Liu, C., Lan, W. R., Liu, M. H., Huang, B., & Zhou, Y. (2019). Autophagy mediates serum starvation-induced quiescence in nucleus pulposus stem cells by the regulation of P27. *Stem Cell Research & Therapy*, *10*(1). https://doi.org/10.1186/S13287-019-1219-8

Li, N., & Clevers, H. (2010). Coexistence of quiescent and active adult stem cells in mammals. *Science*, *327*(5965), 542–545. https://doi.org/10.1126/SCIENCE.1180794/ASSET/07CD8692-391A-4146-AE8B-C1F79ACF275C/ASSETS/GRAPHIC/327_542_F4.JPEG

Liao, Y., Smyth, G. K., & Shi, W. (2014). featureCounts: an efficient general purpose program for assigning sequence reads to genomic features. *Bioinformatics (Oxford, England)*, *30*(7), 923–930. https://doi.org/10.1093/BIOINFORMATICS/BTT656

Llorens-Bobadilla, E., Zhao, S., Baser, A., Saiz-Castro, G., Zwadlo, K., & Martin-Villalba, A. (2015). Single-Cell Transcriptomics Reveals a Population of Dormant Neural Stem Cells that Become Activated upon Brain Injury. *Cell Stem Cell*, *17*(3), 329–340. https://doi.org/10.1016/J.STEM.2015.07.002

Lowe, J., Floyd, K. T., Rastogi, N., Schultz, E. J., Chadwick, J. A., Swager, S. A., Zins, J. G., Kadakia, F. K., Smart, S., Gomez-Sanchez, E. P., Gomez-Sanchez, C. E., Raman, S. V., Janssen, P. M. L., & Rafael-Fortney, J. A. (2016). Similar Efficacy from Specific and Non-Specific Mineralocorticoid Receptor Antagonist Treatment of Muscular Dystrophy Mice. *Journal of Neuromuscular Diseases*, *3*(3), 395–404. https://doi.org/10.3233/JND-160173

Machado, L., Esteves de Lima, J., Fabre, O., Proux, C., Legendre, R., Szegedi, A., Varet, H., Ingerslev, L. R., Barrès, R., Relaix, F., & Mourikis, P. (2017). In Situ Fixation Redefines

Quiescence and Early Activation of Skeletal Muscle Stem Cells. *Cell Reports*, *21*(7), 1982–1993. https://doi.org/10.1016/J.CELREP.2017.10.080

Maesner, C. C., Almada, A. E., & Wagers, A. J. (2016). Established cell surface markers efficiently isolate highly overlapping populations of skeletal muscle satellite cells by fluorescence-activated cell sorting. *Skeletal Muscle*, *6*(1). https://doi.org/10.1186/S13395-016-0106-6

Matsuda, T., Nomi, M., Ikeya, M., Kani, S., Oishi, I., Terashima, T., Takada, S., & Minami, Y. (2001). Expression of the receptor tyrosine kinase genes, Ror1 and Ror2, during mouse development. *Mechanisms of Development*, *105*(1–2), 153–156. https://doi.org/10.1016/S0925-4773(01)00383-5

Matsumura, K., Ohlendieck, K., Ionasescu, V. V., Tomé, F. M. S., Nonaka, I., Burghes, A. H. M., Mora, M., Kaplan, J. C., Fardeau, M., & Campbell, K. P. (1993). The role of the dystrophin-glycoprotein complex in the molecular pathogenesis of muscular dystrophies. *Neuromuscular Disorders : NMD*, *3*(5–6), 533–535. https://doi.org/10.1016/0960-8966(93)90110-6

MAURO, A. (1961). Satellite cell of skeletal muscle fibers. *The Journal of Biophysical and Biochemical Cytology*, *9*(2), 493–495. https://doi.org/10.1083/JCB.9.2.493

Mccarthy, J. J., Mula, J., Miyazaki, M., Erfani, R., Garrison, K., Farooqui, A. B., Srikuea, R., Lawson, B. A., Grimes, B., Keller, C., Van Zant, G., Campbell, K. S., Esser, K. A., Dupont-Versteegden, E. E., & Peterson, C. A. (2011). Effective fiber hypertrophy in satellite cell-depleted skeletal muscle. *Development*, *138*(17), 3657–3666. https://doi.org/10.1242/DEV.068858

McDonald, C. M., Henricson, E. K., Abresch, R. T., Duong, T., Joyce, N. C., Hu, F., Clemens, P. R., Hoffman, E. P., Cnaan, A., Gordish-Dressman, H., Vishwanathan, V., Chidambaranathan,

S., Biggar, W. D., McAdam, L. C., Mah, J. K., Tulinius, M., Morgenroth, L. P., Leshner, R., Tesi-Rocha, C., … Karachunski, P. (2018a). Long-term effects of glucocorticoids on function, quality of life, and survival in patients with Duchenne muscular dystrophy: a prospective cohort study. *Lancet (London, England)*, *391*(10119), 451–461. https://doi.org/10.1016/S0140-6736(17)32160-8

McDonald, C. M., Henricson, E. K., Abresch, R. T., Duong, T., Joyce, N. C., Hu, F., Clemens, P. R., Hoffman, E. P., Cnaan, A., Gordish-Dressman, H., Vishwanathan, V., Chidambaranathan, S., Biggar, W. D., McAdam, L. C., Mah, J. K., Tulinius, M., Morgenroth, L. P., Leshner, R., Tesi-Rocha, C., … Karachunski, P. (2018b). Long-term effects of glucocorticoids on function, quality of life, and survival in patients with Duchenne muscular dystrophy: a prospective cohort study. *Lancet (London, England)*, *391*(10119), 451–461. https://doi.org/10.1016/S0140-6736(17)32160-8

McKellar, D. W., Walter, L. D., Song, L. T., Mantri, M., Wang, M. F. Z., De Vlaminck, I., & Cosgrove, B. D. (2021). Large-scale integration of single-cell transcriptomic data captures transitional progenitor states in mouse skeletal muscle regeneration. *Communications Biology*, *4*(1). https://doi.org/10.1038/S42003-021-02810-X

Megeney, L., Kablar, B., Garrett, K., Anderson, J., & Rudnicki, M. (1996). MyoD is required for myogenic stem cell function in adult skeletal muscle. *Genes & Development*, *10*(10), 1173–1183. https://doi.org/10.1101/gad.10.10.1173

Metzger, T., Gache, V., Xu, M., Cadot, B., Folker, E. S., Richardson, B. E., Gomes, E. R., & Baylies, M. K. (2012). MAP and kinesin-dependent nuclear positioning is required for skeletal muscle function. *Nature*, *484*(7392), 120–124.

https://doi.org/10.1038/NATURE10914

Miller, P. M., Folkmann, A. W., Maia, A. R. R., Efimova, N., Efimov, A., & Kaverina, I. (2009). Golgi-derived CLASP-dependent microtubules control Golgi organization and polarized trafficking in motile cells. *Nature Cell Biology*, *11*(9), 1069–1080. https://doi.org/10.1038/ncb1920

Miller, W. L., & Auchus, R. J. (2011). The molecular biology, biochemistry, and physiology of human steroidogenesis and its disorders. *Endocrine Reviews*, *32*(1), 81–151. https://doi.org/10.1210/ER.2010-0013

Mittelstadt, P. R., Monteiro, J. P., & Ashwell, J. D. (2012). Thymocyte responsiveness to endogenous glucocorticoids is required for immunological fitness. *The Journal of Clinical Investigation*, *122*(7), 2384–2394. https://doi.org/10.1172/JCI63067

Moras, D., & Gronemeyer, H. (1998). The nuclear receptor ligand-binding domain: structure and function. *Current Opinion in Cell Biology*, *10*(3), 384–391. https://doi.org/10.1016/S0955-0674(98)80015-X

Moser, H. (1984). Duchenne muscular dystrophy: pathogenetic aspects and genetic prevention. *Human Genetics*, *66*(1), 17–40. https://doi.org/10.1007/BF00275183

Mouly, V., Aamiri, A., Périé, S., Mamchaoui, K., Barani, A., Bigot, A., Bouazza, B., François, V., Furling, D., Jacquemin, V., Negroni, E., Riederer, I., Vignaud, A., St Guily, J. L., & Butler-Browne, G. S. (2005). Myoblast transfer therapy: is there any light at the end of the tunnel? *Acta Myologica : Myopathies and Cardiomyopathies : Official Journal of the Mediterranean Society of Myology*, *24*(2), 128–133.

Mu, X., Xiang, G., Rathbone, C. R., Pan, H., Bellayr, I. H., Walters, T. J., & Li, Y. (2011). Slow-adhering stem cells derived from injured skeletal muscle have improved regenerative capacity. *The American Journal of Pathology*, *179*(2), 931–941. https://doi.org/10.1016/J.AJPATH.2011.05.004

Murphy, M. M., Lawson, J. A., Mathew, S. J., Hutcheson, D. A., & Kardon, G. (2011a). Satellite cells, connective tissue fibroblasts and their interactions are crucial for muscle regeneration. *Development*, *138*(17), 3625–3637. https://doi.org/10.1242/dev.064162

Murphy, M. M., Lawson, J. A., Mathew, S. J., Hutcheson, D. A., & Kardon, G. (2011b). Satellite cells, connective tissue fibroblasts and their interactions are crucial for muscle regeneration. *Development (Cambridge, England)*, *138*(17), 3625–3637. https://doi.org/10.1242/DEV.064162

Nevo, Y., Shomrat, R., Yaron, Y., Orr-Urtreger, A., Harel, S., & Legum, C. (1999). Fetal muscle biopsy as a diagnostic tool in Duchenne muscular dystrophy. *Prenatal Diagnosis*, *19*(10), 921–926. https://doi.org/10.1002/(sici)1097-0223(199910)19:10<921::aid-pd660>3.0.co;2-a

Nicholas Dias, Yung Peng, R. K. (2017). Microtubule Dynamics: an interplay of biochemistry and mechanics. *Physiology & Behavior*, *176*(3), 139–148. https://doi.org/10.1016/j.physbeh.2017.03.040

Nogales, E., & Wang, H. W. (2006). Structural intermediates in microtubule assembly and disassembly: how and why? *Current Opinion in Cell Biology*, *18*(2), 179–184. https://doi.org/10.1016/J.CEB.2006.02.009

Nomi, M., Oishi, I., Kani, S., Suzuki, H., Matsuda, T., Yoda, A., Kitamura, M., Itoh, K., Takeuchi, S., Takeda, K., Akira, S., Ikeya, M., Takada, S., & Minami, Y. (2001). Loss of mRor1

enhances the heart and skeletal abnormalities in mRor2-deficient mice: redundant and pleiotropic functions of mRor1 and mRor2 receptor tyrosine kinases. *Molecular and Cellular Biology*, *21*(24), 8329–8335. https://doi.org/10.1128/MCB.21.24.8329-8335.2001

Oddoux, S., Randazzo, D., Kenea, A., Alonso, B., Zaal, K. J. M., & Ralston, E. (2019). Misplaced Golgi Elements Produce Randomly Oriented Microtubules and Aberrant Cortical Arrays of Microtubules in Dystrophic Skeletal Muscle Fibers. *Frontiers in Cell and Developmental Biology*, *7*. https://doi.org/10.3389/FCELL.2019.00176

Oddoux, S., Zaal, K. J., Tate, V., Kenea, A., Nandkeolyar, S. A., Reid, E., Liu, W., & Ralston, E. (2013a). Microtubules that form the stationary lattice of muscle fibers are dynamic and nucleated at golgi elements. *Journal of Cell Biology*, *203*(2), 205–213. https://doi.org/10.1083/jcb.201304063

Oddoux, S., Zaal, K. J., Tate, V., Kenea, A., Nandkeolyar, S. A., Reid, E., Liu, W., & Ralston, E. (2013b). Microtubules that form the stationary lattice of muscle fibers are dynamic and nucleated at Golgi elements. *The Journal of Cell Biology*, *203*(2), 205–213. https://doi.org/10.1083/JCB.201304063

Otto, A., Schmidt, C., Luke, G., Allen, S., Valasek, P., Muntoni, F., Lawrence-Watt, D., & Patel, K. (2008). Canonical Wnt signalling induces satellite-cell proliferation during adult skeletal muscle regeneration. *Journal of Cell Science*, *121*(Pt 17), 2939–2950. https://doi.org/10.1242/JCS.026534

P. Seale, L. A. Sabourin, A. Girgis-Gabardo, A. Mansouri, P. Gruss, M. A. R. (2000). Pax7 is required for the specification of myogenic satellite cells. *Cell*, *102*(7), 777–786. https://doi.org/10.1016/s0092-8674(00)00066-0

Partridge, T. A., Grounds, M., & Sloper, J. C. (1978). Evidence of fusion between host and donor myoblasts in skeletal muscle grafts. *Nature*, *273*(5660), 306–308. https://doi.org/10.1038/273306A0

Pasquini, F., Guerin, C., Blake, D., Davies, K., Karpati, G., & Holland, P. (1995). The effect of glucocorticoids on the accumulation of utrophin by cultured normal and dystrophic human skeletal muscle satellite cells. *Neuromuscular Disorders*, *5*(2), 105–114. https://doi.org/10.1016/0960-8966(94)00042-8

Passegué, E., Wagers, A. J., Giuriato, S., Anderson, W. C., & Weissman, I. L. (2005). Global analysis of proliferation and cell cycle gene expression in the regulation of hematopoietic stem and progenitor cell fates. *The Journal of Experimental Medicine*, *202*(11), 1599–1611. https://doi.org/10.1084/JEM.20050967

Pasut, A., Jones, A. E., & Rudnicki, M. A. (2013). Isolation and culture of individual myofibers and their satellite cells from adult skeletal muscle. *Journal of Visualized Experiments : JoVE*, *73*, e50074–e50074. https://doi.org/10.3791/50074

Pasut, A., Oleynik, P., & Rudnicki, M. A. (2012). Isolation of muscle stem cells by fluorescence activated cell sorting cytometry. *Methods in Molecular Biology*, *798*, 53–64. https://doi.org/10.1007/978-1-61779-343-1_3/FIGURES/2

Philippos, M., Sambasivan, R., Castel, D., Rocheteau, P., Bizzarro, V., & Tajbakhsh, S. (2012). A critical requirement for notch signaling in maintenance of the quiescent skeletal muscle stem cell state. *Stem Cells (Dayton, Ohio)*, *30*(2), 243–252. https://doi.org/10.1002/STEM.775

Pratt, W. B., & Toft, D. O. (1997). Steroid receptor interactions with heat shock protein and immunophilin chaperones. *Endocrine Reviews*, *18*(3), 306–360.

https://doi.org/10.1210/EDRV.18.3.0303

Prins, K. W., Humston, J. L., Mehta, A., Tate, V., Ralston, E., & Ervasti, J. M. (2009). Dystrophin is a microtubule-associated protein. *The Journal of Cell Biology*, *186*(3), 363–369. https://doi.org/10.1083/JCB.200905048

Qi, L. L., Rabinowitz, A., Yun, C. C., Yokota, T., Yin, H. F., Alter, J., Jadoon, A., Bou-Gharios, G., & Partridge, T. (2005). Systemic delivery of antisense oligoribonucleotide restores dystrophin expression in body-wide skeletal muscles. *Proceedings of the National Academy of Sciences of the United States of America*, *102*(1), 198–203. https://doi.org/10.1073/PNAS.0406700102

Quattrocelli, M., Barefield, D. Y., Warner, J. L., Vo, A. H., Hadhazy, M., Earley, J. U., Demonbreun, A. R., & McNally, E. M. (2017a). Intermittent glucocorticoid steroid dosing enhances muscle repair without eliciting muscle atrophy. *Journal of Clinical Investigation*, *127*(6), 2418–2432. https://doi.org/10.1172/JCI91445

Quattrocelli, M., Barefield, D. Y., Warner, J. L., Vo, A. H., Hadhazy, M., Earley, J. U., Demonbreun, A. R., & McNally, E. M. (2017b). Intermittent glucocorticoid steroid dosing enhances muscle repair without eliciting muscle atrophy. *The Journal of Clinical Investigation*, *127*(6), 2418–2432. https://doi.org/10.1172/JCI91445

Rafael-Fortney, J. A., Chimanji, N. S., Schill, K. E., Martin, C. D., Murray, J. D., Ganguly, R., Stangland, J. E., Tran, T., Xu, Y., Canan, B. D., Mays, T. A., Delfín, D. A., Janssen, P. M. L., & Raman, S. V. (2011). Early treatment with lisinopril and spironolactone preserves cardiac and skeletal muscle in duchenne muscular dystrophy mice. *Circulation*, *124*(5), 582–588. https://doi.org/10.1161/CIRCULATIONAHA.111.031716/FORMAT/EPUB

Ramamoorthy, S., & Cidlowski, J. A. (2016). Corticosteroids: Mechanisms of Action in Health and Disease. *Rheumatic Diseases Clinics of North America*, *42*(1), 15–31. https://doi.org/10.1016/J.RDC.2015.08.002

Randazzo, D., Khalique, U., Belanto, J. J., Kenea, A., Talsness, D. M., Olthoff, J. T., Tran, M. D., Zaal, K. J., Pak, K., Pinal-Fernandez, I., Mammen, A. L., Sackett, D., Ervasti, J. M., & Ralston, E. (2019). Persistent upregulation of the β-tubulin tubb6, linked to muscle regeneration, is a source of microtubule disorganization in dystrophic muscle. *Human Molecular Genetics*, *28*(7), 1117–1135. https://doi.org/10.1093/HMG/DDY418

Rao, N., Evans, S., Stewart, D., Spencer, K. H., Sheikh, F., Hui, E. E., & Christman, K. L. (2013). Fibroblasts influence muscle progenitor differentiation and alignment in contact independent and dependent manners in organized co-culture devices. *Biomedical Microdevices*, *15*(1), 161–169. https://doi.org/10.1007/S10544-012-9709-9/FIGURES/7

Razafsky, D., & Hodzic, D. (2015). Nuclear envelope: positioning nuclei and organizing synapses. *Current Opinion in Cell Biology*, *34*, 84–93. https://doi.org/10.1016/J.CEB.2015.06.001

Reichardt, H. M., & Schütz, G. (1998). Glucocorticoid signalling - Multiple variations of a common theme. *Molecular and Cellular Endocrinology*, *146*(1–2), 1–6. https://doi.org/10.1016/S0303-7207(98)00208-1

Relaix, F., Bencze, M., Borok, M. J., Der Vartanian, A., Gattazzo, F., Mademtzoglou, D., Perez-Diaz, S., Prola, A., Reyes-Fernandez, P. C., Rotini, A., & Taglietti. (2021). Perspectives on skeletal muscle stem cells. *Nature Communications*, *12*(1). https://doi.org/10.1038/S41467-020-20760-6

Relaix, Frédéric, Rocancourt, D., Mansouri, A., & Buckingham, M. (2005). A Pax3/Pax7-

dependent population of skeletal muscle progenitor cells. *Nature*, *435*(7044), 948–953. https://doi.org/10.1038/NATURE03594

Reul, J. M. H. M., de Kloet, E. R., Van Sluijs, F. J., Rijnberk, A., & Rothuizen, J. (1990). Binding Characteristics of Mineralocorticoid and Glucocorticoid Receptors in Dog Brain and Pituitary. *Endocrinology*, *127*(2), 907–915. https://doi.org/10.1210/ENDO-127-2-907

Rhen, T., & Cidlowski, J. A. (2005). Antiinflammatory action of glucocorticoids--new mechanisms for old drugs. *The New England Journal of Medicine*, *353*(16), 1711–1723. https://doi.org/10.1056/NEJMRA050541

Rimmele, U., Besedovsky, L., Lange, T., & Born, J. (2012). Blocking Mineralocorticoid Receptors Impairs, Blocking Glucocorticoid Receptors Enhances Memory Retrieval in Humans. *Neuropsychopharmacology 2013 38:5*, *38*(5), 884–894. https://doi.org/10.1038/npp.2012.254

Risso, D., Ngai, J., Speed, T. P., & Dudoit, S. (2014). Normalization of RNA-seq data using factor analysis of control genes or samples. *Nature Biotechnology*, *32*(9), 896–902. https://doi.org/10.1038/NBT.2931

Robinson, M. D., McCarthy, D. J., & Smyth, G. K. (2010). edgeR: a Bioconductor package for differential expression analysis of digital gene expression data. *Bioinformatics (Oxford, England)*, *26*(1), 139–140. https://doi.org/10.1093/BIOINFORMATICS/BTP616

Rocheteau, P., Gayraud-Morel, B., Siegl-Cachedenier, I., Blasco, M. A., & Tajbakhsh, S. (2012). A subpopulation of adult skeletal muscle stem cells retains all template DNA strands after cell division. *Cell*, *148*(1–2), 112–125. https://doi.org/10.1016/J.CELL.2011.11.049

Rodgers, J. T., King, K. Y., Brett, J. O., Cromie, M. J., Charville, G. W., Maguire, K. K., Brunson, C., Mastey, N., Liu, L., Tsai, C. R., Goodell, M. A., & Rando, T. A. (2014). mTORC1 controls the adaptive transition of quiescent stem cells from G0 to G(Alert). *Nature*, *510*(7505), 393–396. https://doi.org/10.1038/NATURE13255

Roman, W., & Gomes, E. R. (2018). Nuclear positioning in skeletal muscle. *Seminars in Cell and Developmental Biology*, *82*, 51–56. https://doi.org/10.1016/j.semcdb.2017.11.005

Roman, W., Martins, J. P., Carvalho, F. A., Voituriez, R., Abella, J. V. G., Santos, N. C., Cadot, B., Way, M., & Gomes, E. R. (2017). Myofibril contraction and crosslinking drive nuclear movement to the periphery of skeletal muscle. *Nature Cell Biology 2017 19:10*, *19*(10), 1189–1201. https://doi.org/10.1038/ncb3605

Rosenberg, A. S., Puig, M., Nagaraju, K., Hoffman, E. P., Villalta, S. A., Rao, V. A., Wakefield, L. M., & Woodcock, J. (2015). Immune-mediated pathology in Duchenne muscular dystrophy. *Science Translational Medicine*, *7*(299). https://doi.org/10.1126/scitranslmed.aaa7322

Rossi, S. G., Vazquez, A. E., & Rotundo, R. L. (2000). Local control of acetylcholinesterase gene expression in multinucleated skeletal muscle fibers: individual nuclei respond to signals from the overlying plasma membrane. *The Journal of Neuroscience : The Official Journal of the Society for Neuroscience*, *20*(3), 919–928. https://doi.org/10.1523/JNEUROSCI.20-03-00919.2000

Rovito, D., Rerra, A.-I., Ueberschlag-Pitiot, V., Joshi, S., Karasu, N., Dacleu-Siewe, V., Rayana, K. B., Ghaibour, K., Parisotto, M., Ferry, A., Jelinsky, S. A., Laverny, G., Klaholz, B. P., Sexton, T., Billas, I. M. L., Duteil, D., & Metzger, D. (2021). Myod1 and GR coordinate

myofiber-specific transcriptional enhancers. *Nucleic Acids Research*, *49*(8), 4472–4492. https://doi.org/10.1093/nar/gkab226

Rozo, M., Li, L., & Fan, C. M. (2016). Targeting β1-integrin signaling enhances regeneration in aged and dystrophic muscle in mice. *Nature Medicine 2016 22:8*, *22*(8), 889–896. https://doi.org/10.1038/nm.4116

Ryder-Cook, A. S., Sicinski, P., Thomas, K., Davies, K. E., Worton, R. G., Barnard, E. A., Darlison, M. G., & Barnard, P. J. (1988). Localization of the mdx mutation within the mouse dystrophin gene. *The EMBO Journal*, *7*(10), 3017–3021. https://doi.org/10.1002/J.1460-2075.1988.TB03165.X

Sacco, A., Doyonnas, R., Kraft, P., Vitorovic, S., & Blau, H. M. (2008). Self-renewal and expansion of single transplanted muscle stem cells. *Nature*, *456*(7221), 502–506. https://doi.org/10.1038/NATURE07384

Sakamoto, M., Yuasa, K., Yoshimura, M., Yokota, T., Ikemoto, T., Suzuki, M., Dickson, G., Miyagoe-Suzuki, Y., & Takeda, S. (2002). Micro-dystrophin cDNA ameliorates dystrophic phenotypes when introduced into mdx mice as a transgene. *Biochemical and Biophysical Research Communications*, *293*(4), 1265–1272. https://doi.org/10.1016/S0006-291X(02)00362-5

Salamone, I. M., Quattrocelli, M., Barefield, D. Y., Page, P. G., Tahtah, I., Hadhazy, M., Tomar, G., & McNally, E. M. (2022). Intermittent glucocorticoid treatment enhances skeletal muscle performance through sexually dimorphic mechanisms. *The Journal of Clinical Investigation*, *132*(6). https://doi.org/10.1172/jci149828

Sambasivan, R., Yao, R., Kissenpfennig, A., van Wittenberghe, L., Paldi, A., Gayraud-Morel, B.,

Guenou, H., Malissen, B., Tajbakhsh, S., & Galy, A. (2011). Pax7-expressing satellite cells are indispensable for adult skeletal muscle regeneration. *Development (Cambridge, England)*, *138*(17), 3647–3656. https://doi.org/10.1242/DEV.067587

Sanes, J. R. (2003). The basement membrane/basal lamina of skeletal muscle. *Journal of Biological Chemistry*, *278*(15), 12601–12604. https://doi.org/10.1074/JBC.R200027200

Shin, J., Berg, D. A., Zhu, Y., Shin, J. Y., Song, J., Bonaguidi, M. A., Enikolopov, G., Nauen, D. W., Christian, K. M., Ming, G. L., & Song, H. (2015). Single-Cell RNA-Seq with Waterfall Reveals Molecular Cascades underlying Adult Neurogenesis. *Cell Stem Cell*, *17*(3), 360–372. https://doi.org/10.1016/J.STEM.2015.07.013

Sicinski, P., Geng, Y., Ryder-Cook, A. S., Barnard, E. A., Darlison, M. G., & Barnard, P. J. (1989). The molecular basis of muscular dystrophy in the mdx mouse: a point mutation. *Science (New York, N.Y.)*, *244*(4912), 1578–1580. https://doi.org/10.1126/SCIENCE.2662404

Signer, R. A. J., Magee, J. A., Salic, A., & Morrison, S. J. (2014). Haematopoietic stem cells require a highly regulated protein synthesis rate. *Nature*, *509*(7498), 49–54. https://doi.org/10.1038/NATURE13035

Simsek, T., Kocabas, F., Zheng, J., Deberardinis, R. J., Mahmoud, A. I., Olson, E. N., Schneider, J. W., Zhang, C. C., & Sadek, H. A. (2010). The distinct metabolic profile of hematopoietic stem cells reflects their location in a hypoxic niche. *Cell Stem Cell*, *7*(3), 380–390. https://doi.org/10.1016/J.STEM.2010.07.011

Singh, Paramjeet, Chan, S. W., & Hong, W. (2001). Retinoblastoma protein is functionally distinct from its homologues in affecting glucocorticoid receptor-mediated transcription and apoptosis. *The Journal of Biological Chemistry*, *276*(17), 13762–13770.

https://doi.org/10.1074/JBC.M100137200

Singh, Purva, & Schwarzbauer, J. E. (2012). Fibronectin and stem cell differentiation-lessons from chondrogenesis. *Journal of Cell Science*, *125*, 3703–3712. https://doi.org/10.1242/jcs.095786

Sklar, R. M., & Brown, R. H. (1991). Methylprednisolone increases dystrophin levels by inhibiting myotube death during myogenesis of normal human muscle in vitro. *Journal of the Neurological Sciences*, *101*(1), 73–81. https://doi.org/10.1016/0022-510X(91)90019-4

Skuk, D., Paradis, M., Goulet, M., & Tremblay, J. P. (2007). Ischemic central necrosis in pockets of transplanted myoblasts in nonhuman primates: implications for cell-transplantation strategies. *Transplantation*, *84*(10), 1307–1315. https://doi.org/10.1097/01.TP.0000288322.94252.22

Smith, T., Heger, A., & Sudbery, I. (2017). UMI-tools: modeling sequencing errors in Unique Molecular Identifiers to improve quantification accuracy. *Genome Research*, *27*(3), 491–499. https://doi.org/10.1101/GR.209601.116

So-ichiro Fukada, Akiyoshi Uezumi, Madoka Ikemoto, Satoru Masuda, Masashi Segawa, Naoki Tanimura, Hiroshi Yamamoto, Yuko Miyagoe-Suzuki, S. T. (2007). Molecular signature of quiescent satellite cells in adult skeletal muscle. *Stem Cells*, *25*(10), 2448–2459. https://doi.org/10.1634/stemcells.2007-0019

Study, R., Schultz, E., Gibson, M. C., & Champion, T. (1978). Setellite cells are mitotically quiescent in mature mouse muscle. *J Exp Zool*, *206*, 451–456. https://doi.org/10.1002/jez.1402060314

Surmachevska, N. & Tiwari, V. (n.d.). *Corticosteroid Induced Myopathy - StatPearls - NCBI*

Bookshelf. Retrieved July 7, 2022, from https://www.ncbi.nlm.nih.gov/books/NBK557731/

Takeuchi, S., Takeda, K., Oishi, I., Nomi, M., Ikeya, M., Itoh, K., Tamura, S., Ueda, T., Hatta, T., Otani, H., Terashima, T., Takada, S., Yamamura, H., Akira, S., & Minami, Y. (2000). Mouse Ror2 receptor tyrosine kinase is required for the heart development and limb formation. *Genes to Cells : Devoted to Molecular & Cellular Mechanisms*, *5*(1), 71–78. https://doi.org/10.1046/J.1365-2443.2000.00300.X

Tedesco, F. S., Dellavalle, A., Diaz-Manera, J., Messina, G., & Cossu, G. (2010). Repairing skeletal muscle: regenerative potential of skeletal muscle stem cells. *The Journal of Clinical Investigation*, *120*(1), 11–19. https://doi.org/10.1172/JCI40373

Thomas, K., Engler, A. J., & Meyer, G. A. (2015). Extracellular matrix regulation in the muscle satellite cell niche. *Connective Tissue Research*, *56*(1), 1–8. https://doi.org/10.3109/03008207.2014.947369

Torrente, Y., Belicchi, M., Marchesi, C., D'Antona, G., Cogiamanian, F., Pisati, F., Gavina, M., Giordano, R., Tonlorenzi, R., Fagiolari, G., Lamperti, C., Porretti, L., Lopa, R., Sampaolesi, M., Vicentini, L., Grimoldi, N., Tiberio, F., Songa, V., Baratta, P., … Bresolin, N. (2007). Autologous transplantation of muscle-derived CD133+ stem cells in Duchenne muscle patients. *Cell Transplantation*, *16*(6), 563–577. https://doi.org/10.3727/000000007783465064

Uezumi, A., Fukada, S. I., Yamamoto, N., Takeda, S., & Tsuchida, K. (2010). Mesenchymal progenitors distinct from satellite cells contribute to ectopic fat cell formation in skeletal muscle. *Nature Cell Biology 2010 12:2*, *12*(2), 143–152. https://doi.org/10.1038/ncb2014

Uhlén, M., Fagerberg, L., Hallström, B. M., Lindskog, C., Oksvold, P., Mardinoglu, A., Sivertsson,

Å., Kampf, C., Sjöstedt, E., Asplund, A., Olsson, I. M., Edlund, K., Lundberg, E., Navani, S., Szigyarto, C. A. K., Odeberg, J., Djureinovic, D., Takanen, J. O., Hober, S., … Pontén, F. (2015). Tissue-based map of the human proteome. *Science*, *347*(6220). https://doi.org/10.1126/SCIENCE.1260419/SUPPL_FILE/1260419_UHLEN.SM.PDF

Urciuolo, A., Quarta, M., Morbidoni, V., Gattazzo, F., Molon, S., Grumati, P., Montemurro, F., Tedesco, F. S., Blaauw, B., Cossu, G., Vozzi, G., Rando, T. A., & Bonaldo, P. (2013). Collagen VI regulates satellite cell self-renewal and muscle regeneration. *Nature Communications*, *4*. https://doi.org/10.1038/NCOMMS2964

Verma, M., Asakura, Y., Murakonda, B. S. R., Pengo, T., Latroche, C., Chazaud, B., McLoon, L. K., & Asakura, A. (2018). Muscle Satellite Cell Cross-Talk with a Vascular Niche Maintains Quiescence via VEGF and Notch Signaling. *Cell Stem Cell*, *23*(4), 530-543.e9. https://doi.org/10.1016/J.STEM.2018.09.007/ATTACHMENT/5877889C-78EC-470F-A34F-B3703636AE2F/MMC2.XLSX

Wallace, A. D., & Cidlowski, J. A. (2001). Proteasome-mediated Glucocorticoid Receptor Degradation Restricts Transcriptional Signaling by Glucocorticoids. *Journal of Biological Chemistry*, *276*(46), 42714–42721. https://doi.org/10.1074/JBC.M106033200

Wang, L., Jin, S., Dai, P., Zhang, T., Shi, Y., Ai, G., Shao, X., Xie, Y., Xu, J., Chen, Z., & Gao, Z. (2020). p57 Kip2 is a master regulator of human adipose derived stem cell quiescence and senescence. *Stem Cell Research*, *44*. https://doi.org/10.1016/J.SCR.2020.101759

Wang, Y. X., Feige, P., Brun, C. E., Hekmatnejad, B., Dumont, N. A., Renaud, J. M., Faulkes, S., Guindon, D. E., & Rudnicki, M. A. (2019). EGFR-Aurka Signaling Rescues Polarity and Regeneration Defects in Dystrophin-Deficient Muscle Stem Cells by Increasing Asymmetric

Divisions. *Cell Stem Cell*, *24*(3), 419-432.e6. https://doi.org/10.1016/J.STEM.2019.01.002

Watson, M. L., Baehr, L. M., Reichardt, H. M., Tuckermann, J. P., Bodine, S. C., & David Furlow, J. (2012). A cell-autonomous role for the glucocorticoid receptor in skeletal muscle atrophy induced by systemic glucocorticoid exposure. *American Journal of Physiology. Endocrinology and Metabolism*, *302*(10). https://doi.org/10.1152/AJPENDO.00512.2011

Webster, C., & Blau, H. M. (1990). Accelerated age-related decline in replicative life-span of Duchenne muscular dystrophy myoblasts: implications for cell and gene therapy. *Somatic Cell and Molecular Genetics*, *16*(6), 557–565. https://doi.org/10.1007/BF01233096

Wilson, M. H., & Holzbaur, E. L. F. (2015). Nesprins anchor kinesin-1 motors to the nucleus to drive nuclear distribution in muscle cells. *Development*, *142*(1), 218–228. https://doi.org/10.1242/DEV.114769

Wiper-Bergeron, N., Salem, H. A., Tomlinson, J. J., Wu, D., & Haché, R. J. G. (2007). Glucocorticoid-stimulated preadipocytes differentiation is mediated through acetylation of C/EBPβ by GCN5. *Proceedings of the National Academy of Sciences of the United States of America*, *104*(8), 2703–2708. https://doi.org/10.1073/pnas.0607378104

Wiper-Bergeron, N., Wu, D., Pope, L., Schild-Poulter, C., & Haché, R. J. G. (2003). Stimulation of preadipocyte differentiation by steroid through targeting of an HDAC1 complex. *EMBO Journal*, *22*(9), 2135–2145. https://doi.org/10.1093/emboj/cdg218

Wloga, D., Joachimiak, E., & Fabczak, H. (2017). Tubulin Post-Translational Modifications and Microtubule Dynamics. *International Journal of Molecular Sciences*, *18*(10). https://doi.org/10.3390/IJMS18102207

Wosczyna, M. N., Konishi, C. T., Perez Carbajal, E. E., Wang, T. T., Walsh, R. A., Gan, Q., Wagner, M. W., & Rando, T. A. (2019). Mesenchymal Stromal Cells Are Required for Regeneration and Homeostatic Maintenance of Skeletal Muscle. *Cell Reports*, *27*(7), 2029-2035.e5. https://doi.org/10.1016/J.CELREP.2019.04.074

Wu, T., Hu, E., Xu, S., Chen, M., Guo, P., Dai, Z., Feng, T., Zhou, L., Tang, W., Zhan, L., Fu, X., Liu, S., Bo, X., & Yu, G. (2021). clusterProfiler 4.0: A universal enrichment tool for interpreting omics data. *Innovation (Cambridge (Mass.))*, *2*(3). https://doi.org/10.1016/J.XINN.2021.100141

Yao, G., Lee, T. J., Mori, S., Nevins, J. R., & You, L. (2008). A bistable Rb-E2F switch underlies the restriction point. *Nature Cell Biology*, *10*(4), 476–482. https://doi.org/10.1038/NCB1711

Yin, H., Price, F., & Rudnicki, M. A. (2013). Satellite Cells and the Muscle Stem Cell Niche. *Physiol Rev*, *93*, 23–67. https://doi.org/10.1152/physrev.00043.2011.-Adult

Zaal, K. J. M., Reid, E., Mousavi, K., Zhang, T., Mehta, A., Bugnard, E., Sartorelli, V., & Ralston, E. (2011). Who needs microtubules? Myogenic reorganization of MTOC, Golgi complex and ER exit sites persists despite lack of normal microtubule tracks. *PloS One*, *6*(12). https://doi.org/10.1371/JOURNAL.PONE.0029057

Zammit, P. S., Golding, J. P., Nagata, Y., Hudon, V., Partridge, T. A., & Beauchamp, J. R. (2004). Muscle satellite cells adopt divergent fates: a mechanism for self-renewal? *The Journal of Cell Biology*, *166*(3), 347–357. https://doi.org/10.1083/JCB.200312007

Zammit, P. S., Relaix, F., Nagata, Y., Ruiz, A. P., Collins, C. A., Partridge, T. A., & Beauchamp, J. R. (2006). Pax7 and myogenic progression in skeletal muscle satellite cells. *Journal of Cell Science*, *119*(Pt 9), 1824–1832. https://doi.org/10.1242/JCS.02908

Zhang, S., Chen, L., Cui, B., Chuang, H. Y., Yu, J., Wang-Rodriguez, J., Tang, L., Chen, G., Basak, G. W., & Kipps, T. J. (2012). ROR1 is expressed in human breast cancer and associated with enhanced tumor-cell growth. *PloS One*, *7*(3). https://doi.org/10.1371/JOURNAL.PONE.0031127

Zhang, S., Chen, L., Wang-Rodriguez, J., Zhang, L., Cui, B., Frankel, W., Wu, R., & Kipps, T. J. (2012). The onco-embryonic antigen ROR1 is expressed by a variety of human cancers. *The American Journal of Pathology*, *181*(6), 1903–1910. https://doi.org/10.1016/J.AJPATH.2012.08.024

Zhao, W., Qin, W., Pan, J., Wu, Y., Bauman, W. A., & Cardozo, C. (2009). Dependence of dexamethasone-induced Akt/FOXO1 signaling, upregulation of MAFbx, and protein catabolism upon the glucocorticoid receptor. *Biochemical and Biophysical Research Communications*, *378*(3), 668–672. https://doi.org/10.1016/J.BBRC.2008.11.123

Zou, Y., Zhang, R.-Z., Sabatelli, P., Chu, M.-L., & Bönnemann, C. G. (2008). Muscle Interstitial Fibroblasts Are the Main Source of Collagen VI Synthesis in Skeletal Muscle: Implications for Congenital Muscular Dystrophy Types Ullrich and Bethlem. *J Neuropathol Exp Neurol*, *67*((2)), 144–154. http://www.jneuropath.com.

APPENDICES

A. Supplemental Figure 1

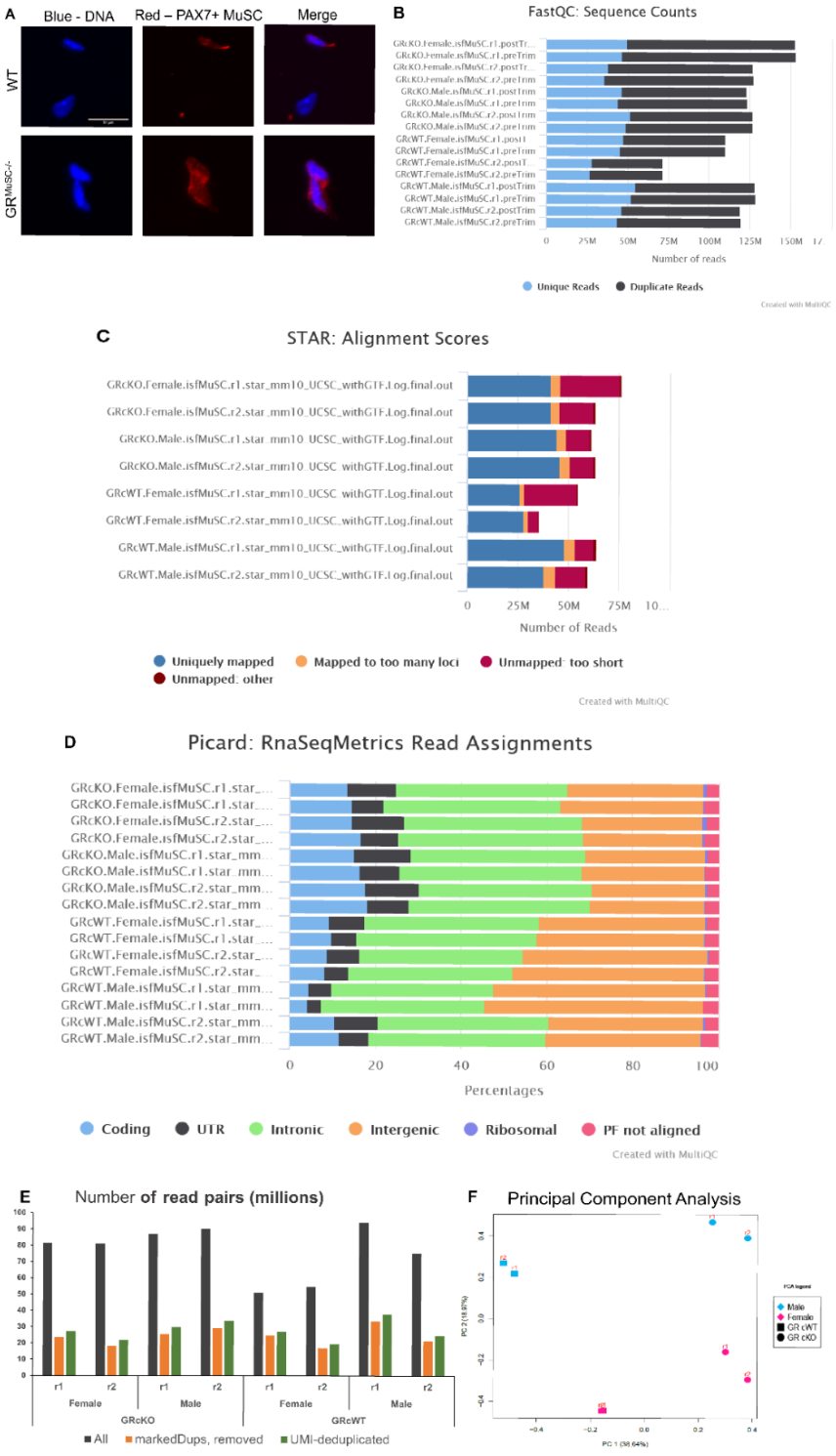

Supplemental Figure 1: PCA analysis on bulk RNA sequenced from male and female WT and $GR^{MuSC-/-}$ FFPE fixed MuSCs revealed distinct clusters between genotypes and sex.
(A) Representative images of PAX7+ (red) (*in situ*) fixed MuSCs from WT and $GR^{MuSC-/-}$ FFPE samples from n=2 male and female mice. Nuclei were counterstained with DAPI (blue). Scale bar, 50 μm. **(B)** FastQC sequence read quality in RNA sequenced from WT and $GR^{MuSC-/-}$ FFPE (*in situ*) fixed MuSCs from n=2 male and female mice. **(C)** STAR alignment scores in RNA sequenced from *in situ* fixed MuSCs from (A). **(D)** Picard RNA-seq metric analysis using RNA sequenced from (A). **(E)** Difference in number of read pairs before and after removal of duplicates in RNA sequenced from MuSCs from (A). **(F)** Principal Component Analysis plot showing clusters of samples based on their similarity in RNA sequenced from *in situ* fixed MuSCs from males in (A).

B. Curriculum Vitae

RASHIDA RAJGARA

HIGHLIGHTS OF QUALIFICATIONS

- Currently, a PhD candidate in the laboratory of Dr. Nadine Wiper Bergeron since May 2017.
- More than 10 years of lab research experience in stem cell-based therapies for treating muscular dystrophy (2012-present).
- Trained in basic and advanced laboratory techniques, including *in vivo* animal work, *in vitro* cell culture, extraction, quantification, and analysis of macromolecules.
- Adept at designing experiments, interpreting data, experimental troubleshooting, statistical analysis and presenting to various audiences through written reports or oral presentations.
- Self- motivated individual with an eye for detail, commendable organization, time-management, and analytic skills.
- Maintains composure, value, and flexibility under pressure independently and as part of a team.

EDUCATION

Doctor of Philosophy, Cellular and Molecular Medicine **May 2017-May 2023**
University of Ottawa, Ottawa, ON
Department: Cellular and Molecular Medicine
Thesis title: *The Role of Glucocorticoid Signaling in Adult Muscle Stem Cell and Myogenic Differentiation.*
Supervisor: Dr. Nadine Wiper-Bergeron

Master of Science, Biochemistry **Sep 2012- Aug 2014**
University of Ottawa, Ottawa, ON
Department: Biochemistry, Microbiology, and Immunology
Thesis title: *The role of Sox7 in the activation of satellite cells and regulation of skeletal myogenesis.*
Supervisor: Dr. Ilona Skerjanc

Fourth year bachelor's diploma **Sep 2011 – Apr 2012**
Carleton University, Ottawa, ON
Areas of Concentration: Biology and Biochemistry

Bachelor of Science, Life Sciences and Biochemistry **Jun 2008- Jun 2011**
University of Mumbai, Mumbai, India
Honors: Chemistry

PROFESSIONAL EXPERIENCE

Research Technician II **Sep 2014 – Apr 2017**
Ilona Skerjanc's Laboratory

University of Ottawa, Ottawa, ON

- Prepared purchase orders, monitored inventory, calibrated, and maintained equipment.
- Coordinated undergraduate and graduate student projects, laboratory meeting schedules and other laboratory affairs.
- Consulted directly with the pharmaceutical sector on issues regarding laboratory products, procedures, and promotions.
- Maintained mouse colonies, coordinated *in vivo* and *in vitro* experiments and prepared specimens for other lab members.

RESEARCH PUBLICATIONS

- Albadrani, H., Ammar, T., Rajgara, R. **(3rd),** Bader, M., Wiper-Bergeron, N., & Renaud, J. M. (2022). Angiotensin 1-7 increases fiber cross-sectional area and force in juvenile mouse skeletal muscle. *American journal of physiology-Cell physiology*, 323(6), C1681–C1696. DOI: 10.1152/ajpcell.00271.2021. Total number of authors: 6.
- Collao N., Akohene-Mensah P., Nallabelli J., Binet E., Askarian A., Lloyd J., Niemiro G., Beals J., van Vliet S., **Rajgara R. (10th),** Saleh A., Wiper-Bergeron N., Paluska S., Burd N., and De Lisio M. The Role of L-type Amino Acid Transporter 1 (Slc7a5) During *In vitro* Myogenesis. (2022). *American Journal of Physiology-Cell Physiology* (impact factor 4.25). DOI: 10.1152/ajpcell.00162.2021. Total number of authors: 15.
- AlSudais H., **Rajgara R. (2nd),** Saleh A., Wiper-Bergeron N. C/EBPβ promotes the expression of atrophy-inducing factors by tumors and is a central regulator of cancer cachexia (2022). *Journal of Cachexia, Sarcopenia and Muscle* (impact factor 12.91). DOI: 10.1002/jcsm.12909. Total number of authors: 4.
- Lamarche É., AlSudais H., **Rajgara R. (3rd),** Fu D., Omaiche S., Wiper-Bergeron N. SMAD2 promotes myogenin expression and terminal myogenic differentiation (2021). *Development.* Volume 148, Issue 3: dev195495 (impact factor 6.9). DOI: 10.1242/dev.195495. PMID: 33462116. Total number of authors: 6.
- Zakariyah A., **Rajgara R**. **(2nd)**, Shelton M., Blais A., Skerjanc I., Burgon P. Combinatorial Utilization of Murine Embryonic Stem Cells, and *In vivo* Models to Study Human Congenital Heart Disease (2019). *Current Protocols in Stem Cell Biology*, Volume 48, Issue:1 (impact factor 1.92). DOI: 10.1002/cpsc.75. Total number of authors: 6.
- Zakariyah A., **Rajgara R. (2nd),** Ellias Horner E., Cattin M., Blais A., Skerjanc I., Burgon P. *In vitro* Modeling of Congenital Heart Defects Associated with an NKX2-5 Mutation Revealed a Dysregulation in BMP/Notch-Mediated Signaling (2018). *Stem Cells.* Volume 36, Issue: 4, 514 -526 (impact factor 5.59). DOI:10.1002/stem.2766. Total number of authors: 7.
- **Rajgara R. (1st),** Lala-Tabbert N., Marchildon F., Lamarche E., MacDonald J., Scott D., Blais A., Skerjanc S., Wiper-Bergeron N. SOX7 is required for muscle satellite cell development and maintenance (2017). *Stem Cell Reports*, Volume 9, Issue: 4, 1139 – 1151 (impact factor 7.34). DOI: 10.1016/j.stemcr.2017.08.014. Total number of authors: 9.

- Zakariyah A., **Rajgara R. (2nd),** Veinot J., Skerjanc I., Burgon P. Congenital heart defect causing mutation in Nkx2.5 displays *in vivo* functional deficit (2017). *Journal of Molecular and Cellular Cardiology.* Volume 105, Issue: 36, 89-98 (impact factor 5.68). DOI: 10.1016/j.yjmcc.2017.03.003. Total number of authors: 5.
- Fair J, Voronova A., Bosiljcic N., **Rajgara R. (4th),** Blais A., Skerjanc I. BRG1 interacts with GLI2 and binds Mef2c gene in a hedgehog signaling dependent manner during *in vitro* cardiomyogenesis (2016). *BMC Developmental Biology*. Aug 2; 16(1):27 (impact factor 2.28). DOI: 10.1186/s12861-016-0127-8. Total number of authors: 6.

RESEARCH ABSTRACTS

- Ngo C., Mardiros L., **Rajgara R (last).** (2020). Scinapse 2019-2020 Undergraduate Science Case Competition: Augmented Biology. *URNCST Journal.* Volume 4, Issue 3, 1-12. https://doi.org/10.26685/urncst.184.
- Cyr D., Ghossein J., **Rajgara R (last)**. (2019). Scinapse 2018-2019 Undergraduate Science Case Competition: Cannabis, Harm or Health? *URNCST Journal.* Volume 3, Issue: 9*, 1-19.* https://doi.org/10.26685/urncst.163
- Bajwa D., Cornila I., Ghossein J., **Rajgara R (last)**. (2018). Scinapse 2017-2018 Undergraduate Science Case Competition: What the frack is this? *URNCST Journal.* Volume 2, Issue: 3, 1-20. https://doi.org/10.26685/urncst.47

CONFERENCE POSTER PRESENTATIONS & RESEARCH DAYS

- **Rajgara R.,** AlSudais H., Wiper-Bergeron N. Poster presentation title: The Role of Glucocorticoid Signaling in Adult Muscle Stem Cells. CMM/NSC Departmental Research Day, on the 24th of October 2019.
- **Rajgara R.,** AlSudais H., Wiper-Bergeron N. Poster Presentation title: The Role of Glucocorticoid Signaling in Adult Muscle Stem Cells. 5th Ottawa International Conference on Neuromuscular Disease and Biology, held in Ottawa from 17-19th October 2019.
- **Rajgara R.,** AlSudais H., Wiper-Bergeron N. Poster Presentation title: The Role of Glucocorticoid Signaling in Adult Muscle Stem Cells. 1st Annual Faculty of Medicine Research Day, on the 25th of September 2019. Abstract published in the special edition of the University of Ottawa Journal of Medicine (UOJM).
- **Rajgara R.**, Lala-Tabbert N., Marchildon F., Lamarche É., MacDonald J., Scott D., Blais A., Skerjanc I., Wiper-Bergeron N. Poster Presentation title: SOX7 is required for muscle satellite cell development and maintenance. 4th Ottawa International Conference on Neuromuscular Disease and Biology, held in Ottawa from 7-9th September 2017.
- **Rajgara R.**, Shelton M., Metz J., Liu J., Carpenedo R., Demers S., Stanford W., Skerjanc I. Poster Presentation title: Inhibition of GSK3-β enhances skeletal myogenesis in embryonic

stem cells. 3rd Ottawa International Conference on Neuromuscular Disease and Biology, held in Ottawa from 24-26th September 2015.

- Presented a poster at the 7th Canadian Developmental Biology Conference held in Mont Tremblant in March 2013.

VOLUNTEER EXPERIENCE

President, CMM/NSC Graduate Student Council **Sep 2020-Aug 2021**
University of Ottawa

- Overseeing the general functioning of the graduate student council. More specifically leading the biweekly meetings, setting meeting agendas, and moderating discussion; helping to coordinate and present at the Welcome Week orientation as well as the CMM/NSC GSA annual general meeting. The role also involves coordinating with and providing support to the VPs for specific events; consulting with BMI and SEPH GSA heads; organizing the annual CMM/NSC GSA elections; and attending other program-related meetings with the FMGSC (Faculty of Medicine Graduate Studies Committee).

Vice-President, CMM/NSC Graduate Student Council **Sep 2018- Aug 2020**
University of Ottawa

- Function as a liaison between the graduate student body and the Faculty of Medicine council by attending meetings with the Dean and departmental heads, ensuring that the needs of students are effectively conveyed to the council and all decisions involving students are discussed with total transparency and approved accordingly.

President, SciNapse Undergraduate Science Case Competition **Jun 2017- Jun 2020**
University of Ottawa, Ottawa ON

- Lead a non-profit organization consisting of student leaders from universities across North America and a provincial team of students here at the University of Ottawa that aims to provide undergraduates with opportunities to explore science build skills and stand out by proposing an original research idea for a real-world challenge.
- Planning a gala, awards ceremony, and a conference with workshops for a 100+ finalists
- Organizing monthly team meetings, individual consulting with leaders and team members, procuring judges, finding sponsors/funding, and answering all SciNapse related inquiries from participants.
- Setting up collaborations between students and senior scientists in the Ottawa community.

Co-VP Academic, CMM/NSC Graduate Student Council **Sep 2017- Aug 2018**
University of Ottawa, ON

- Represented the graduate student body and ensured that the academic needs of students were effectively conveyed to the faculty.
- Organized academic and professional events such as Career Day, Scholarship, Transfer/Comprehensive exam, Statistics and Thesis Writing workshops. for graduate students to provide a transformative and enriching academic experience.

VP Social, BMI Graduate Student Association **Sep 2012- Aug 2015**
University of Ottawa, ON

- Liaised the interpersonal graduate students needs with council members by organizing social networking events.
- Planned orientation week activities for new graduate students to acquaint themselves with the department and fellow graduates.
- Organized food socials, summer BBQ's and dance lessons, the annual Halloween and Holiday celebrations as well as several events at popular locals to potentiate further interactions between students.

SCHOLARSHIPS/AWARDS

- Ontario Graduate Scholarship **May 2019- Apr 2022**
- Faculty of Medicine Leadership Award, Graduate Studies CMM/NSC GSA **Dec 2021**
- Faculty of Medicine Leadership Award, Graduate Studies CMM/NSC GSA **Dec 2020**
- RBC Students leading Change Scholarship, Royal Bank of Canada **Sep 2018- Apr 2019**
- Faculty of Medicine Leadership Award, University of Ottawa **Dec 2014**
- OMG Exchange Program, University of Mumbai/ Carleton University **Sep 2011- Apr 2012**